KUNGL
TEKNISKA
HÖGSKOLAN

TRITA-EES–0004
ISSN 1100-1607

Control Lyapunov Functions: A Control Strategy for Damping of Power Oscillations in Large Power Systems

Mehrdad Ghandhari

Stockholm 2000

Doctoral Dissertation
Royal Institute of Technology
Dept. of Electric Power Engineering
Electric Power Systems

KTH Högskoletryckeriet, Stockholm 2000

Abstract

In the present climate of deregulation and privatisation, the utilities are often separated into generation, transmission and distribution companies so as to help promote economic efficiency and encourage competition. Also, environmental concerns, right-of-way and cost problems have delayed the construction of both generation facilities and new transmission lines while the demand for electric power has continued to grow, which must be met by increased loading of available lines. A consequence is that power system damping is often reduced which leads to a poor damping of electromechanical power oscillations and/or impairment of transient stability.

The aim of this thesis is to examine the ability of Controllable Series Devices (CSDs), such as

- Unified Power Flow Controller (UPFC)
- Controllable Series Capacitor (CSC)
- Quadrature Boosting Transformer (QBT)

for improving transient stability and damping of electromechanical oscillations in a power system.

For these devices, a general model is used in power system analysis. This model is referred to as injection model which is valid for load flow and angle stability analysis. The model is also helpful for understanding the impact of the CSDs on power system stability.

A control strategy for damping of electromechanical power oscillations is also derived based on Lyapunov theory. Lyapunov theory deals with dynamical systems without input. For this reason, it has traditionally been applied only to closed–loop control systems, that is, systems for which the input has been eliminated through the substitution of a predetermined feedback control. However, in this thesis, Lyapunov function candidates are used in feedback design itself by making the Lyapunov derivative negative when choosing the control. This control strategy is called Control Lyapunov Function (CLF) for systems with control input.

Keywords: Controllable Series Devices (CSDs), Unified Power Flow Controller (UPFC), Quadrature Boosting Transformer (QBT), Controllable Series Capacitor (CSC), Lyapunov function, Control Lyapunov Function (CLF), SIngle Machine Equivalent (SIME), Variable Structure Control (VSC).

TRITA-EES–0004 • ISSN 1100-1607

Acknowledgments

First of all, I would like to express my deepest gratitude and appreciation to my supervisor, Professor Göran Andersson, for his support and guidance throughout this project.

I would like to extend my warmest thanks to Dr. Ian A. Hiskens for his constant support, inspiring discussions and valuable suggestions, especially during my visit at the University of Newcastle, Australia.

I gratefully acknowledge numerous useful comments by the members of the project steering committee, namely, Mojtaba Noroozian, Lennart Ängquist, Bertil Berggren of ABB and Magnus Danielsson of Svenska Kraftnät. Also, financial support from these companies through the Elektra program is gratefully acknowledged.

Many thanks to the staff of Electric Power Systems for providing stimulating and friendly atmosphere for study and research and help in different aspects. My special thanks to Mrs. Lillemor Hyllengren for all her assistance.

A special thanks to Lars Lindkvist for his assistance with SIMPOW.

Many thanks to Professor Mania Pavella and Damien Ernst for helping me with SIME during my visit at the University of Liège, Belgium.

Finally, I would like to extend my deepest gratitude and personal thanks to those closest to me. In particular, I would like to thank my dear mother for teaching me the value of education and my lovely Karin for her support and encouragement during this period of late working hours.

Mehrdad Ghandhari
Stockholm
September 2000

Acronyms

Acronym	Description
AC	Alternating Current
AVR	Automatic Voltage Regulator
BT	Boosting Transformer
CLF	Control Lyapunov Function
CSC	Controllable Series Capacitor
CSDs	Controllable Series Devices
DAE	Differential–Algebraic Equations
DC	Direct Current
ET	Excitation Transformer
FACTS	Flexible AC Transmission Systems
GOMIB	Generalized One–Machine Infinite Bus
OMIB	One–Machine Infinite Bus
PSS	Power System Stabilizer
QBT	Quadrature Boosting Transformer
RNM	Reduced Network Model
s.e.p	Stable Equilibrium Point
SIME	SIngle Machine Equivalent
SPM	Structure Preserving Model
TCSC	Thyristor Controlled Series Capacitors
TSSC	Thyristor Switched Series Capacitors
UPFC	Unified Power Flow Controller
VSC	Variable Structure Control

Contents

List of Figures

Chapter 1

Introduction

1.1 Background and Motivation of Project

Historically, power systems were designed and operated with large margins. It was comparatively easy to match load growth with new generation and transmission equipment. So, systems normally operated in a region where behavior was fairly linear. Only occasionally would systems be forced to extremes where nonlinearities could begin to have some significant effect. However, because of political and environmental issues, such as the building and the locations of new generation and impediments of the building transmission facilities, there is a greater need to make maximum use of existing facilities. As a consequence, some transmission lines become more loaded than was planned (when they were built) which leads to reduced power system damping of oscillations and to decreased system stability margins. Also, as the electricity industry moves toward an open access market, operating strategies will become much less predictable. Hence, the reliance on nearly linear behavior (which was adequate in the past) must give way to an acceptance that nonlinearities are going to play an increasingly important role in power system operation. It is therefore vital that analysis tools perform accurately and reliably in the presence of nonlinearities [1].

Development of devices for increasing the transmission capacity of lines, and controlling the power flow in transmission system goes on presently. Many of these new apparatuses can be materialized only due to the latest

development in high–power electronics to be used in the main circuits[1] combined with control strategies that rely on the modern control system software and hardware.

By using power electronics controllers a Flexible AC Transmission System (FACTS) can be produced which offers greater control of power flow, secure loading and damping of power system oscillations [2]. The device concepts can be classified into those operating in shunt with the power line in which cases the injected currents are controlled, and those operating in series with the power line in which cases the inserted voltages are controlled. The first category includes system components, such as the Static Var Compensator (SVC), and the latter category includes system components, such as

- Unified Power Flow Controller (UPFC)
- Controllable Series Capacitor (CSC)
- Quadrature Boosting Transformer (QBT)

which all henceforth will be called Controllable Series Devices (CSDs). Application of these devices to power flow control and damping control in electric power systems is described in [3].

Generally, in the modeling of such devices for studies of power system behavior, the fast switching action inherent in power electronics is ignored. Instead, the devices are represented by approximate models which exhibit continuous behavior. The aim is to ensure that the exact and approximate representations have a similar "average" effect on the system. Of course, any physical limitations in the actual device must be accurately reflected in the approximate model [1].

1.2 Aims of the Performed Work

Modern power systems are large scale and complex. Disturbances typically change the network topology and result in nonlinear system response. Also, because of deregulation the configuration of the interconnected grid will routinely be in a state of change. Therefore, the traditional control laws based on linearized system models are often of limited

[1] The circuits of the device where the power is flowing are usually referred to as main circuits

value. Thus, a control strategy that will counteract a wide variety of disturbances that may occur in the power system is attractive.

The aim of this project is to investigate and evaluate the enhancement of the performance of the control laws which are derived for nonlinear systems. Also, a question of great importance is the selection of the input signals for the CSDs in order to damp power oscillations in an effective and robust manner. For a CSD controller sited in the transmission system, it is attractive to extract an input signal from the locally measurable quantities at the controller location.

In the first part of the project, two control strategies, namely:

- Variable Structure Control
- Energy Function Method

were studied and the results were reported in [4]–[6]. It was concluded that the Energy Function Method was more suitable than the Variable Structure Control for controlling CSDs in a multi–machine power system. Therefore, further research regarding Energy Function Method was motivated.

It should be noted that Energy Function Method will henceforth be renamed to Control Lyapunov Function (CLF).

The overall aim of the research of this part of the project is to try to resolve some issues regarding CLF and verify its applicability to realistic power systems. The following topics are planned to be addressed:

- Influence of losses.
- Influence of more detailed models.
- Use of local input signals and coordination of different controllers.

These items will be elaborated below.

So far Control Lyapunov Function (CLF) is proven to work in power systems without losses. One issue is the unavailability of CLF to effectively handle power system losses, where the losses are either from transmission systems or from the transfer conductances in the reduced system admittance matrix after the elimination of load buses. This is a profound

theoretical problem. This problem is also valid when voltage dependence of real loads and more detailed models of synchronous machines included Automatic Voltage regulator (AVR) and turbine regulator are considered.

One of the aims of the proposed project is to study the effects that can be expected when control laws for the CSDs (which are based upon simplified system models) are applied to realistic systems.

In the somewhat simplified model used to derive the CLF based control law, it can be verified that local input signals, e.g. power flows on lines, can successfully be used to damp power oscillations. However, there are two issues that will be investigated further in this project to gain a better basis and understanding, namely:

- Are local signals sufficient also when more complicated and realistic models of the power system components are used?
- Even if it can be proven that local signals can stabilize the system, a remote input signal may be more effective for this purpose. A pertinent question is for which power system conditions this is the case.

A related question (at least from a theoretical point of view) concerns the coordination of several CSD controller. A relevant question is then:

- Do CSDs with CLF control adversely affect each other?

The aim of the project is to answer the above questions through analytical work and simulations of realistic power systems.

The project can be seen as a very natural extension and continuation of the work done at the department and reported in [7]. The emphasis in [7] was on (steady– state) power flow control and on linear analysis of power systems with CSDs, but some possibilities of nonlinear control were also briefly investigated.

The project was also coordinated with a project by the NUTEK REGINA project on Coordinated and Robust Control of Power Systems which was reported in [8]. The main issues of [8] involve the design of control strategies of power systems for the case when several interacting controllers are present, both in steady–state and dynamically. The proposed project and

the project reported in [8] have some points of interactions which were coordinated, and it is believed that these two projects have benefited from each other in fruitful way.

Another project was dealing with damping of power oscillations by use of High Voltage Direct Current (HVDC) systems and was reported in [9]. Many of the questions and problems of the proposed project are similar to those of [9], but the studied solutions are of course different. A fruitful interaction took also place in this case. All the described projects together are part of long term plan of the department to develop and investigate the possibilities and virtues of controllable devices in power systems. This plan includes also the development of relevant analysis and simulation tools.

1.3 Outline of the Thesis

Chapter 2 briefly explains the effects and consequence of power system oscillations in a power system. This chapter also outlines how these oscillations are mitigated in a power system. Discussion in this chapter largely follows that in [10] and references therein.

Chapter 3 presents the mathematical models for a power system required in formulating the stability problem. Both Reduced Network Model (RNM) and Structure Preserving Model (SPM) are presented in this chapter. Discussion in this chapter largely follows that in [11], [12] and references therein.

Chapter 4 explains the operating principles of the Unified Power Flow Controller (UPFC), the Quadrature Boosting Transformer (QBT) and Controllable Series Capacitor (CSC). A general model is also derived for these devices. This model which is referred to as injection model, is helpful for understanding the impact of these components on power systems.

Chapter 5 starts by reviewing some relevant concepts from nonlinear dynamical systems theory. Then, this chapter analyzes stability of equilibrium points by applying Lyapunov theorems. For mechanical and electrical systems, the physical energy (or energy–like) functions are often used as Lyapunov function candidates. The time derivatives of these energy functions are however negative semidefinite, and therefore, these functions fail to prove the asymptotic stability of an equilibrium point. However, by

applying the La Salle's invariance principle and the theorem of Barbashin and Krasovskii, the asymptotic stability of an equilibrium point can also be justified by the energy functions. Discussion in this chapter largely follows that in [13]–[16].

Chapter 6 introduces the concept of Control Lyapunov Function for systems with control input. The so–called affine systems are studied in this chapter. Discussion in this chapter largely follows that in [17] and references therein.

Chapter 7 provides the results of numerical examples. In this chapter, the control laws derived in Chapter 6 are applied to various test systems.

Chapter 8 introduces the concept of SIngle Machine Equivalent (SIME). SIME is a hybrid direct-temporal transient stability method, which transforms the trajectories of a multi–machine power system into the trajectory of a Generalized One–Machine Infinite Bus (GOMIB) system. Basically, SIME deals with the post-fault configuration of a power system subjected to a disturbance which presumably drives it to instability. Under such condition, SIME uses a time–domain simulation program in order to identify the mode of separation of its machines into two groups, namely, critical and non-critical machines which are replaced by successively a two–machine equivalent. Then, this two–machine equivalent is replaced by a GOMIB system. Discussion in this chapter largely follows that in [12].

Chapter 9 introduces the concept of Variable Structure Control (VSC) and VSC with sliding mode. With VSC, dynamical systems are controlled with discontinuous feedback controllers. VSC has been developed during the last four decades, and is characterized by a control law which is designed to drive the system trajectories onto a specified line (or surface) in the state space. The sliding mode describes the particular case when the system trajectories are constrained to lie upon a line (or surface). Discussion in this chapter largely follows that in [44] and [48].

Finally, in Chapter 10, we provide the conclusions and also some suggestions for future work are given.

1.4 List of Publications

Work performed during this project has been published in the following publications:

1. M. Norrozian, L. Ängquist, M. Ghandhari and G. Andersson, "Use of UPFC for Optimal Power Flow Control", *Proceedings of Stockholm Power Tech.*, pp. 506–511, June 1995.

2. M. Norrozian, L. Ängquist, M. Ghandhari and G. Andersson, "Series–Connected FACTS Devices Control Strategy for Damping of Electromechanical Oscillations", *Proceedings of* 12^{th} *PSCC*, pp. 1090–1096, August 1996.

3. M. Norrozian, L. Ängquist, M. Ghandhari and G. Andersson, "Use of UPFC for Optimal Power Flow Control", *IEEE Trans. on Power Delivery*, Vol. 12, No. 4, pp. 1629–1635, October 1997.

4. M. Norrozian, L. Ängquist, M. Ghandhari and G. Andersson, "Improving Power System Dynamics by Series–Connected FACTS Devices", *IEEE Trans. on Power Delivery*, Vol. 12, No. 4, pp. 1636–1642, October 1997.

5. M. Ghandhari, G. Andersson, M. Norrozian and L. Ängquist, "Nonlinear Control of Controllable Series Devices (CSD)", *Proceedings of the* 29^{th} *North American Power Symposium (NAPS)*, pp. 398–403, October 1997.

6. M. Ghandhari, *Control of Power Oscillations in Transmission Systems Using Controllable Series Devices*, *Licentiate Thesis, Royal Institute of Technology*, TRITA–EES–9705, ISSN 1100–1607, 1997.

7. M. Ghandhari and G. Andersson, "Two Various Control Laws for Controllable Series Capacitor (CSC)", *Power Tech. Budapest 99*, September 1999.

8. M. Ghandhari and G. Andersson, "A Damping Control Strategy for Controllable Series Capacitor (CSC)", *Proceedings of the* 31^{th} *North American Power Symposium (NAPS)*, pp. 398–403, October 1999.

9. M. Ghandhari, G. Andersson and I. A. Hiskens, "Control Lyapunov Functions for Controllable Series Devices", *SEPOPE, Brazil, (invited paper)*, May 2000.

10. M. Ghandhari, G. Andersson and I. A. Hiskens, "Control Lyapunov Functions for Controllable Series Devices", *Submitted to IEEE Trans. on Power Systems.*

11. M. Ghandhari, G. Andersson, D. Ernst and M. Pavella, "A Control Strategy for Controllable Series Capacitor in Electric power Systems", *Submitted to Automatica.*

Chapter 2

Power System Oscillations

An electrical power system consists of many individual elements connected together to form a large, complex system capable of generating, transmitting and distributing electrical energy over a large geographical area. Because of this interconnection of elements, a large variety of dynamic interactions are possible, some of which will only affect some of elements, others will affect parts of the system, while others may affect the system as a whole.

In general, power system stability can be divided into (rotor) angle stability and voltage stability. In this thesis, the angle stability is considered. Power system stability is a term applied to alternating current electric power systems, denoting a condition in which the various synchronous machines of the system remain "in synchronism", or "in step" with each other. Conversely, instability denotes a condition involving "loss of synchronism", or falling "out of step" [19]. The stability problem involves the study of the electromechanical oscillations inherent in power systems.

Power systems exhibit various modes of oscillation due to interactions among system components. Many of the oscillations are due to synchronous generator rotors swinging relative to each other. The electromechanical modes involving these masses usually occur in the frequency range of 0.1 to 2 Hz. Particularly troublesome are the interarea oscillations, which typically are in the frequency range of 0.1 to 1 Hz. The interarea modes are usually associated with groups of machines swinging relative to other groups across a relatively weak transmission path. The higher frequency electromechanical modes (1 to 2 Hz) typically involve

one or two generators swinging against the rest of the power system or electrically close machines swinging against each other (called also local modes). In many systems, the damping of these electromechanical swing modes is a critical factor for operating in a secure manner.

Because of political and environmental issues, such as the building and the locations of new generation and impediments of the building transmission facilities, there is a greater need to make maximum use of existing facilities. As a consequence, some transmission lines become more loaded than was planned when they were built. In particular, heavy power transfers can create interarea damping problems that constrain system operation. The oscillations themselves may be triggered through some event or disturbance on the power system or by shifting the system operating point across some steady-state stability boundary where oscillations may be spontaneously created. Controller proliferation makes such boundaries increasingly difficult to anticipate. Once started, undamped oscillations often grow in magnitude over the span of many seconds. These oscillations may persist for many minutes and be limited in amplitude only by system nonlinearities. In some cases, large generator groups loose synchronism and part or all of the electrical network is lost. The same effect can be reached through slow cascading outages when the oscillations are strong and persistent enough to cause uncoordinated automatic disconnection of key generators or loads. Sustained oscillations can disrupt the power system in other ways, even when they do not produce network separation or loss of resources. For example, power swings that are not troublesome in themselves may have associated voltage or frequency swings, which are unacceptable. Such considerations can limit power transfers even when stability is not a direct concern.

2.1 Sources of Mitigating Power System Oscillations

The torques which influence the machine oscillations can be conceptually split into synchronizing and damping components of torque. The synchronizing component "holds" the machines together and is important for system transient stability following large disturbances. For small disturbances, the synchronizing component of torque determines the frequency of an oscillation.

The damping component determines the decay of oscillations and is important for system stability following recovery from the initial swing. Damping is influenced by many system parameters. It is usually small and can sometimes become negative in the presence of controls, which are practically the only "source" of negative damping. Negative damping can lead to spontaneous growth of oscillations until relays begin to trip system elements.

Much history exists in the power system literature on the application of supplemental modulation controls to existing regulators in order to aid damping of power swings. When a device, its regulator and supplemental control are added to the power system, they must operate satisfactorily in the presence of multiple power swing modes over a wide range of operating conditions.

Conventionally, the damping of power system oscillations is performed by Power System Stabilizer (PSS) which is an added device to Automatic Voltage Regulator (AVR) of the generator. The basic function of the PSS is to extend stability limits by modulating generator voltage through the exciter to provide positive damping torque to power swing modes. By modulating the terminal voltage the PSS affects the power flow from the generator, which efficiently damps local modes. PSS has the disadvantage of working through the same element that had resulted in the negative damping originally. Also, the achievable damping of interarea modes is less than that of local modes. Since system damping is small at best, it is reasonable to use new devices for more damping. For effective damping without disturbing the network synchronizing torques, it is essential that the damping device generate a torque whose phase is precisely defined and can operate continuously. Theses requirements seem best satisfied by the fast response and static character of power electronics devices.

In recent years, the fast progress in the field of power electronics has opened new opportunities for the power industry via utilization of the FACTS devices which offer an alternative means to mitigate power system oscillations. They are operated synchronously with the transmission line and may be connected either in parallel producing controllable shunt reactive current for voltage regulation, or in series with the line for controlling power flow on the transmission line.

Unlike PSS control at a generator location, the speed deviations of the machines of interest used as input signals (measurements) are not readily available to the FACTS devices sited in the transmission line. Further,

since the usual intent is to damp interarea modes, which involve a large number of generators, speed signals themselves are not necessarily the best choice for an input signal for devices in the transmission line. For the FACTS devices, it is typically desirable to extract an input signal from locally measurable quantities. Selecting appropriate measurements is usually a very most important aspect of control design.

2.2 Summary

Power systems exhibit various modes of oscillation due to interactions among system components. Particularly troublesome are the interarea oscillations, which typically are in the frequency range of 0.1 to 1 Hz. Conventionally, the damping of power system oscillations is performed by Power System Stabilizer (PSS). However, due to the fast progress in the field of power electronics, the FACTS devices offer an alternative means to mitigate power system oscillations.

Chapter 3

Modeling of Power Systems

In this chapter, the mathematical models for a power system required in formulating the stability problem will be presented. Both Reduced Network Model (RNM) and Structure Preserving Model (SPM) are presented in this chapter.

Figure 3.1 shows a multi–machine power system which has a total of $n+N$ nodes of which the first n are internal machine nodes and the remaining N are load buses, that is, network nodes.

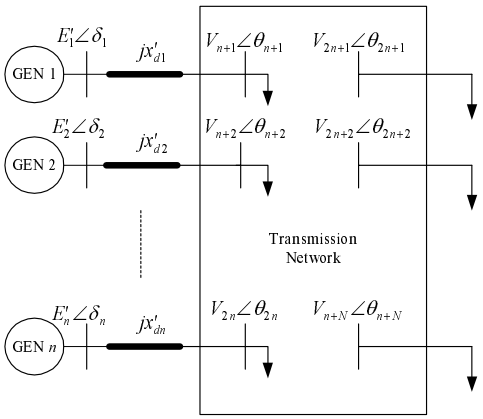

Figure 3.1. A multi–machine power system.

In Figure 3.1, $\bar{E}'_k = E'_k\angle\delta_k$ $(k = 1\cdots n)$ is the internal machine voltage phasor behind the transient reactance x'_{dk} which includes the reactance

of transformer. E'_k is the magnitude of the internal machine voltage and δ_k is the internal machine angle of the k–th machine. All the angles are measured with respect to a synchronously rotating reference in the system. $\bar{V}_k = V_k \angle \theta_k$ $(k = n+1 \cdots n+N)$ is the load bus voltage phasor with magnitude V_k and phase angle θ_k.

Historically, loads are presented by the following three types or models in terms of their load voltage characteristics (also called "static loads"), namely:

- Constant power
- Constant current
- Constant impedance

They form fundamental basis in modeling a majority of loads with the exception of some motor loads requiring special consideration during large disturbances. A static load is described by

$$\begin{aligned} P_L &= P_{Lo}\,(\frac{V}{V_o})^{mp} \\ Q_L &= Q_{Lo}\,(\frac{V}{V_o})^{mq} \end{aligned} \tag{3.1}$$

where P_{Lo} and Q_{Lo} are the active and reactive powers at the nominal voltage V_o, respectively. mp and mq are the voltage exponents of the active power and the reactive power which can assume any value ranging from 0 to 3 based on the nature of the composite load characteristic at a given bus. V is the current voltage.

Having $mp = mq = 0$, the active and reactive components of the static load have constant power characteristics. For $mp = mq = 1$ and $mp = mq = 2$, the active and reactive components of the static load have constant current and constant impedance characteristics, respectively.

A frequently used representation of the static loads as functions of voltage and frequency deviations may be written as (also called ZIP model)

$$\begin{aligned} P_L &= P_{Lo}(a_0 V^0 + a_1 V^1 + a_2 V^2)(1 + k_P \Delta f) \\ Q_L &= Q_{Lo}(b_0 V^0 + b_1 V^1 + b_2 V^2)(1 + k_Q \Delta f) \end{aligned} \tag{3.2}$$

where a_i, b_i, k_P and k_Q are the respective voltage and frequency sensitivity parameters for the load model.

3.1 Reduced Network Model

The Reduced Network Model (RNM) is based on the following assumptions:

- The various network components are assumed to be insensitive to changes in frequency.
- Each synchronous machine is represented by a voltage phasor with constant magnitude E' behind its transient reactance.
- The mechanical angle of the synchronous machine rotor is assumed to coincide with the electrical phase angle of the voltage phasor behind the transient reactance.
- Loads are represented as constant impedances, i.e. $mp = mq = 2$ in (3.1).
- Mechanical power input to generators is assumed constant.
- Saliency is neglected, i.e. $x'_d = x'_q$.
- Stator resistance is neglected.

This is the simplest power system model used in stability studies. It is usually limited to analysis of first–swing transients.

Power systems are most naturally described by Differential–Algebraic Equations (DAE). An advantage of the assumption of constant impedance loads is that it is possible to eliminate the network nodes to obtain an equivalent system which only consists of nonlinear differential equations. This is achieved by the following steps:

1. Perform a pre–fault load flow calculation. Calculate the equivalent steady–state impedance loads in the form of admittances as

$$\bar{y}_{Lk} = \frac{P_{Lk} - jQ_{Lk}}{V_k^2} \quad , \quad k = n+1 \cdots n+N$$

   for each load bus, and add these elements to the $\bar{Y}_{bus}$ matrix.

2. Calculate the internal machine voltages behind transient reactances as

$$\bar{E}'_k = \bar{V}_{n+k} + jx'_{dk}\frac{P_{Gk} - jQ_{Gk}}{\bar{V}^*_{n+k}} \quad , \quad k = 1 \cdots n$$

for each of the n machines.

3. Augment the $\bar{Y}_{bus}$ matrix by admittances corresponding to the machine transient reactances as

$$\bar{y}_k = \frac{1}{jx'_{dk}} \quad , \quad k = 1 \cdots n$$

to create the n internal machine nodes.

4. This augmented admittance matrix can symbolically be partitioned as

$$\hat{\bar{Y}}_{BUS} = \begin{matrix} \\ n \\ N \end{matrix} \begin{matrix} \begin{matrix} n & N \end{matrix} \\ \begin{bmatrix} \bar{Y}_A & \bar{Y}_B \\ \bar{Y}_C & \bar{Y}_D \end{bmatrix} \end{matrix}$$

The relation between injected currents and node voltages is now given by

$$\begin{bmatrix} \bar{I}_G \\ 0 \end{bmatrix} = \begin{bmatrix} \bar{Y}_A & \bar{Y}_B \\ \bar{Y}_C & \bar{Y}_D \end{bmatrix} \begin{bmatrix} \bar{E}_G \\ \bar{V}_L \end{bmatrix}$$

where $\bar{E}_G$ is the vector of the internal machine voltages behind the transient reactances and $\bar{V}_L$ is the vector of load bus voltages. Since there is no injected currents in the network nodes, this system can be reduced to internal machine nodes as

$$\bar{I}_G = (\bar{Y}_A - \bar{Y}_B\bar{Y}_D^{-1}\bar{Y}_C)\bar{E}_G = \bar{Y}_{int}\bar{E}_G$$

The power injected in the internal machine node k can now be calculated by

$$\begin{aligned} P_{Gk} &= Re\{\bar{E}'_k \bar{I}^*_{Gk}\} \\ &= E'^2_k G_{kk} + \sum_{\substack{l=1 \\ l \neq k}}^{n} E'_k E'_l (B_{kl}\sin(\delta_{kl}) + G_{kl}\cos(\delta_{kl})) \end{aligned} \tag{3.3}$$

where

$\delta_{kl} = \delta_k - \delta_l$

G_{kk} is the short-circuit conductance of the k–th machine.

G_{kl} is the transfer conductance in $\bar{Y}_{int}$, $k \neq l$.

B_{kl} is the transfer susceptance in $\bar{Y}_{int}$, $k \neq l$.

Let

$$\begin{aligned} \mathcal{C}_{kl} &= E'_k E'_l B_{kl} \\ \mathcal{F}_{kl} &= E'_k E'_l G_{kl} \end{aligned} \tag{3.4}$$

Now, the motion of the k–th machine is given by ($k = 1 \cdots n$)

$$\begin{aligned} \dot{\delta}_k &= \omega_k \\ M_k \dot{\omega}_k &= P_{mk} - D_k \omega_k - P_{Gk} \end{aligned} \tag{3.5}$$

or

$$\begin{aligned} \dot{\delta}_k &= \omega_k \\ M_k \dot{\omega}_k &= P_k - D_k \omega_k - \sum_{\substack{l=1 \\ l \neq k}}^{n} (\mathcal{C}_{kl} \sin(\delta_{kl}) + \mathcal{F}_{kl} \cos(\delta_{kl})) \end{aligned} \tag{3.6}$$

where

$P_k = P_{mk} - {E'_k}^2 G_{kk}$

P_{mk} is the mechanical power input to the k–th machine.

$D_k > 0$ is the damping constant of the k–th machine.

$M_k > 0$ is the moment of inertia constant of the k–th machine.

ω_k is the rotor speed deviation of the machine k with respect to a synchronously rotating reference.

In the analysis of angle stability, the focus of attention is on the behavior of the machine angles with respect to each other. In order to clearly distinguish between the forces that accelerate the whole system and those that tend to separate the system into different parts, swing equations (3.6)

are transformed into the Center Of Inertia (COI) reference frame. The position of the COI is defined by

$$\delta_{COI} = \frac{1}{M_T}\sum_{k=1}^{n} M_k\delta_k \quad , \quad M_T = \sum_{k=1}^{n} M_k \tag{3.7}$$

Next, the state variables δ_k and ω_k are transformed to the COI variables as

$$\begin{aligned} \tilde{\delta}_k &= \delta_k - \delta_{COI} \\ \tilde{\omega}_k &= \omega_k - \omega_{COI} \end{aligned}$$

These COI variables are constrained by

$$\begin{aligned} \sum_{k=1}^{n} M_k\tilde{\delta}_k = 0 \\ \sum_{k=1}^{n} M_k\tilde{\omega}_k = 0 \end{aligned} \tag{3.8}$$

Swing equations (3.6) can now be rewritten in the COI reference frame as ($k = 1 \cdots n$)

$$\begin{aligned} \dot{\tilde{\delta}}_k &= \tilde{\omega}_k \\ \dot{\tilde{\omega}}_k &= \frac{1}{M_k}[P_k - \sum_{\substack{l=1 \\ l\neq k}}^{n} \mathcal{C}_{kl}\sin(\delta_{kl}) + \frac{M_k}{M_T}P_{COI} - D_k\tilde{\omega}_k] \\ &\quad - \frac{1}{M_k}\sum_{\substack{l=1 \\ l\neq k}}^{n} \mathcal{F}_{kl}\cos(\delta_{kl}) \\ &= f_k + p_k \end{aligned} \tag{3.9}$$

where

$$\begin{aligned} P_{COI} &= \sum_{k=1}^{n}(P_{mk} - P_{Gk}) \\ f_k &= \frac{1}{M_k}[P_k - \sum_{\substack{l=1 \\ l\neq k}}^{n} \mathcal{C}_{kl}\sin(\delta_{kl}) + \frac{M_k}{M_T}P_{COI} - D_k\tilde{\omega}_k] \\ p_k &= -\frac{1}{M_k}\sum_{\substack{l=1 \\ l\neq k}}^{n} \mathcal{F}_{kl}\cos(\delta_{kl}) \end{aligned} \tag{3.10}$$

Note that $\tilde{\delta}_{kl} = \tilde{\delta}_k - \tilde{\delta}_l = \delta_{kl}$ and uniform damping is considered.

System (3.9) can indeed be considered as an Ordinary Differential Equation (ODE) of the form

$$\dot{x} = F(x) = f_o(x) + p(x) \tag{3.11}$$

where $x = [\,\tilde{\delta} \quad \tilde{\omega}\,]^T$ is the vector of the state variables. In (3.11)

$$f_o(x) = [\,\tilde{\omega} \quad [f_1 \cdots f_n]\,]^T \quad , \quad p(x) = [\,0 \quad [p_1 \cdots p_n]\,]^T$$

and

$$\tilde{\delta} = [\,\tilde{\delta}_1 \cdots \tilde{\delta}_n\,] \quad , \quad \tilde{\omega} = [\,\tilde{\omega}_1 \cdots \tilde{\omega}_n\,]$$

3.2 Structure Preserving Model

It is known that load characteristics have a significant effect on system dynamics. Inaccurate load modeling may lead to a power system operating in modes that result in actual system collapse or separation. In the Reduced Network Model (RNM), impedance loads are assumed. Hence, in the context of system modeling, RNM precludes consideration of load behaviors (i.e. voltage and frequency variations) at load buses. Furthermore, in the context of physical explanation of results, reduction of the transmission network leads to loss of network topology.

Structure Preserving Model (SPM) have been proposed (first in [20]) to overcome some of the shortcomings of the RNM, and to improve the modeling of generators and load representations. An advantage of using SPM is that from a modeling viewpoint, it allows more realistic representations of power system components, especially load behaviors.

Consider again the multi–machine power system shown in Figure 3.1. It is assumed that the mechanical power input is constant and the stator resistance is neglected. The one–axis generator model is used for the generators. This model includes one circuit for the field winding of the rotor, i.e. this model considers the effects of field flux decay. Note that in the one–axis generator model, the voltage behind the direct transient reactance is no longer a constant. The loads are modeled by equation (3.1) with $mp = 0$ and arbitrary mq. The transmission lines are given by an admittance matrix of order $(N \times N)$ formed without considering the

loads and the d–axis transient reactances x'_d. The kl–th element of the admittance matrix is defined by $\bar{Y}_{kl} = G_{kl} + jB_{kl}$, where G_{kl} represents solely the resistances of the respective transmission lines. In general, because of the high ratio of reactance to resistance, the transmission line resistances can be neglected. Thus, $\bar{Y}_{kl} = jB_{kl}$.

The dynamics of the k–th generator are described by the following differential equations with respect to the COI reference frame. Note that in the following equations $\tilde{\delta}_k - \tilde{\theta}_l = \delta_k - \theta_l$ and $\tilde{\theta}_k - \tilde{\theta}_l = \theta_k - \theta_l$. Thus, for $k = 1 \cdots n$

$$\begin{aligned} \dot{\tilde{\delta}}_k &= \tilde{\omega}_k \\ M_k \dot{\tilde{\omega}}_k &= P_{mk} - P_{Gk} - D_k \tilde{\omega}_k - \frac{M_k}{M_T} P_{COI} \\ T'_{dok} \dot{E}'_{qk} &= \frac{x_{dk} - x'_{dk}}{x'_{dk}} V_{n+k} \cos(\delta_k - \theta_{n+k}) \\ &\quad + E_{fdk} - \frac{x_{dk}}{x'_{dk}} E'_{qk} \end{aligned} \tag{3.12}$$

where

$$\begin{aligned} P_{Gk} = &\frac{1}{x'_{dk}} E'_{qk} V_{n+k} \sin(\delta_k - \theta_{n+k}) \\ &- \frac{x'_{dk} - x_{qk}}{2 x'_{dk} x_{qk}} V_{n+k}^2 \sin(2(\delta_k - \theta_{n+k})) \end{aligned} \tag{3.13}$$

P_{COI} is given by (3.10).

x_{dk}, x_{qk} are the d–axis and the q–axis synchronous reactances of the k–th machine.

E'_{qk} is the q-axis voltage behind transient reactance of the k–th machine.

T'_{dok} is the d–axis transient open–circuit time constant of the k–th machine.

E_{fdk} is the exciter voltage of the k–th machine which is assumed constant.

E_{fd} can be either constant (fixed excitation) or can vary due to Automatic Voltage Regulator (AVR) action. When the exciter control action is included in the generator model, due to AVR modeling, at least one additional differential equation is needed in (3.12).

For the lossless system the following equations can be written at bus k where P_k is the real power and Q_k is the reactive power injected into the system from bus k.

For $k = (n+1)\cdots 2n$

$$P_k = \sum_{l=n+1}^{n+N} B_{kl}V_kV_l\sin(\theta_k-\theta_l) + \frac{E'_{q(k-n)}V_k\sin(\theta_k-\delta_{k-n})}{x'_{d(k-n)}} + \frac{x'_{d(k-n)}-x_{q(k-n)}}{2x'_{d(k-n)}x_{q(k-n)}}V_k^2\sin(2(\theta_k-\delta_{k-n}))$$

$$Q_k = -\sum_{l=n+1}^{n+N} B_{kl}V_kV_l\cos(\theta_k-\theta_l) + \frac{V_k^2 - E'_{q(k-n)}V_k\cos(\theta_k-\delta_{k-n})}{x'_{d(k-n)}} - \frac{x'_{d(k-n)}-x_{q(k-n)}}{2x'_{d(k-n)}x_{q(k-n)}}V_k^2[\cos(2(\theta_k-\delta_{k-n}))-1]$$

and for $k = (2n+1)\cdots(n+N)$

$$P_k = \sum_{l=n+1}^{n+N} B_{kl}V_kV_l\sin(\theta_k-\theta_l)$$

$$Q_k = -\sum_{l=n+1}^{n+N} B_{kl}V_kV_l\cos(\theta_k-\theta_l)$$

Therefore, for $k = (n+1)\cdots(n+N)$ the power flow equations can be written as

$$\begin{aligned} P_k + P_{Lk} &= 0 \\ Q_k + Q_{Lk} &= 0 \end{aligned} \tag{3.14}$$

3.3 Summary

Dynamics of multi–machine power systems are described by the Reduced Network Model or the Structure Preserving Model. In the Reduced Network Model impedance loads are assumed. Thus, it is possible to eliminate the network nodes to obtain an equivalent system which only consists of

nonlinear differential equations. However, in the context of physical explanation of results, reduction of the transmission network leads to loss of network topology.

In the Structure Preserving Model, dynamics of multi–machine power systems are described by Differential–Algebraic Equations. Thus, from a modeling viewpoint, it allows more realistic representations of power system components, especially load behaviors.

Chapter 4

Modeling of Controllable Series Devices

In this chapter, the operating principles of a Unified Power Flow Controller (UPFC), a Quadrature Boosting Transformer (QBT) and a Controllable Series Capacitor (CSC) are described. Also, a general model is derived for these devices. The models are derived in a single–phase positive–sequence phasor frame. This model which is referred to as injection model, is helpful for understanding the impact of these components on power systems. Furthermore, this model can easily be implemented into existent power system analysis programs.

4.1 Operating Principle of Controllable Series Devices

4.1.1 Unified Power Flow Controller

A unified power flow controller consists of two voltage source converters [21]. These converters are operated from a common DC link provided by a DC capacitor, see Figure 4.1. Converter 2 provides the main function of the UPFC by injecting an AC voltage with controllable magnitude and phase angle in series with the transmission line via a series transformer. The basic function of converter 1 is to supply or absorb the real power demand by converter 2 at the common DC link. Converter 1 can also

generate or absorb controllable reactive power if it is desired. This converter can thereby provide independent shunt reactive compensation for the line. Converter 2 supplies or absorbs locally the required reactive power, and exchanges the active power as a result of the series injection voltage.

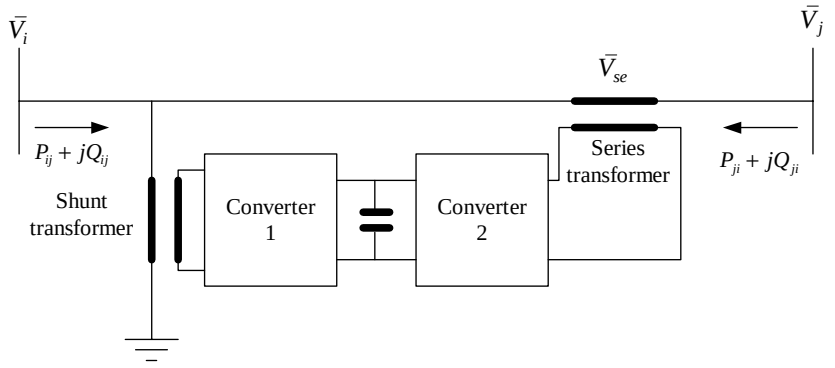

Figure 4.1. Basic circuit arrangement of a UPFC.

4.1.2 Quadrature Boosting Transformer

Based on feasible semiconductor switches and converter topologies for high–power applications, different Phase Shifting Transformer (PST) circuit configurations are identified. In this thesis, the so–called Quadrature Boosting Transformer (QBT) (i.e. the injected voltage is perpendicular to the input terminal voltage) is considered. Figure 4.2 shows the basic circuit of a Quadrature Boosting Transformer (QBT). The phase angle difference between the QBT terminal voltages is achieved by serially connecting a Boosting Transformer (BT) into the transmission line. The power which is injected into the transmission line by this boosting transformer must be taken from the network by the Excitation Transformer (ET). The converter controls the magnitude and the phase angle of $\bar{V}_{se}$.

4.1.3 Controllable Series Capacitor

A Controllable Series Capacitor (CSC) can be materialized by Thyristor Controlled Series Capacitors (TCSC) and Thyristor Switched Series Ca-

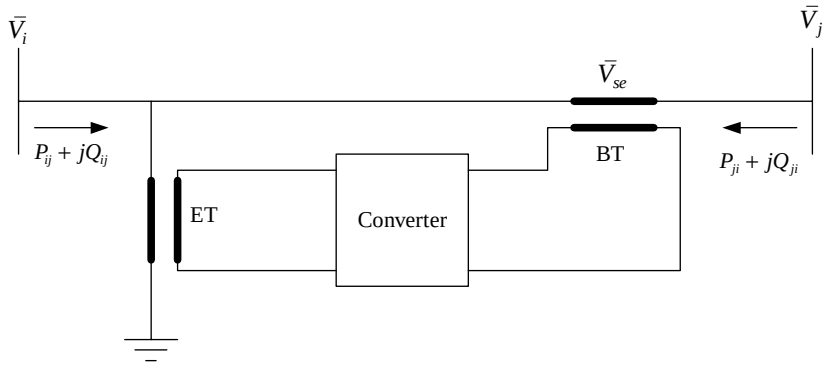

Figure 4.2. Basic circuit arrangement of a QBT.

pacitors (TSSC), as shown in Figure 4.3. In a simplified study, a CSC can be considered as a continuously controllable reactance (normally capacitive) which is connected in series with the transmission line.

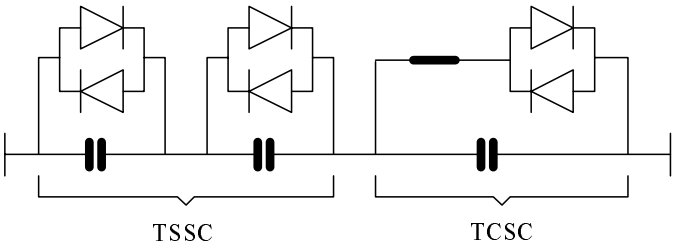

Figure 4.3. Basic circuit arrangement of a CSC.

4.2 Injection Model

Figure 4.4 shows the equivalent circuit diagram of a CSD which is located between buses **i** and **j** in a transmission system. A UPFC and a QBT inject a voltage $\bar{V}_{se}$ in series with the transmission line through a series transformer, see Section 4.1. The active power P_{se} involved in the series injection is taken from the transmission line (i.e. P_{sh}) through a shunt

transformer. The UPFC generates or absorbs the needed reactive power (i.e. Q_{se} and Q_{sh}) locally by the switching operation of its converters, while the reactive power Q_{se} injected in series with the transmission line by the QBT, is taken from the transmission line (i.e. Q_{sh}). In Figure 4.4, x_s is the effective reactance of the UPFC (or the QBT) seen from the transmission line side of the series transformer.

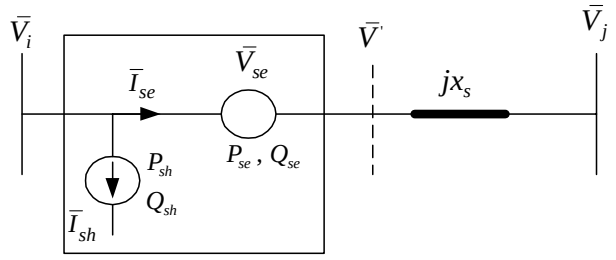

Figure 4.4. Equivalent circuit diagram of a CSD.

Figure 4.5 shows the vector diagram of the equivalent circuit diagram of a CSD.

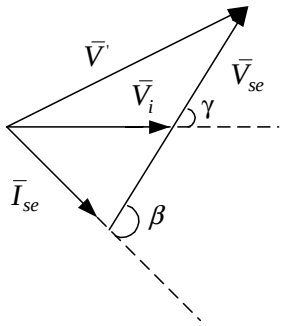

Figure 4.5. Vector diagram of the equivalent circuit diagram.

4.2.1 Injection Model of UPFC

To obtain an injection model for a UPFC, we first consider the series part of the UPFC as shown in Figure 4.6.

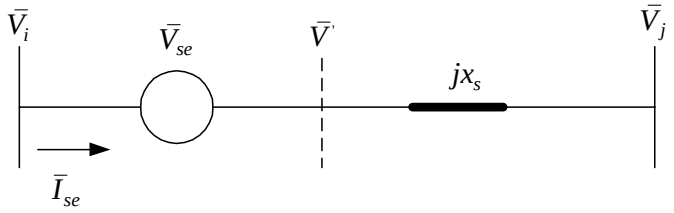

Figure 4.6. Representation of the series connected voltage source.

The series connected voltage source is modeled by an ideal series voltage $\bar{V}_{se}$ which is controllable in magnitude and phase, that is, $\bar{V}_{se} = r\bar{V}_i e^{j\gamma}$ where $0 \leq r \leq r_{max}$ and $0 \leq \gamma \leq 2\pi$.

The injection model is obtained (as shown in Figure 4.7) by replacing the voltage source $\bar{V}_{se}$ by a current source $\bar{I}_{inj} = -jb_s\bar{V}_{se}$ in parallel with x_s. Note that $b_s = 1/x_s$.

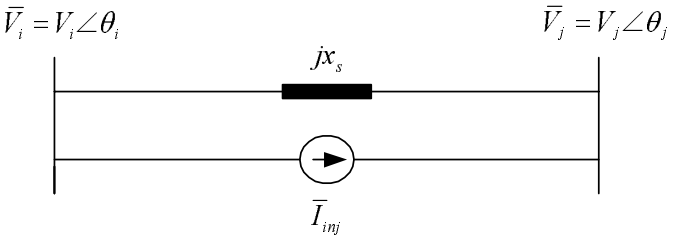

Figure 4.7. Replacement of the series voltage source by a current source.

The current source $\bar{I}_{inj}$ corresponds to injection powers $\bar{S}_i$ and $\bar{S}_j$ which are defined by

$$\begin{aligned} \bar{S}_i &= \bar{V}_i(-\bar{I}_{inj})^* = -rb_sV_i^2\sin(\gamma) - jrb_sV_i^2\cos(\gamma) \\ \bar{S}_j &= \bar{V}_j(\bar{I}_{inj})^* = rb_sV_iV_j\sin(\theta_{ij}-\gamma) + jrb_sV_iV_j\cos(\theta_{ij}-\gamma) \end{aligned}$$

where $\theta_{ij} = \theta_i - \theta_j$.

Figure 4.8 shows the injection model of the series part of the UPFC, where

$$\begin{aligned} P_i = -real(\bar{S}_i) \quad , \quad Q_i = -imag(\bar{S}_i) \\ P_j = -real(\bar{S}_j) \quad , \quad Q_j = -imag(\bar{S}_j) \end{aligned} \tag{4.1}$$

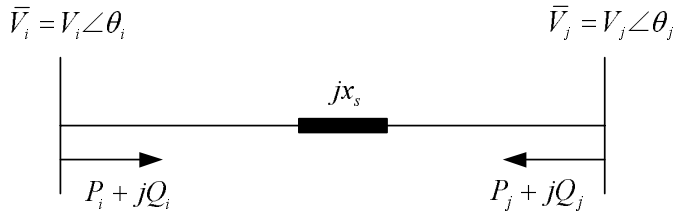

Figure 4.8. Injection model of the series part of the UPFC.

The apparent power supplied by the series voltage source is calculated from

$$\bar{S}_{se} = \bar{V}_{se}\bar{I}^*_{se} = re^{j\gamma}\bar{V}_i(\frac{\bar{V}' - \bar{V}_j}{jx_s})^*$$

Active and reactive powers supplied by the series voltage source are distinguished as:

$$\begin{aligned} P_{se} &= rb_sV_iV_j\sin(\theta_{ij}+\gamma) - rb_sV_i^2\sin(\gamma) \\ Q_{se} &= -rb_sV_iV_j\cos(\theta_{ij}+\gamma) + rb_sV_i^2\cos(\gamma) + r^2b_sV_i^2 \end{aligned}$$

Assuming an ideal UPFC (i.e. losses are neglected in the UPFC), we have then $P_{sh} = P_{se}$. For the UPFC, Q_{sh} is independently controllable, and we assume that $Q_{sh} = 0$. Note that Q_{sh} can also have a nonzero value.

The injection model of the UPFC is constructed from the series connected voltage source model shown in Figure 4.8 by adding $P_{sh} + jQ_{sh}$ to bus **i**. Figure 4.9 shows the injection model of the UPFC.

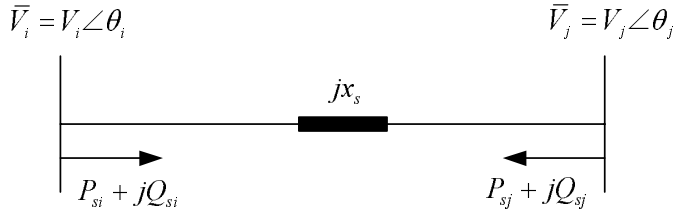

Figure 4.9. Injection model of the UPFC.

In Figure 4.9

$$\begin{aligned} P_{si} &= rb_s V_i V_j \sin(\theta_{ij} + \gamma) \\ P_{sj} &= -P_{si} \\ Q_{si} &= rb_s V_i^2 \cos(\gamma) \\ Q_{sj} &= -rb_s V_i V_j \cos(\theta_{ij} + \gamma) \end{aligned} \tag{4.2}$$

where r and γ are the control variables of the UPFC.

For the purpose of developing a control strategy for the UPFC, it is useful to apply the following control variables.

Since

$$\begin{aligned} r\sin(\theta_{ij} + \gamma) &= r\cos(\gamma)\sin(\theta_{ij}) + r\sin(\gamma)\cos(\theta_{ij}) \\ r\cos(\theta_{ij} + \gamma) &= r\cos(\gamma)\cos(\theta_{ij}) - r\sin(\gamma)\sin(\theta_{ij}) \end{aligned} \tag{4.3}$$

let

$$u_{up1} = r\cos(\gamma) \quad , \quad u_{up2} = r\sin(\gamma) \tag{4.4}$$

Substituting (4.3) and (4.4) into (4.2), the following is obtained.

$$\begin{aligned} P_{si} &= b_s V_i V_j (u_{up1}\sin(\theta_{ij}) + u_{up2}\cos(\theta_{ij})) \\ P_{sj} &= -P_{si} \\ Q_{si} &= u_{up1} b_s V_i^2 \\ Q_{sj} &= -b_s V_i V_j (u_{up1}\cos(\theta_{ij}) - u_{up2}\sin(\theta_{ij})) \end{aligned} \tag{4.5}$$

Note that

$$r = \sqrt{u_{up1}^2 + u_{up2}^2} \quad , \quad \gamma = \arctan(\frac{u_{up2}}{u_{up1}})$$

4.2.2 Injection Model of QBT

The argument given in Subsection 4.2.1 is also valid for constructing an injection model for a QBT. For this device, the injected voltage $\bar{V}_{se}$ is perpendicular to the input terminal voltage $\bar{V}_i$. Thus, $\gamma = \pm\pi/2$, see Figure 4.5.

Assuming an ideal QBT (i.e. losses are neglected in the QBT), we have then $P_{sh} = P_{se}$. For the QBT, the reactive power injected in series with

the transmission line is taken from the shunt part of the QBT. Therefore, $Q_{sh} = Q_{se}$.

The injection model of the QBT is constructed from the series connected voltage source model shown in Figure 4.8 by adding $P_{sh} + jQ_{sh}$ to bus **i**. Thus, Figure 4.9 also shows the injection model of the QBT, where

$$\begin{aligned} P_{si} &= u_q b_s V_i V_j \cos(\theta_{ij}) \\ P_{sj} &= -P_{si} \\ Q_{si} &= u_q b_s V_i^2 + u_q b_s V_i V_j \sin(\theta_{ij}) \\ Q_{sj} &= u_q b_s V_i V_j \sin(\theta_{ij}) \end{aligned} \tag{4.6}$$

In (4.6), $u_q = r\sin(\gamma)$ and $-r_{max} \leq u_q \leq r_{max}$ since $\gamma = \pm\pi/2$.

Note that

$$r = \mid u_q \mid \quad , \quad \gamma = sgn(u_q)\frac{\pi}{2}$$

where $sgn(.)$ is the sign function.

4.2.3 Injection Model of CSC

Suppose a CSC is is located between buses **i** and **j** in a lossless transmission line as shown in Figure 4.10.

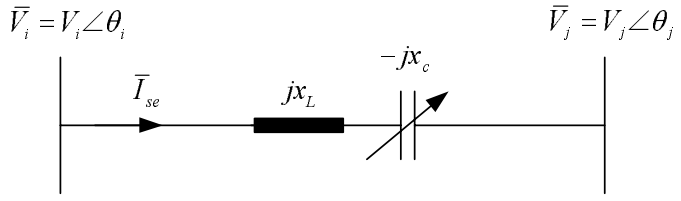

Figure 4.10. CSC located in a lossless transmission line.

For studies involving load flow and angle stability analysis, the CSC is modeled as a variable reactance, i.e x_c in Figure 4.10. However, for the purpose of developing a control strategy and having same models for the CSDs, it is useful to have an injection model representation for the CSC.

Figure 4.4 is also valid for the CSC if $\bar{I}_{sh}$ is set to zero and x_s is the transmission line reactance, i.e. $x_s = x_L$. Furthermore, $\beta = \pi/2$ in Figure 4.5. Thus, Figure 4.10 can be replaced by Figure 4.4 where $x_s = x_L$ and $\bar{I}_{sh} = 0$. From Figure 4.10, we have

$$\bar{I}_{se} = \frac{\bar{V}_i - \bar{V}_j}{j(x_L - x_c)}$$

In Figure 4.4, $\bar{V}_{se} = -jx_c\bar{I}_{se}$ and in Figure 4.7, we have

$$\bar{I}_{inj} = \frac{\bar{V}_{se}}{jx_L} = -\frac{jx_c\bar{I}_{se}}{jx_L} = -\frac{x_c}{x_L}\bar{I}_{se}$$

The injection model of the CSC is then obtained by (4.1). Note that since $\bar{I}_{sh} = 0$, we have $P_{sh} = Q_{sh} = 0$. Thus, Figure 4.9 is also valid for the CSC, where

$$\begin{aligned} P_{si} &= u_c b_s V_i V_j \sin(\theta_{ij}) \\ P_{sj} &= -P_{si} \\ Q_{si} &= u_c b_s (V_i^2 - V_i V_j \cos(\theta_{ij})) \\ Q_{sj} &= u_c b_s (V_j^2 - V_i V_j \cos(\theta_{ij})) \end{aligned} \tag{4.7}$$

and

$$u_c = \frac{x_c}{x_L - x_c} \tag{4.8}$$

4.3 Summary

The injection models of the Controllable Series Devices are derived in a single–phase positive–sequence phasor frame. The injection model is helpful for understanding the impact of the Controllable Series Devices on power systems. This model can easily be used for the purpose of developing control laws. Furthermore, this model can be implemented into existent power system analysis programs.

Chapter 5

Lyapunov Stability

This chapter starts by reviewing some relevant concepts from nonlinear dynamical systems theory. Stability of equilibrium points in the sense of Lyapunov is also presented. Lyapunov stability theorems give sufficient conditions for stability. They do not say whether the given conditions are necessary. There are however theorems which establish (at least conceptually) that for many of Lyapunov stability theorems the given conditions are indeed necessary. Such theorems are usually called converse Lyapunov theorems. These theorems have been a basis for the introduction of Control Lyapunov Function for systems with control input.

5.1 Mathematical Preliminaries

Consider the nonlinear system

$$\dot{x} = f_o(x) \tag{5.1}$$

where x is the n–dimensional state vector which belongs to the Euclidean space R^n. The system is specified by the vector field function $f_o : \mathcal{D} \to R^n$ which is continuous and has continuous first-order partial derivatives with respect to x on a domain $\mathcal{D} \subset R^n$ into R^n. System (5.1) is also called

autonomous since time does not appear explicitly in f_o. Let the solution to (5.1) be given by

$$x(t) = \phi(t - t_o, x_o)$$

where x_o is the initial conditions and t_o is the initial time which is arbitrary. Since the dependence of the solution on the initial time is not essential, we can assume without loss of generality that $t_o = 0$. Thus,

$$x(t) = \phi(t, x_o)$$

Since $f_o(x)$ is continuous, and has continuous first-order partial derivatives with respect to x, a solution to (5.1) (satisfying the initial conditions $x(0) = \phi(0, x_o) = x_o$) exists on some time interval $a < t < b$ containing 0, and that the time interval can be extended at both ends as long as $\|f_o[x(t)]\|$ remains bounded. Furthermore, the solution is unique and differentiable in both t and x_o.

One of the most important geometric properties of autonomous systems of the form (5.1) is that there is only one solution $x(t) = \phi(t, x_o)$ passing through any given initial state $x(0) = \phi(0, x_o) = x_o$. Hence, trajectories in state space can never intersect each other. In contrast, for nonautonomous systems, the solution $x(t) = \phi(t, t_o, x_o)$ depends on the starting time t_o, so that the solution from x_o at $t_o = 0$ will generally not be the same as the solution starting from x_o at some other initial time $t_o \neq 0$.

An equilibrium point x_e for (5.1) is defined by $f_o(x_e) = 0$. The point x_e is Lyapunov stable (or stable in the sense of Lyapunov) if solutions that start near x_e remain near x_e for all $t \geq 0$. More precisely, an equilibrium point x_e is Lyapunov stable if for any $\epsilon > 0$ (no matter how small) there exists a $\delta = \delta(\epsilon) > 0$ such that for every $x(0)$ in which

$$\|x(0) - x_e\| < \delta$$

the solution $x(t)$ satisfies

$$\|x(t) - x_e\| < \epsilon \quad , \quad \forall\, t > 0$$

If, in addition,

$$\|x(t) - x_e\| \to 0 \quad as \quad t \to \infty$$

then x_e is asymptotically stable. An equilibrium point x_e that is not stable is called unstable.

Lyapunov stability of a solution to a system of nonlinear equations (at least locally) can be defined by examining the linearized equations of motion. This approach is known as Lyapunov's first (or indirect) method. Linearizing the nonlinear system (5.1) around an equilibrium point x_e, we obtain

$$\Delta \dot{x} = A\Delta x$$

where

$$A = \left[\frac{\partial f_o(x)}{\partial x}\right]_{x=x_e} = \left[\begin{array}{ccc} \frac{\partial f_1(x)}{\partial x_1} & \cdots & \frac{\partial f_1(x)}{\partial x_n} \\ \vdots & \ddots & \vdots \\ \frac{\partial f_n(x)}{\partial x_1} & \cdots & \frac{\partial f_n(x)}{\partial x_n} \end{array}\right]_{x=x_e}$$

which is also called the Jacobian matrix at x_e. We say x_e is hyperbolic if A has no eigenvalues (λ) with zero real part. Matrix A is called a stability matrix or a Hurwitz matrix if all eigenvalues of A satisfy $Re\lambda_i < 0$.

Theorem 5.1. *Let x_e be an equilibrium point for the nonlinear system* (5.1). *Then,*

1. *x_e is asymptotically stable if A is a Hurwitz matrix.*
2. *x_e is exponentially stable if and only if A is a Hurwitz matrix.*
3. *x_e is unstable if $Re\lambda_i > 0$ for one or more of the eigenvalues of A.*

The proof can be found in [13].

An asymptotically or exponentially stable equilibrium point is henceforth denoted by x_s. A few topological concepts of R^n are reviewed in the following. The stability region of x_s (denoted by $S(x_s)$) is a region in the state space from which all trajectories converge to x_s. More precisely,

$$S(x_s) = \{x : \lim_{t\to\infty} \phi(t, x_o) = x_s\}$$

A subset $S \subset R^n$ is said to be open, if for every vector $x \in S$, one can find an ϵ–neighborhood of x

$$N(x, \epsilon) = \{z \in R^n : \|z - x\| < \epsilon\}$$

such that $N(x, \epsilon) \in S$. A set S is bounded if there is $r > 0$ such that $\|x\| \leq r$ for all $x \in S$. A point p is a boundary point of a set S if

every neighborhood of p contains at least one point of S and one point not belonging to S. Boundary of the stability region $S(x_s)$ is called the stability boundary of x_s, denoted by $\partial S(x_s)$. A closed set contains all its boundary points. A set S is compact if it is closed and bounded. An open set S is connected if every pair of points in S can be joined by an arc lying in S. A set S is said to be positively invariant set if

$$x(0) \in S \Rightarrow x(t) \in S, \forall\, t \geq 0 \tag{5.2}$$

Let $\mathcal{E}$ denote the set of equilibrium points of nonlinear system (5.1). Let also x_e be a hyperbolic equilibrium point of (5.1). The stable manifolds ($W_s(x_e)$) and the unstable manifolds ($W_u(x_e)$) of x_e are expressed by

$$\begin{aligned} W_s(x_e) &= \{x : \phi(t, x_o) \to x_e \quad \text{as} \quad t \to \infty\} \\ W_u(x_e) &= \{x : \phi(t, x_o) \to x_e \quad \text{as} \quad t \to -\infty\} \end{aligned}$$

We say two manifolds satisfy the transversality conditions if either [22]

- at every point of their intersection, their tangent spaces span R^n at the intersection point, or
- they do not intersect at all.

Consider again the nonlinear system (5.1). Assume that this system satisfies the following assumptions:

- All equilibrium points on the stability boundary are hyperbolic.
- The stable and the unstable manifolds of equilibrium points on the stability boundary satisfy the transversality conditions.
- Every trajectory on the stability boundary approaches one of the equilibrium points on the stability boundary as $t \to \infty$.

Characterization of the stability boundary is given by the following theorem.

Theorem 5.2. *Let x_{e_i} $(i = 1, 2, \dots)$ be the unstable equilibrium points of (5.1) on $\partial S(x_s)$. The stability boundary $\partial S(x_s)$ is then contained in the set which is the union of the stable manifolds of the unstable equilibrium points on the stability boundary $\partial S(x_s)$. More precisely,*

$$\partial S(x_s) = \bigcup_{x_{e_i} \in \mathcal{E} \bigcap \partial S(x_s)} W_s(x_{e_i})$$

The proof can be found in [22].

An algorithm to determine the stability boundary would involve the following steps:

1. Find all equilibrium points, i.e. solve $f_o(x) = 0$.
2. Identify those unstable equilibrium points whose unstable manifolds contain trajectories approaching the stable equilibrium point x_s. These unstable equilibrium points will be on the stability boundary.
3. Find the union of the stable manifolds of the unstable equilibrium points identified in step 2. This step would in practice involve numerical integration.

Example 5.1:

Consider the following nonlinear system

$$\begin{aligned} \dot{x}_1 &= -8x_1 + 2x_1x_2^2 \\ \dot{x}_2 &= -18x_2 + 2x_2x_1^2 \end{aligned} \tag{5.3}$$

Step 1 gives the following equilibrium points.

$$\begin{aligned} x_{e_1} &= (-3,-2) \quad , \quad x_{e_2} = (3,2) \\ x_{e_3} &= (-3,2) \quad , \quad x_{e_4} = (3,-2) \end{aligned}$$

and

$$x_{e_5} = (0,0)$$

Linearization of (5.3) gives

$$A = \left[\begin{array}{cc} -8 + 2x_2^2 & 4x_1x_2 \\ 4x_1x_2 & -18 + 2x_1^2 \end{array} \right]_{x=x_e}$$

Applying Theorem 5.1, we find that $x_{e_5} = (0,0)$ is the only asymptotically stable point, i.e. $x_s = x_{e_5}$. Step 2 and step 3 give Figure 5.1 which shows the stability region and the stability boundary of x_s.

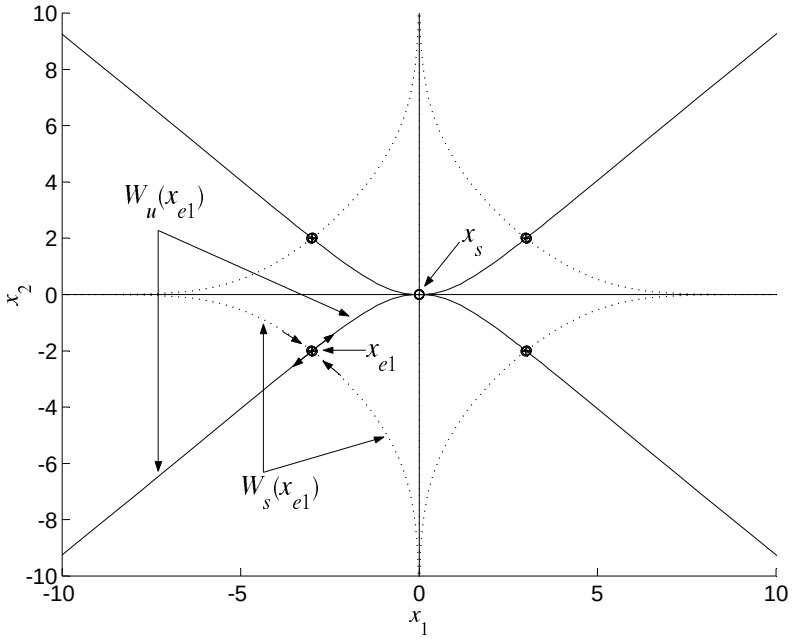

Figure 5.1. Stability boundary (dotted lines) and stability region of x_s.

5.2 Lyapunov Function

In this section we present a qualitative approach to stability analysis (valid for both linear and nonlinear systems) known as Lyapunov's second (or direct) method. The objective of this method is to answer questions of stability of differential equations, utilizing the given form of the equations but without explicit knowledge of the solutions.

The principal idea of Lyapunov's second method is closely related to the energy of a system. If the rate of change $dE(x)/dt$ of the energy $E(x)$ of an isolated physical system is negative for every possible state x, except for a single equilibrium state x_e, the energy will then continually decrease until it finally assumes its minimum value $E(x_e)$. In other words, a dissipative system perturbed from its equilibrium point will always return to it; this is the intuitive concept of stability [23]. Thus, by examining the time derivative of E along the trajectories of the system, it is possible to determine the stability of the equilibrium point. In 1892, Lyapunov

showed that certain other functions could be used instead of energy to determine stability of an equilibrium point.

Consider again the system (5.1). We present the analysis in terms of the zero equilibrium point, i.e. $x_e = 0$. The stability of any other equilibrium point can be obtained by simply translating the coordinate system so that the equilibrium of interest is at the origin in the new coordinates. Let $\mathcal{V} : \mathcal{D} \to R$ be a continuously differentiable function defined in a domain $\mathcal{D} \subset R^n$ that contains the origin. The time derivative of $\mathcal{V}$ along the trajectories of (5.1) (denoted by $\dot{\mathcal{V}}$) is given by

$$\begin{aligned}
\dot{\mathcal{V}} &= \sum_{i=1}^{n} \frac{\partial \mathcal{V}}{\partial x_i} f_i(x) \\
&= \left[\frac{\partial \mathcal{V}}{\partial x_1}, \frac{\partial \mathcal{V}}{\partial x_2}, \cdots, \frac{\partial \mathcal{V}}{\partial x_n} \right] \cdot \begin{bmatrix} f_1(x) \\ f_2(x) \\ \vdots \\ f_n(x) \end{bmatrix} = \frac{\partial \mathcal{V}}{\partial x} \cdot f_o(x) \\
&= grad(\mathcal{V}(x)) \cdot f_o(x)
\end{aligned}$$

The time derivative of $\mathcal{V}$ along the trajectories of a system is dependent on the system's equation. Hence, $\dot{\mathcal{V}}$ will be different for different systems.

Theorem 5.3. *Let $x = 0$ be an equilibrium point for (5.1) and $\mathcal{D} \subset R^n$ be a domain containing $x = 0$. Let $\mathcal{V} : \mathcal{D} \to R$ be a continuously differentiable function, such that*

$$\mathcal{V}(0) = 0 \quad and \quad \mathcal{V}(x) > 0 \quad in \quad \mathcal{D} - \{0\} \tag{5.4}$$

$$\dot{\mathcal{V}}(x) = grad(\mathcal{V}(x)) \cdot f_o(x) \leq 0 \quad in \quad \mathcal{D} \tag{5.5}$$

Then, the origin is stable. Moreover, if

$$\dot{\mathcal{V}}(x) = grad(\mathcal{V}(x)) \cdot f_o(x) < 0 \quad in \quad \mathcal{D} - \{0\} \tag{5.6}$$

the origin is asymptotically stable.

The proof can be found in [13].

A continuously differentiable function $\mathcal{V}$ satisfying (5.4) and (5.5) (or (5.6)) is called a Lyapunov function.

A function $\mathcal{V}(x)$ satisfying condition (5.4), that is, $\mathcal{V}(0) = 0$ and $\mathcal{V}(x) > 0$ for $x \neq 0$, is said to be positive definite. If it satisfies the weaker condition $\mathcal{V}(x) \geq 0$ for $x \neq 0$, it is said to be positive semidefinite. A function $\mathcal{V}(x)$ is said to be negative definite or negative semidefinite if $-\mathcal{V}(x)$ is positive definite or positive semidefinite, respectively. With this terminology, we rephrase Lyapunov's theorem to say that the origin is stable if there is a continuously differentiable positive definite function $\mathcal{V}(x)$ so that $\dot{\mathcal{V}}(x)$ is negative semidefinite, and it is asymptotically stable if $\dot{\mathcal{V}}(x)$ is negative definite.

Theorem 5.4. *Let $x = 0$ be an equilibrium point for (5.1) and $\mathcal{D} \subset R^n$ be a domain containing $x = 0$. Let $\mathcal{V} : \mathcal{D} \to R$ be a continuously differentiable function, such that $\mathcal{V}(0) = 0$ and $\mathcal{V}(x^o) > 0$ for some x^o with arbitrarily small $\|x^o\|$. Choose $r > 0$, such that the ball $B_r = \{x \in R^n : \|x\| \leq r\}$ is contained in $\mathcal{D}$, and let*

$$U = \{x \in B_r : \mathcal{V}(x) > 0\}$$

Suppose that $\dot{\mathcal{V}}(x) > 0$ in U. Then, the origin is unstable.

The proof can be found in [13].

Example 5.2:

Consider the scalar system

$$\dot{x} = ax^3 \tag{5.7}$$

Linearization of the system about the origin $x = 0$ yields

$$A = 3ax^2|_{x=0} = 0$$

Thus, A is not Hurwitz. Applying Theorem 5.1, the origin is therefore not exponentially stable. However, Theorem 5.1 fails to determine stability of the origin. This failure is genuine in the sense that the origin could be asymptotically stable, stable or unstable depending on the value of the parameter a. Stability of the origin can be however determined by applying Theorems 5.3 and 5.4. Choosing the positive definite function $\mathcal{V}(x) = x^4$, its time derivative along the trajectories of system (5.7) is given by

$$\dot{\mathcal{V}}(x) = 4ax^6$$

If $a < 0$, the origin is asymptotically stable since $\dot{\mathcal{V}}(x) < 0$. If $a = 0$, the origin is stable since $\dot{\mathcal{V}}(x) = 0$. Finally, if $a > 0$, the origin is then unstable since $\dot{\mathcal{V}}(x) > 0$.

As was mentioned, Lyapunov functions for a given system are not unique. Furthermore, while the conditions in Lyapunov's stability theorem are sufficient conditions, they are not constructive conditions; they do not tell us how to find a Lyapunov function for a particular system. There are however theorems which establish (at least conceptually) that the given conditions in Theorem 5.3 are also necessary for stability. Such theorems are usually called converse Lyapunov theorems. These theorems do not give direct help in the practical search for a Lyapunov function. However, the theorems are useful in using Lyapunov theory to draw conceptual conclusions about the behavior of dynamical systems. They have also been a basis for the introduction of Control Lyapunov Function for systems with control input. In this Section, one of these converse theorems is given. For a comprehensive treatment of converse Lyapunov theorems, see [14]–[15] and [23].

Theorem 5.5. *Let $x = 0$ be an asymptotically stable equilibrium point for system* (5.1) *and $\mathcal{D} \subset R^n$ be a domain containing $x = 0$. Let also $\mathcal{D}_o \subset \mathcal{D}$, containing $x = 0$. Then, there is a continuously differentiable positive definite function $\mathcal{V} : \mathcal{D}_o \to R$ whose time derivative is negative definite.*

Quite often, it is not sufficient to determine that a given system has an asymptotically stable equilibrium point. Rather, it is important to find the stability region of that point, or at least an estimate of it. Theorem 5.2 may give the stability region of an asymptotically stable equilibrium point. However, application of this theorem may be difficult (if not impossible) to large and complex systems. Lyapunov's second method can be used to find the stability region $S(x_s)$ or an estimate of it. By an estimate of $S(x_s)$, we mean a set $\Omega \subset S(x)$, such that every trajectory starting in Ω approaches the origin as $t \to \infty$.

Consider again the nonlinear system (5.3) in Example 5.1. The stability region and the stability boundary of this system were shown in Figure 5.1 by applying Theorem 5.2. Now, an estimate of the stability region is defined by using Lyapunov function. The simplest estimate is provided by the set

$$\Omega_c = \{x \in R^n : \mathcal{V}(x) < c\}$$

Consider the positive definite function $\mathcal{V} = x_1^2 + x_2^2$ whose time derivative along the trajectories of the system is given by

$$\dot{\mathcal{V}} = -4(4x_1^2 + 9x_2^2 - 2x_1^2x_2^2)$$

Since our interest is in estimating the stability region, we need to determine a domain $\mathcal{D}$ about the origin where $\dot{\mathcal{V}}$ is negative definite and a set $\Omega_c \subset \mathcal{D}$, which is bounded. We can find c by minimizing $\mathcal{V}$ subject to $\dot{\mathcal{V}} = 0$. Doing this, we easily find $c = 12.5$. Thus, $\mathcal{V} < 12.5$ is the estimate of the stability region as shown in Figure 5.2.

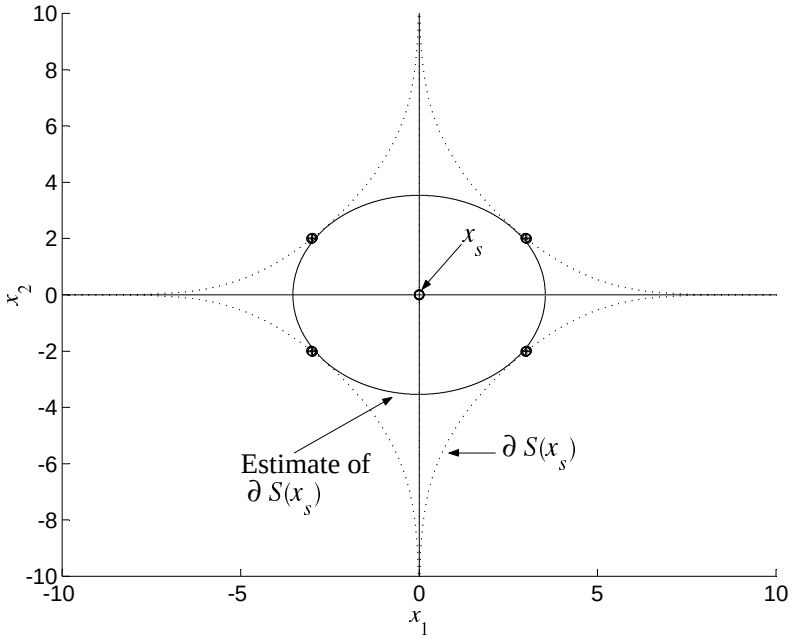

Figure 5.2. Estimate of the stability region of x_s.

For mechanical and electrical systems, the physical energy (or energy–like) functions are often used as Lyapunov function candidates. The time derivatives of these energy functions are however negative semidefinite. Therefore, these functions fail to satisfy condition (5.6) for Lyapunov function.

Example 5.3:

Consider the One–Machine Infinite Bus (OMIB) system shown in Figure 5.3 in which x_L includes line reactance ($x_{line} = 0.5$ $(p.u)$), transformer reactance ($x_t = 0.15$ $(p.u)$) and generator transient reactance ($x'_d = 0.2$ $(p.u)$).

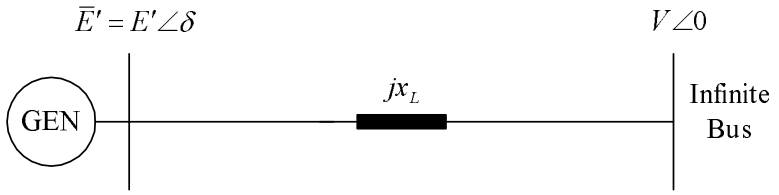

Figure 5.3. The OMIB system.

The dynamics of this system are given by

$$\begin{aligned} \dot{\delta} &= \omega \\ \dot{\omega} &= \frac{1}{M}[P_m - P_{max}\sin(\delta) - D\omega] \end{aligned} \tag{5.8}$$

where

$$\begin{aligned} M =& \frac{2H}{\omega_o} = \frac{8}{100\pi},\ D = \frac{60}{\omega_o},\ P_m = 1.1\ (p.u),\ P_{max} = bE'V \\ b =& \frac{1}{x_L} = \frac{1}{0.85},\ E' = 1.075\ (p.u),\ V = 1\ (p.u) \end{aligned} \tag{5.9}$$

The equilibrium points of this system are given by

$$\begin{aligned} (\delta_{e_1}, \omega_{e_1}) &= (\pi - \arcsin(P_m/P_{max}), 0) \\ (\delta_{e_2}, \omega_{e_2}) &= (-\pi - \arcsin(P_m/P_{max}), 0) \\ (\delta_{e_3}, \omega_{e_3}) &= (\arcsin(P_m/P_{max}), 0) \end{aligned} \tag{5.10}$$

Applying Theorem 5.1, it can be found that $(\delta_{e_1}, \omega_{e_1})$ and $(\delta_{e_2}, \omega_{e_2})$ are unstable, but $(\delta_{e_3}, \omega_{e_3})$ is an asymptotically (and also exponentially) stable point. Let $x = [\delta \quad \omega]^T$ and $x_s = [\delta^s \quad 0]^T = [\delta_{e_3} \quad 0]^T$. The stability of $(\delta^s, 0)$ (or x_s) is studied by applying Theorem 5.3. For system (5.8), the following energy function (which is positive definite in a certain domain surrounding $(\delta^s, 0)$) exists.

$$\mathcal{V} = 0.5M\omega^2 - P_m\delta - P_{max}\cos(\delta) + C_o \tag{5.11}$$

where C_o is a constant, such that $\mathcal{V} = 0$ at $(\delta^s, 0)$. The time derivative of (5.11) along the trajectories of (5.8) is given by

$$\begin{aligned}\dot{\mathcal{V}} &= grad(\mathcal{V}) \cdot f_o(x) \\ &= [-P_m + P_{max}\sin(\delta) \quad M\omega] \cdot \begin{bmatrix} \omega \\ \frac{P_m - P_{max}\sin(\delta) - D\omega}{M} \end{bmatrix} \\ &= -D\omega^2 \leq 0\end{aligned} \tag{5.12}$$

which is negative semidefinite. It is not negative definite because $\dot{\mathcal{V}} = 0$ for $\omega = 0$ irrespective of the value of δ. Therefore, we can only conclude that $(\delta^s, 0)$ is stable, since $\dot{\mathcal{V}}$ fails to satisfy condition (5.6) for Lyapunov function. However, we found based on Theorem 5.1 that $(\delta^s, 0)$ is asymptotically stable. Furthermore, Figure 5.4 shows that $(\delta^s, 0)$ is asymptotically stable.

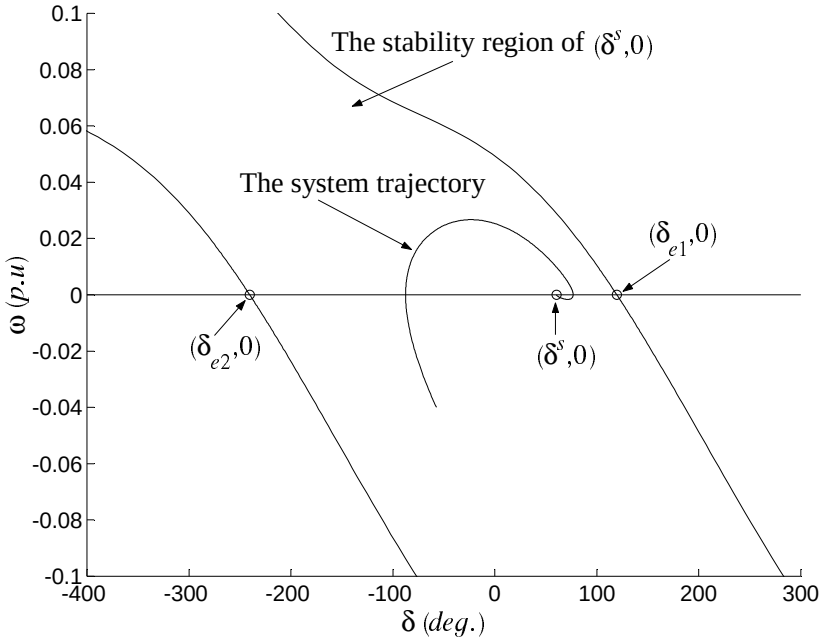

Figure 5.4. Phase portrait of the OMIB system.

Note, however, that $\dot{\mathcal{V}}$ is negative everywhere except on the line $\omega = 0$, where $\dot{\mathcal{V}} = 0$. For the system to maintain the $\dot{\mathcal{V}} = 0$ condition, the

trajectory of the system must be confined to the line $\omega = 0$. Unless $\delta = \delta^s$, this is impossible because from (5.8)

$$\omega = 0 \Rightarrow \dot{\omega} = 0 \Rightarrow P_m - P_{max}\sin(\delta) = 0$$

Hence, on the segment $\delta_{e_2} < \delta < \delta_{e_1}$ of the $\omega = 0$ line, the system can maintain the $\dot{\mathcal{V}} = 0$ only at the $(\delta^s, 0)$. Therefore, $\mathcal{V}$ must decrease towards 0, and consequently $(\delta, \omega) \to (\delta^s, 0)$ as $t \to \infty$.

The above argument follows La Salle's invariance principle and the theorem of Barbashin and Krasovskii. We first state La Salle's theorem.

Theorem 5.6. *Let $\Omega \subset \mathcal{D}$ be a compact set that is positively invariant with respect to* (5.1). *Let $\mathcal{V} : \mathcal{D} \to R$ be a continuously differentiable function, such that $\dot{\mathcal{V}} \leq 0$ in Ω. Let $\mathcal{Z}$ be the set of all points in Ω where $\dot{\mathcal{V}} = 0$. Let $\mathcal{M}$ be the largest invariant set in $\mathcal{Z}$. Then, every solution starting in Ω approaches $\mathcal{M}$ as $t \to \infty$.*

A positively invariant set is defined by (5.2). It is clear that under the assumptions of Theorem 5.6 the maximal invariant set $\mathcal{M}$ is not empty, it indeed contains at least the equilibrium point $x = 0$. Thus, one will be able to conclude that the given equilibrium point is asymptotically stable, whenever $\mathcal{M}$ reduces to the equilibrium point. This is done by showing that no solution can stay identically in $\mathcal{Z}$, other than the trivial solution $x(t) = 0$. We are now ready to state the theorem of Barbashin and Krasovskii.

Theorem 5.7. *Let $x = 0$ be an equilibrium point for* (5.1). *Let also $\mathcal{V} : \mathcal{D} \to R$ be a continuously differentiable positive definite function on a domain $\mathcal{D}$ containing the origin $x = 0$, such that $\dot{\mathcal{V}} \leq 0$ in $\mathcal{D}$. Let $S = \{x \in \mathcal{D} : \dot{\mathcal{V}} = 0\}$ and suppose that no solution can stay identically in S, other than the trivial solution. Then, the origin is asymptotically stable.*

The proofs of the above theorems can be found in [13].

Unlike Theorem 5.7, Theorem 5.6 does not require the function $\mathcal{V}(x)$ to be positive definite. Furthermore, this theorem gives an estimate of the stability region which is not necessarily of the form $\Omega_c = \{x \in R^n : \mathcal{V}(x) \leq c\}$ by which we estimated the stability region of system (5.3), see Figure 5.2. The set Ω of Theorem 5.6 can be any compact positively

invariant set which may give less conservative estimates of the stability region.

Note, however, that these two theorems cannot be considered as an extension of Lyapunov's theorem. If the origin is asymptotically stable, there must then exist a "true" Lyapunov function by virtue of Theorem 5.5. However, since it is (in general) difficult to find a "true" Lyapunov function, these theorems are therefore useful for testing stability.

5.3 Total Stability

Consider the system

$$\dot{x} = F(x) \tag{5.13}$$

which describes an actual real system. This system has the same properties as system (5.1). Since it is difficult to find a Lyapunov function for the actual system (5.13), we (based on the reasonable conditions) simplify this system, such that a Lyapunov function can be found. The dynamics of the simplified system are then given by

$$\dot{x} = f_o(x) \tag{5.14}$$

System (5.14) is henceforth called the nominal system.

With simple manipulation, the actual system (5.13) can be rewritten as

$$\begin{aligned} \dot{x} = F(x) =& f_o(x) + [F(x) - f_o(x)] \\ =& f_o(x) + p(x) \end{aligned} \tag{5.15}$$

where $p(x) = [F(x) - f_o(x)]$. We think of this system as a perturbation of the nominal system (5.14), see also (3.11).

Suppose the nominal system (5.14) has an asymptotically stable equilibrium point at the origin. The question arises, what we can say about the stability behavior of the perturbed system (5.15). Lyapunov stability accounts for the robustness of an equilibrium point with respect to perturbations of the initial state. However, a concept of stability was introduced (usually referred to as total stability) expressing the robustness of the nominal system with respect to perturbations acting on the right–hand side of the nominal system.

Let the origin be an equilibrium point for the nominal system (5.14). Let also $\mathcal{X}(t)$ denote the solution of the perturbed system. We say that the origin is totally stable, if for every positive number ϵ (however small), there are two positive numbers $\eta_1(\epsilon)$ and $\eta_2(\epsilon)$, such that

$$\|\mathcal{X}(t)\| < \epsilon \qquad \text{for} \qquad t > 0$$

provided that

$$\|\mathcal{X}(0)\| < \eta_1(\epsilon)$$

,and that in the domain $\|x\| < \epsilon$ and $t > 0$, the inequality

$$\|p(x)\| < \eta_2(\epsilon)$$

is satisfied.

Note that in the definition of the total stability, it is not required that $p(x)$ should be zero at the origin, i.e. $p(0) \neq 0$. The only requirement on function $p(x)$ is that this function is bounded in modulus for sufficiently small values of x, i.e. $p(x)$ remains small for all $t > 0$.

Theorem 5.8. *If the origin of the nominal system* (5.14) *is asymptotically stable, it is also totally stable.*

Applying the converse Lyapunov theorem (i.e. Theorem 5.5), we can state the following theorem.

Theorem 5.9. *If there exists a Lyapunov function for the nominal system* (5.14)*, the origin is totally stable.*

The proofs of the above theorems can be found in [14].

The requirement that function $p(x)$ be small for all $t > 0$ is not realistic. It is more realistic to require that $p(x)$ may assume large values in certain small intervals of time while being small most of the time. A function $p(x)$ with this property is called bounded in the mean. It can be shown that Theorem 5.9 is also valid for $p(x)$ that is bounded in the mean [15].

5.4 Application of Lyapunov Function to Power Systems

As noted in Section 5.2, for mechanical and electrical systems, the physical energy (or energy–like) functions are often used as Lyapunov function candidates. The time derivatives of these energy functions are however negative semidefinite. Therefore, these functions fail to satisfy condition (5.6) for Lyapunov function. However, applying La Salle's invariance principle and/or the theorem of Barbashin and Krasovskii (i.e. Theorems 5.6 and 5.7), the energy functions satisfy the asymptotic stability condition and they can be considered as Lyapunov function candidates.

In the following, energy functions for both Reduced Network Model and Structure Preserving Model are presented. For a detailed analysis of energy functions in power systems, see [11] and references therein.

5.4.1 Energy Function for Reduced Network Model

Application of energy functions to power systems began in the former Soviet Union in the 1930's, and in the western world in 1947 with Magnusson [24]. All early work on energy function methods was based on the Reduced Network Model (RNM) of power systems, i.e. system (3.11) for which Lyapunov theory was already established. However, by assuming constant impedance load models, the RNM excludes the use of general nonlinear and dynamic loads, that is, network structure is lost in this model. Furthermore, to find a rigorous energy function, $p(x)$ must be zero in (3.11), that is, transfer conductances must be ignored. However, the concept of total stability may give an analytical justification of this approximation, i.e setting $p(x)$ to zero.

Now, consider system (3.11). Setting $p(x) = 0$, the dynamics of the system are described by

$$\begin{aligned} \dot{\tilde{\delta}}_k &= \tilde{\omega}_k \\ \dot{\tilde{\omega}}_k &= \frac{1}{M_k}[P_k - \sum_{\substack{l=1 \\ l \neq k}}^{n} \mathcal{C}_{kl} \sin(\delta_{kl}) + \frac{M_k}{M_T} P_{COI} - D_k \tilde{\omega}_k] \end{aligned} \tag{5.16}$$

The following energy function is given for system (5.16)

$$\mathcal{V}(\tilde{\delta},\tilde{\omega}) = \frac{1}{2}\sum_{k=1}^{n} M_k\tilde{\omega}_k^2 - \sum_{k=1}^{n} P_k\tilde{\delta}_k - \sum_{k=1}^{n-1}\sum_{l=k+1}^{n} \mathcal{C}_{kl}\cos(\delta_{kl}) + C_o \qquad (5.17)$$

where C_o is a constant, such that at the stable equilibrium point $(\delta^s, 0)$, the energy function is zero. Thus,

$$C_o = \sum_{k=1}^{n} P_k\tilde{\delta}_k^s + \sum_{k=1}^{n-1}\sum_{l=k+1}^{n} \mathcal{C}_{kl}\cos(\delta_{kl}^s)$$

It can be shown that the energy function (5.17) is positive definite in a certain region surrounding $(\delta^s, 0)$.

The time derivative of the energy function along the trajectories of system (5.16) is given by

$$\begin{aligned}
\dot{\mathcal{V}} &= grad(\mathcal{V})\cdot f_o(x) \\
&= \sum_{k=1}^{n}\left[M_k\dot{\tilde{\omega}}_k - P_k + \sum_{\substack{l=1\\ l\neq k}}^{n}\mathcal{C}_{kl}\sin(\delta_{kl})\right]\tilde{\omega}_k \\
&= \sum_{k=1}^{n}\left[\frac{M_k}{M_T}P_{COI} - D_k\tilde{\omega}_k\right]\tilde{\omega}_k \\
&= -\sum_{k=1}^{n} D_k\tilde{\omega}_k^2
\end{aligned} \qquad (5.18)$$

since,

$$\sum_{k=1}^{n}\frac{P_{COI}}{M_T}M_k\tilde{\omega}_k = \frac{P_{COI}}{M_T}\sum_{k=1}^{n} M_k\tilde{\omega}_k = 0$$

by virtue of (3.8).

Also, by virtue of Theorem 5.7, the energy function (5.17) satisfies the asymptotic stability condition and it can be considered as a Lyapunov function candidate.

5.4.2 Energy Function for Structure Preserving Model

As noted in Section 3.2, Structure Preserving Model (SPM) has been proposed to overcome some of the shortcomings of the RNM and to improve

the modeling of generators and load representations. In general, SPM is mathematically described by a set of Differential–Algebraic Equations (DAE) of the form:

$$\begin{aligned} \dot{x} &= f(x, y) \\ 0 &= g(x, y) \end{aligned} \tag{5.19}$$

Here, the differential equations describe the dynamics of the generators (see (3.12)), while the algebraic equations express the power flow equations at each bus (see (3.14)). The algebraic states y are related to the dynamic states x through the algebraic equations g. Note that in (5.19), each trajectory must satisfy the algebraic constraint $g(x, y) = 0$ at all time. Therefore, (5.19) can be interpreted as a dynamical system on the algebraic manifold $L = \{(x, y) : g(x, y) = 0\}$. Generally, there exist certain points within L where the trajectories may run into conflicts in satisfying constraint $g(x, y) = 0$. These points are called the singular or the impasse points of the network.

Given a point on L, say $(x_o, y_o) \in L$. If the Jacobian $G_y = \frac{\partial g}{\partial y}$ is non-singular (i.e. $det(G_y) \neq 0$ at (x_o, y_o)), by virtue of the Implicit Function Theorem, there exists a unique solution, $y = h(x)$, of the network equations which satisfies $g(x, h(x)) = 0$ locally near (x_o, y_o). Therefore locally near (x_o, y_o), the dynamics of (5.19) exists as a well defined smooth system described by

$$\dot{x} = f(x, h(x)) = F(x) \tag{5.20}$$

which is indeed an ODE system.

Note that once the trajectory intersects the singular surface

$$S = \{(x, y) \in L : det(G_y) = 0\}$$

a DAE cannot be reduced to an ODE. This is usually referred to as a singularity induced bifurcation [25].

To obtain an energy function for system (5.20), it might be necessary to simplify this system. For example, differential–algebraic equations (3.12) and (3.14) are based on that the power system is lossless, the real load is constant and the generators are modeled by the one–axis model excluding

AVR and turbine regulator. Let $f_o(x)$ describe the simplified system. Then, (5.20) can be rewritten as

$$\begin{aligned}\dot{x} =& f(x, h(x)) = F(x) \\ =& f_o(x) + (F(x) - f_o(x)) \\ =& f_o(x) + p(x)\end{aligned} \tag{5.21}$$

Note that for both RNM and SPM modeling of the power systems, $F(x)$ has been used to denote the actual system and $f_o(x)$ to denote the simplified system, see (3.11) and (5.21), in order to facilitate the application of the theorems in Section 5.3. However, it does not mean that $F(x)$ and $f_o(x)$ are identical in (3.11) and (5.21).

It is also possible to infer dynamical behavior of a DAE via a singular perturbation approach. This approach treats the algebraic equations as a limit of fast dynamics $\epsilon\dot{y} = g(x, y)$. In other words, as ϵ approaches zero, the fast dynamics will approach the algebraic manifold. Therefore for DAE system (5.19), an associated singularly perturbed system can be defined by

$$\begin{aligned}\dot{x} &= f(x, y) \\ \epsilon\dot{y} &= g(x, y)\end{aligned} \tag{5.22}$$

where ϵ is a sufficiently small positive number. If f and g are both smooth functions and bounded for all (x, y), the vector field is then globally well defined.

Although the DAE system (5.19) and the corresponding singularly perturbed system (5.22) have some different dynamic models, they still share several similar dynamical properties. For instance, they have the same equilibrium points, but the trajectories of the singularly perturbed system (5.22) are not exactly the same as the trajectories of the original DAE system (5.19). However, Tikhonov's theorem over the infinite time interval can be applied to provide a theoretical justification to ensure that the difference of solution trajectories between the original DAE system (5.19) and the singularly perturbed system (5.22) is uniformly bounded by the order of $O(\epsilon)$ [13]. Thus, trajectories generated by the singular perturbed system are still valid approximations to that of the DAE system. Application of the singular perturbation approach to the power systems can be found in [26]–[28].

Based on the theorems in [29] and [30], the following energy function is given for equations (3.12) and (3.14), or indeed for system (5.21) with $p(x) = 0$.

$$\mathcal{V}(\tilde{\omega}, \tilde{\delta}, E'_q, V, \tilde{\theta}) = \mathcal{V}_1 + \sum_{k=1}^{8} \mathcal{V}_{2k} + C_o \tag{5.23}$$

where

$$\begin{aligned}
\mathcal{V}_1 &= \frac{1}{2}\sum_{k=1}^{n} M_k \tilde{\omega}_k^2 \\
\mathcal{V}_{21} &= -\sum_{k=1}^{n} P_{mk}\tilde{\delta}_k \\
\mathcal{V}_{22} &= \sum_{k=n+1}^{n+N} P_{Lk}\tilde{\theta}_k \\
\mathcal{V}_{23} &= \sum_{k=n+1}^{n+N} \int \frac{Q_{Lk}}{V_k}\, dV_k \\
\mathcal{V}_{24} &= \sum_{k=n+1}^{2n} \frac{1}{2x'_{dk-n}}[E'^2_{qk-n} + V_k^2 - 2E'_{qk-n}V_k\cos(\delta_{k-n} - \theta_k)] \\
\mathcal{V}_{25} &= -\frac{1}{2}\sum_{k=n+1}^{n+N}\sum_{l=n+1}^{n+N} B_{kl}V_kV_l\cos(\theta_k - \theta_l) \\
\mathcal{V}_{26} &= \sum_{k=n+1}^{2n} \frac{x'_{dk-n} - x_{qk-n}}{4x'_{dk-n}x_{qk-n}}[V_k^2 - V_k^2\cos(2(\delta_{k-n} - \theta_k))] \\
\mathcal{V}_{27} &= -\sum_{k=1}^{n} \frac{E_{fdk}E'_{qk}}{x_{dk} - x'_{dk}} \\
\mathcal{V}_{28} &= \sum_{k=1}^{n} \frac{E'^2_{qk}}{2(x_{dk} - x'_{dk})}
\end{aligned}$$

$\mathcal{V}_1$ is known as the kinetic energy and $\mathcal{V}_{2k}$ as the potential energy. C_o is a constant, such that at the stable equilibrium point, the energy function is zero.

Using the notation

$$[\frac{d\mathcal{V}}{dt}]_{\tilde{\omega}} \quad \text{for} \quad \frac{\partial \mathcal{V}}{\partial \tilde{\omega}} \frac{d\tilde{\omega}}{dt}$$

and similarly for the other states, we have

$$\begin{aligned}[\frac{d\mathcal{V}_1}{dt}]_{\tilde{\omega}} + [\frac{d\mathcal{V}_{21}}{dt} + \frac{d\mathcal{V}_{24}}{dt} + \frac{d\mathcal{V}_{26}}{dt}]_{\tilde{\delta}} \\ = -\sum_{k=1}^{n} D_k(\tilde{\omega}_k)^2\end{aligned} \tag{5.24}$$

$$\begin{aligned}[\frac{d\mathcal{V}_{22}}{dt} + \frac{d\mathcal{V}_{24}}{dt} + \frac{d\mathcal{V}_{25}}{dt} + \frac{d\mathcal{V}_{26}}{dt}]_{\tilde{\theta}} \\ = \sum (P_k + P_{Lk})\dot{\tilde{\theta}}_k = 0\end{aligned} \tag{5.25}$$

$$\begin{aligned}[\frac{d\mathcal{V}_{23}}{dt} + \frac{d\mathcal{V}_{24}}{dt} + \frac{d\mathcal{V}_{25}}{dt} + \frac{d\mathcal{V}_{26}}{dt}]_{V} \\ = \sum (Q_k + Q_{Lk})\frac{\dot{V}_k}{V_k} = 0\end{aligned} \tag{5.26}$$

$$\begin{aligned}[\frac{d\mathcal{V}_{27}}{dt} + \frac{d\mathcal{V}_{28}}{dt} + \frac{d\mathcal{V}_{24}}{dt}]_{E'_q} \\ = -\sum_{k=1}^{n} \frac{T'_{dok}}{x_{dk} - x'_{dk}} (\dot{E}'_{qk})^2\end{aligned} \tag{5.27}$$

Thus, the time derivative of the energy function is

$$\frac{d\mathcal{V}}{dt} = -\sum_{k=1}^{n} D_k(\tilde{\omega}_k)^2 - \sum_{k=1}^{n} \frac{T'_{dok}}{x_{dk} - x'_{dk}} (\dot{E}'_{qk})^2 \leq 0 \tag{5.28}$$

5.5 Summary

The existence of a Lyapunov function is necessary and sufficient for the stability of a system. For mechanical and electrical systems, the physical energy (or energy–like) functions are often used as Lyapunov function candidates. The time derivatives of these energy functions are however negative semidefinite. Therefore, these functions fail to satisfy condition (5.6) for Lyapunov function. However, Theorem 5.7 and/or Theorem 5.6 justifies the use of the energy functions as Lyapunov function candidates.

Since it is difficult to find a Lyapunov function for an actual real system, it is reasonable to simplify the actual system, such that a Lyapunov function can be found. Then, based on the concepts of the total stability, it can be shown that the stability of the simplified system also implies the stability of the actual system, see Theorem 5.8 and Theorem 5.9.

Chapter 6

Control Lyapunov Function

Lyapunov theory deals with dynamical systems without input. For this reason, it has traditionally been applied only to closed–loop control systems, that is, systems for which the input has been eliminated through the substitution of a predetermined feedback control. However, some authors, [31]–[33], started using Lyapunov function candidates in feedback design itself by making the Lyapunov derivative negative when choosing the control. Such ideas have been made precise with the introduction of the concept of a Control Lyapunov Function for systems with control input [34].

6.1 General Framework

Consider the following autonomous system depending on a parameter $u \in R^m$

$$\dot{x} = f(x, u) \quad , \quad x \in \Omega \tag{6.1}$$

where Ω is an open connected region of R^n. System (6.1) is referred to as a control system in which u is the control input and x is the state variables.

Let the origin be an equilibrium point for (6.1) and $0 \in \Omega$. The stabilizability problem can then be stated in the following way. We want to find

conditions for the existence of a feedback control $u = u(x)$ defined in a neighborhood of the origin such that the closed–loop system

$$\dot{x} = f(x, u(x)) = \tilde{f}(x)$$

has a stable equilibrium point at the origin. If such a function $u(x)$ exists, we say that (6.1) is stabilizable at the origin and the function $u(x)$ is called a stabilizing feedback law or (simply) a stabilizer. Throughout this work, we are mainly interested in achieving asymptotic stability of the closed–loop system.

Consider system (6.1) and assume that this system is continuously stabilizable. According to the converse Lyapunov theorem (i.e. Theorem 5.5), there must be a positive definite function $\mathcal{V}(x)$, such that

$$\dot{\mathcal{V}}(x) = grad(\mathcal{V}(x)) \cdot f(x, u) < 0 \tag{6.2}$$

for each $x \neq 0$ in some neighborhood $\mathcal{D}$ of the origin.

A function $\mathcal{V}(x)$ satisfying (5.4) and (6.2) is called a Control Lyapunov Function (CLF). Henceforth, we study a special form of (6.1) which is called affine systems, that is, systems of the form

$$\dot{x} = f(x, u) = f_o(x) + \sum_{i=1}^{m} u_i f_i(x) \tag{6.3}$$

where $x \in \Omega \subset R^n$, $u \in R^m$ and $f_o(x)$ is the system without control input. We assume that $f_o,\ f_1,\ \ldots,\ f_m$ are C^∞, (C^r denotes r–time differentiable). We also assume that for some $\bar{u} = (\bar{u}_1,\ \ldots,\ \bar{u}_m) \in R^m$ the equality

$$\dot{x} = f_o(0) + \sum_{i=1}^{m} \bar{u}_i f_i(0) = 0 \tag{6.4}$$

holds. Indeed, for each stabilizing feedback $u(x)$, the value $\bar{u} = u(0)$ must satisfy (6.4). We are now ready to state the following theorem which was obtained first by Artstein [31].

Theorem 6.1. *Let $u = (u_1,\ \ldots,\ u_m) \in R^m$. Let also $\bar{u}$ be a solution of (6.4). There exists a continuous feedback law $u(x)$ which makes (6.3) asymptotically stable if and only if there exists a function $\mathcal{V}(x)$ which*

satisfies condition (5.4)*, and also for every* $\epsilon > 0$*, a* $\delta > 0$ *exists such that whenever* $\|x\| < \delta$*, the inequality*

$$grad(\mathcal{V}(x)) \cdot [f_o(x) + u_1 f_1(x) + \cdots + u_m f_m(x)] < 0$$

holds for $\|u - \bar{u}\| < \epsilon$*.*

Since Artstein's proof is not constructive, a question arises whether it is possible to write an explicit formula for a stabilizing feedback under the assumptions of Theorem 6.1.

Now, consider system (6.3) with $R^m = R$, that is,

$$\dot{x} = f_o(x) + u f_1(x) \tag{6.5}$$

Moreover, we assume $f_o(0) = 0$, so that we can also take $u(0) = 0$. Note that if (6.5) has a stabilizing control law $u(x)$ such that $u(0) = \bar{u}$, then the system

$$\dot{x} = [f_o(x) + \bar{u} f_1(x)] + v f_1(x)$$

can be stabilized setting $v(x) = u(x) - \bar{u}$, where $v(0) = 0$. This could suggest that we can limit ourselves to consider affine systems whose drift term vanishes at the origin, as well as any admissible feedback law.

Let $\mathcal{V}(x)$ be a positive definite function and let

$$a(x) = grad(\mathcal{V}(x)) \cdot f_o(x)$$
$$b(x) = grad(\mathcal{V}(x)) \cdot f_1(x)$$

Now consider the expression

$$u(x) = -\frac{a(x) + \psi(x)}{b(x)} \tag{6.6}$$

where $\psi(x)$ is a positive real function. Obviously, the feedback law (6.6) makes (6.5) asymptotically stable since $\dot{\mathcal{V}} = -\psi(x) < 0$. Thus, $\mathcal{V}(x)$ is a CLF for (6.5). However, a question arises how (6.6) should be defined when $b(x) = 0$.

Sontag proved that defining $u(x) = 0$ when $b(x) = 0$ and taking

$$\psi(x) = \sqrt{a^2(x) + b^4(x)}$$

then (6.6) is a stabilizer [32].

Example 6.1:

Consider the following system

$$\begin{aligned} \dot{x}_1 &= -\, x_2 \\ \dot{x}_2 &= x_1 + u x_2 \end{aligned} \tag{6.7}$$

which can be written in the form (6.5) with

$$f_o(x) = \begin{bmatrix} -x_2 \\ x_1 \end{bmatrix} \quad , \quad f_1(x) = \begin{bmatrix} 0 \\ x_2 \end{bmatrix}$$

Taking

$$\mathcal{V}(x) = \frac{x_1^2 + x_2^2}{2} \tag{6.8}$$

we have then

$$\begin{aligned} a(x) &= grad(\mathcal{V}(x)) \cdot f_o(x) = 0 \\ b(x) &= grad(\mathcal{V}(x)) \cdot f_1(x) = x_2^2 \end{aligned}$$

Thus, Sontag's formula (6.6) reduces to

$$u(x) = -x_2^2 \tag{6.9}$$

The time derivative of $\mathcal{V}(x)$ along the trajectories of the closed–loop system is given by

$$\dot{\mathcal{V}}(x) = -x_2^4$$

which does not satisfy (6.2). However, applying Theorem 5.7, it can be shown that the closed–loop system is asymptotically stable and the feedback law (6.9) is therefore a stabilizer.

Since the system (6.7) is stabilizable, by the converse Lyapunov theorem it must exist a function which satisfies the conditions (5.4) and (6.2), that is, there must exist another function than (6.8) that satisfies the conditions (5.4) and (6.2).

Taking

$$\mathcal{V}(x) = x_1^2 - x_1 x_2 + x_2^2 \tag{6.10}$$

it can be shown that this function satisfies the conditions (5.4) and (6.2). However, there is no real advantage in using the "true" Lyapunov function

(6.10) instead of (6.8). Indeed, using (6.10), the feedback law defined according to Sontag's formula is then given by

$$u(x) = -\frac{(x_2^2 - x_1^2) + \sqrt{(x_2^2 - x_1^2)^2 + x_2^4(2x_2 - x_1)^4}}{x_2(2x_2 - x_1)}$$

which is more complicated than (6.9).

Function (6.8) is indeed the energy function of system (6.7) without control input, that is, the energy function of $f_0(x)$. The treatment of such systems fits better in the framework of the Jurdjevic–Quinn approach as explained below.

We say that (6.3) satisfies a Lyapunov condition of the Jurdjevic–Quinn type if there is a C^∞ function $\mathcal{V}(x)$ which satisfies (5.4) and

$$grad(\mathcal{V}(x)) \cdot f_o(x) \leq 0 \quad \text{for} \quad x \in \mathcal{D} \tag{6.11}$$

According to the Jurdjevic–Quinn approach, a stabilizing feedback law is typically defined componentwise, setting $u(x) = [u_1(x), \ldots, u_m(x)]$ and

$$u_i(x) = -grad(\mathcal{V}(x)) \cdot f_i(x)\ , \quad i = 1, \ldots, m \tag{6.12}$$

Thus, the time derivative of $\mathcal{V}(x)$ for $x \in \mathcal{D}$ with respect to the closed-loop system is given by

$$\begin{aligned} \dot{\mathcal{V}}(x) &= grad(\mathcal{V}(x)) \cdot f_o(x) + \sum_{i=1}^{m} u_i\, grad(\mathcal{V}(x)) \cdot f_i(x) \\ &\leq \sum_{i=1}^{m} u_i\, grad(\mathcal{V}(x)) \cdot f_i(x) \\ &= -\sum_{i=1}^{m} (grad(\mathcal{V}(x)) \cdot f_i(x))^2 < 0 \end{aligned} \tag{6.13}$$

by virtue of (6.11) and (6.12) [33].

Based on La Salle's invariance principle, the trajectories of the closed–loop system are attracted by the largest invariant set contained in

$$\begin{aligned} \mathcal{Z} &= \{x \in \mathcal{D} : \dot{\mathcal{V}}(x) = 0\} \\ &= \{x \in \mathcal{D} : grad(\mathcal{V}(x)) \cdot f_i(x) = 0\ ,\ i = 0, \ldots, m\} \end{aligned}$$

Hence, to prove that (6.12) provides a stabilizing feedback, we need some technical assumptions excluding the existence of nontrivial sets in $\mathcal{Z}$. Thus, the following theorem is stated (compare to Theorem 5.7).

Theorem 6.2. *Consider the affine system* (6.3) *with* C^∞ *vector fields and* $f_o(0) = 0$. *Assume that there exists a Lyapunov function* $\mathcal{V}(x)$ *of the Jurdjevic–Quinn type. Then, the functions* (6.12) *define a smooth stabilizing feedback law if and only if there exists a positive real number* c_o, *such that for each* $c \in [0 \cdots c_o]$, *no trajectory of the vector field* f_o *is contained in the set*

$$\mathcal{L}_c = \{x \in \mathcal{D} : \mathcal{V}(x) = c \quad \text{and} \quad grad(\mathcal{V}(x)) \cdot f_i(x) = 0\ ,\ i = 1, \ldots, m\}$$

The proof can be found in [18].

Note that the feedback law provided by Sontag's formula does not coincide in general with (6.12), apart from the special case where

$$grad(\mathcal{V}(x)) \cdot f_o(x) = 0$$

In general, it is natural to expect that the feedback law (6.12) is "simpler" than the one defined by (6.6).

Example 6.2:

Consider the OMIB system with a CSD as shown in Figure 6.1. A three-phase fault occurs at point F. The fault is cleared after 100 ms by opening of the faulted line. The post–fault system data is as given by (5.9) in Example 5.3, but $D = 2/\omega_o$. The post–fault stable equilibrium point (s.e.p) is given by $(\delta_{e_3}, 0)$ in (5.10).

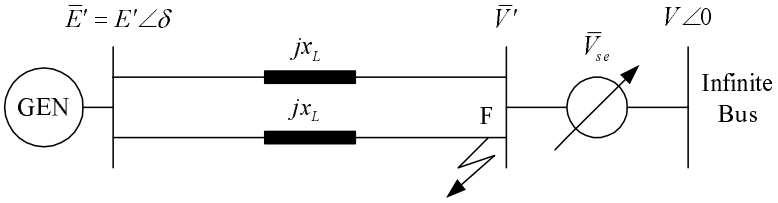

Figure 6.1. The OMIB system with a CSD.

Neglecting x_s (see Section 4.2), we have for UPFC

$$\bar{V}_{se} = rVe^{j\gamma} = V(r\cos(\gamma) + jr\sin(\gamma)) = V(u_{up1} + ju_{up2})$$

and for QBT

$$\bar{V}_{se} = rVe^{j\gamma} = V(r\cos(\gamma) + jr\sin(\gamma)) = jVu_q$$

since $\gamma = \pm\pi/2$, see Section 4.2.

Let $\bar{V}' = \bar{V}_{se} + V$. The post–fault electric power is then given by

$$P_e = real(jb\bar{E}'(\bar{E}' - \bar{V}')^*)$$

Thus, the post–fault electric power of the OMIB system in which a UPFC is installed, is given by

$$P_e = P_{max}\sin(\delta) + u_{up1}P_{max}\sin(\delta) - u_{up2}P_{max}\cos(\delta) \tag{6.14}$$

Having a QBT in the system, then

$$P_e = P_{max}\sin(\delta) - u_q P_{max}\cos(\delta) \tag{6.15}$$

Finally, having a CSC in the system, the post–fault electric power is given by

$$P_e = real\left[\bar{E}'\left(\frac{\bar{E}' - V}{j(x_L - x_c)}\right)^*\right] = P_{max}\sin(\delta) + u_c P_{max}\sin(\delta) \tag{6.16}$$

where u_c is given by (4.8).

Let $x = [\delta \quad \omega]^T$ and $x_s = [\delta^s \quad 0]^T = [\delta_{e_3} \quad 0]^T$. The post–fault dynamics of the system with CSD are then described by the affine system of the form (6.3), that is,

$$\dot{x} = f(x,u) = f_o(x) + \sum_{i=1}^{m} u_i f_i(x)$$

where $f_o(x)$ is given by the right–hand side of (5.8). Note that $f_o(x_s) = 0$, so that we can take also $u(x_s) = 0$.

Having a UPFC in the system, the post–fault dynamics of the system are given by

$$\dot{x} = f_o(x) + u_{up1}f_{up1}(x) + u_{up2}f_{up2}(x) \tag{6.17}$$

For QBT,

$$\dot{x} = f_o(x) + u_q f_{qbt}(x) \tag{6.18}$$

and for CSC,

$$\dot{x} = f_o(x) + u_c f_{csc}(x) \tag{6.19}$$

where

$$\begin{aligned} f_{up1}(x) &= f_{csc}(x) = [\ 0 \quad -c_1\sin(\delta)\ ]^T \\ f_{up2}(x) &= f_{qbt}(x) = [\ 0 \quad c_1\cos(\delta)\ ]^T \end{aligned}$$

and $c_1 = \frac{P_{max}}{M}$.

Using the energy function (5.11) of the uncontrolled system (5.8) as a Lyapunov function candidate for the control systems (6.17)–(6.19), we have then for

UPFC:

$$\begin{aligned}\dot{\mathcal{V}} &= grad(\mathcal{V}) \cdot [f_o(x) + u_{up1} f_{up1}(x) + u_{up2} f_{up2}(x)] \\ &\leq u_{up1}\ grad(\mathcal{V}) \cdot f_{up1}(x) + u_{up2}\ grad(\mathcal{V}) \cdot f_{up2}(x) \\ &= P_{max}[-u_{up1} \sin(\delta)\ \omega + u_{up2} \cos(\delta)\ \omega]\end{aligned} \tag{6.20}$$

QBT:

$$\begin{aligned}\dot{\mathcal{V}} &= grad(\mathcal{V}) \cdot [f_o(x) + u_q f_{qbt}(x)] \\ &\leq u_q\ grad(\mathcal{V}) \cdot f_{qbt}(x) \\ &= P_{max} u_q \cos(\delta)\ \omega\end{aligned} \tag{6.21}$$

CSC:

$$\begin{aligned}\dot{\mathcal{V}} &= grad(\mathcal{V}) \cdot [f_o(x) + u_c f_{csc}(x)] \\ &\leq u_c\ grad(\mathcal{V}) \cdot f_{csc}(x) \\ &= -P_{max} u_c \sin(\delta)\ \omega\end{aligned} \tag{6.22}$$

since $grad(\mathcal{V}) \cdot f_o(x) \leq 0$, see (5.12). By virtue of the Jurdjevic–Quinn approach, the following stabilizing control laws are given

UPFC:

$$\begin{aligned}u_{up1} &= k_1 \sin(\delta)\ \omega \\ u_{up2} &= -k_2 \cos(\delta)\ \omega\end{aligned} \tag{6.23}$$

QBT:

$$u_q = -k_3 \cos(\delta)\ \omega \tag{6.24}$$

CSC:

$$u_c = k_4 \sin(\delta)\ \omega \tag{6.25}$$

since $P_{max} > 0$. k_1–k_4 are positive gains which are chosen individually to obtain appropriate damping.

Thus, with the control laws (6.23)–(6.25), the energy function (5.11) becomes a CLF for the control systems (6.17)–(6.19).

Note that u_c and x_c have the same sign, since x_c is (normally) less than x_L, see (4.8). Thus, u_c can be replaced by x_c in (6.25), that is,

$$x_c = k_5 \sin(\delta)\, \omega \tag{6.26}$$

The CSDs have the following data (r_{max} and x_{cmax} in $(p.u)$)

- **UPFC:** $r_{max} = 0.10, \quad 0 \le r \le r_{max}$, $k_1 = 0.2$ and $k_2 = 0.25$.
- **QBT:** $r_{max} = 0.26, \quad 0 \le r \le r_{max}$ and $k_3 = 1$.
- **CSC:** $x_{cmax} = 0.125, \ 0 \le x_c \le x_{cmax}$ and $k_5 = 0.4$.

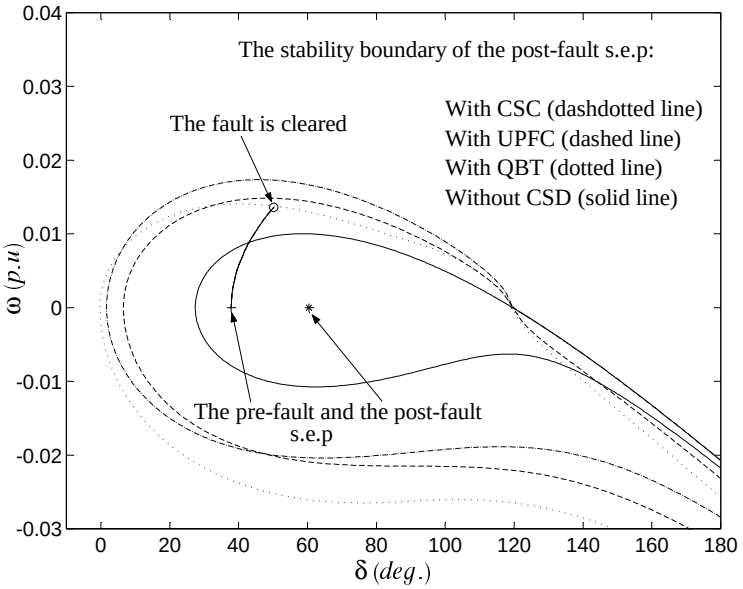

Figure 6.2. Phase portrait of the OMIB system during the fault.

Figure 6.2 shows the stability boundary of the post–fault s.e.p for the OMIB system without CSD and with CSD. The CSDs are controlled by the control laws (6.23), (6.24) and (6.26). Figure 6.2 shows that the stability region of the post–fault s.e.p is significantly enlarged by the CLF controlled CSDs. Without a CSD, the system trajectory lies outside the

corresponding stability region at fault clearing. Therefore, the system is unstable for the proposed fault, see Figure 6.3. However, the CSDs ensure that the post–fault system trajectory lies within the corresponding enlarged stability region. The control system is therefore stable for the proposed fault, see Figure 6.3.

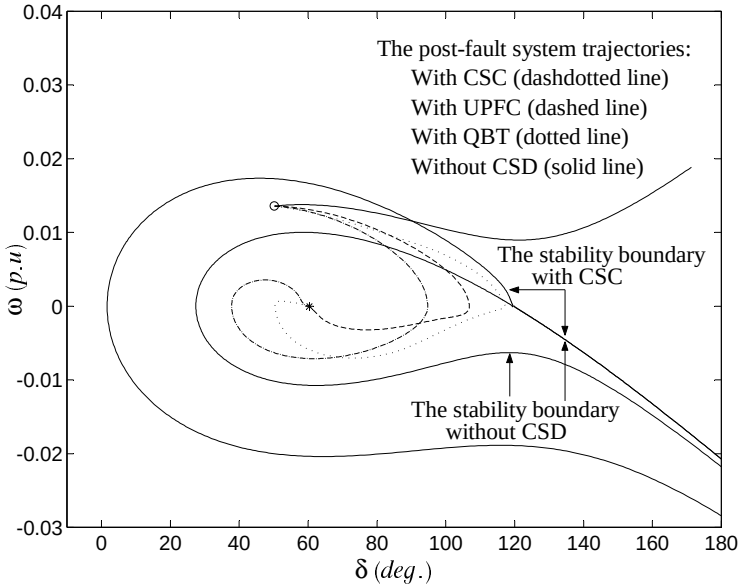

Figure 6.3. Phase portrait of the OMIB system after the fault.

Example 6.3:

Consider now the test system shown in Figure 6.4. The terminal buses have been eliminated in Figure 6.4, and the transient reactances have been incorporated into the transmission line reactances. The dynamics of this system are given by

$$\begin{aligned}
\dot{\delta}_1 &= \omega_1 \\
\dot{\delta}_2 &= \omega_2 \\
\dot{\omega}_1 &= \frac{1}{M_1}[P_{m1} - \mathcal{C}_{12}\sin(\delta_{12}) - \mathcal{C}_{13}\sin(\delta_1) - D_1\omega_1] \\
\dot{\omega}_2 &= \frac{1}{M_2}[P_{m2} - \mathcal{C}_{12}\sin(\delta_{21}) - \mathcal{C}_{23}\sin(\delta_2) - D_2\omega_2]
\end{aligned} \tag{6.27}$$

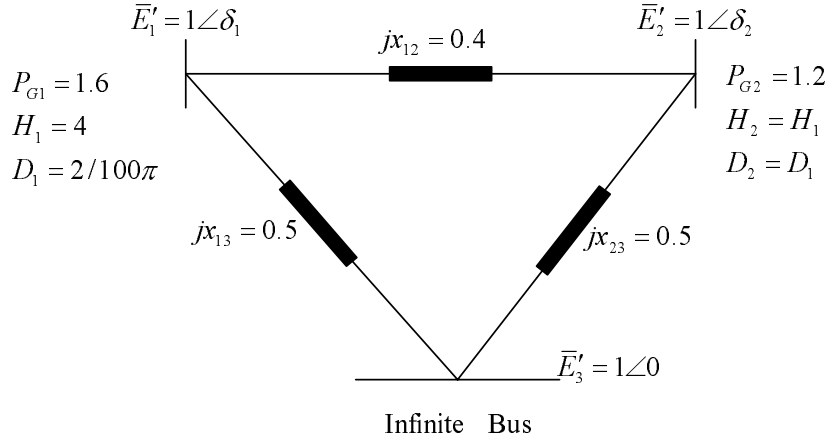

Figure 6.4. The 2–machine infinite bus test system

or

$$\dot{x} = f_o(x)$$

where $\mathcal{C}_{12} = E_1' E_2'/x_{12}$, $\mathcal{C}_{13} = E_1' E_3'/x_{13}$ and $\mathcal{C}_{23} = E_2' E_3'/x_{23}$.

It should be noted that (6.27) is similar to (5.16) with $P_k = P_{mk}$. Since bus 3 is assumed to be an infinite bus, we have $M_3 \to \infty$. Therefore, $M_T \to \infty$, $\delta_{COI} \to 0$ in (3.7) and $\frac{M_k}{M_T} P_{COI} = 0$ in (5.16). Thus, the energy function (5.17) (in which $\tilde{\delta}$ and $\tilde{\omega}$ are replaced by δ and ω, respectively) is also an energy function for the system (6.27), that is,

$$\mathcal{V}(\delta, \omega) = \frac{1}{2} \sum_{k=1}^{2} M_k \omega_k^2 - \sum_{k=1}^{2} P_{mk} \delta_k - \sum_{k=1}^{2} \sum_{l=k+1}^{3} \mathcal{C}_{kl} \cos(\delta_{kl}) + C_o \quad (6.28)$$

The gradient of the energy function is given by

$$grad(\mathcal{V}) = \begin{bmatrix} -P_{m1} + \mathcal{C}_{12} \sin(\delta_{12}) + \mathcal{C}_{13} \sin(\delta_1) \\ -P_{m2} + \mathcal{C}_{12} \sin(\delta_{21}) + \mathcal{C}_{23} \sin(\delta_2) \\ M_1 \omega_1 \\ M_2 \omega_2 \end{bmatrix}^T$$

Thus, the time derivative of (6.28) along the trajectories of (6.27) is given by (see also (5.18))

$$\dot{\mathcal{V}} = grad(\mathcal{V}) \cdot f_o(x) = -\sum_{k=1}^{2} D_k \omega_k^2 \leq 0$$

Having two CSCs in the lines between bus 1 and bus 3, and between bus 2 and bus 3, respectively, the dynamics of the system can be described by the affine system

$$\dot{x} = f_o(x) + u_{c1} f_1(x) + u_{c2} f_2(x) \tag{6.29}$$

where

$$f_1(x) = \frac{1}{M_1} \begin{bmatrix} 0 \\ 0 \\ -\mathcal{C}_{13} \sin(\delta_1) \\ 0 \end{bmatrix} \quad , \quad f_2(x) = \frac{1}{M_2} \begin{bmatrix} 0 \\ 0 \\ 0 \\ -\mathcal{C}_{23} \sin(\delta_2) \end{bmatrix}$$

Using the energy function (6.28) as a Lyapunov function candidate for the system (6.29), we have then

$$\begin{aligned} \dot{\mathcal{V}} &= grad(\mathcal{V}) \cdot f_o(x) + u_{c1}\ grad(\mathcal{V}) \cdot f_1(x) + u_{c2}\ grad(\mathcal{V}) \cdot f_2(x) \\ &\leq u_{c1}\ grad(\mathcal{V}) \cdot f_1(x) + u_{c2}\ grad(\mathcal{V}) \cdot f_2(x) \end{aligned} \tag{6.30}$$

By virtue of the Jurdjevic–Quinn approach (and (4.8)), the following stabilizing control laws are given

$$\begin{aligned} x_{c1} &= -grad(\mathcal{V}) \cdot f_1(x) = k_1 \sin(\delta_1)\ \omega_1 \\ x_{c2} &= -grad(\mathcal{V}) \cdot f_2(x) = k_2 \sin(\delta_2)\ \omega_2 \end{aligned} \tag{6.31}$$

which make (6.28) as a CLF for the system (6.29).

An important issue with this example is to show that several CLF controlled devices do not adversely affect each other. The reason is that each device (independent of the other devices) contributes to make $\dot{\mathcal{V}}(x)$ negative. With several CLF controlled devices in the system, the negativeness of $\dot{\mathcal{V}}(x)$ indeed becomes larger, that is, the slope of $\mathcal{V}(x)$ becomes

sharper which implies that the energy decreases faster to its minimum value, i.e., $\mathcal{V}(x_s) = 0$. Consequently, the system trajectories tend faster to its post–fault stable equilibrium point, that is, we have better damping in the system. The above argument is illustrated in Figure 6.5 and Figure 6.6. These figures show the variation of the rotor angles and the energy function after the fault. The uncontrolled system (solid line) is stable for the proposed fault, but it is not well damped. Using one CLF controlled CSC in the system (dotted line), the system is then better damped for the proposed fault. However, with two CLF controlled CSCs (dashed line), the system is much better damped.

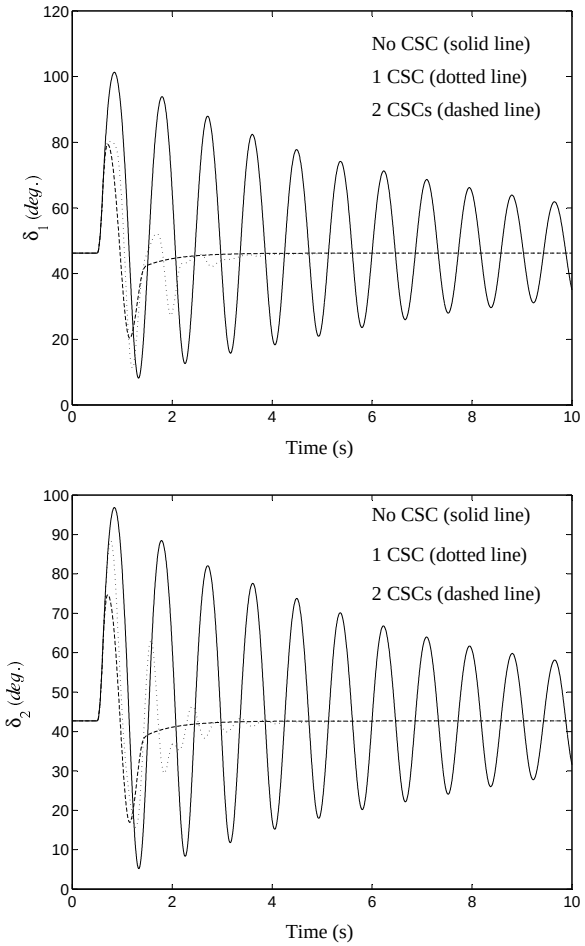

Figure 6.5. Variation of the rotor angles.

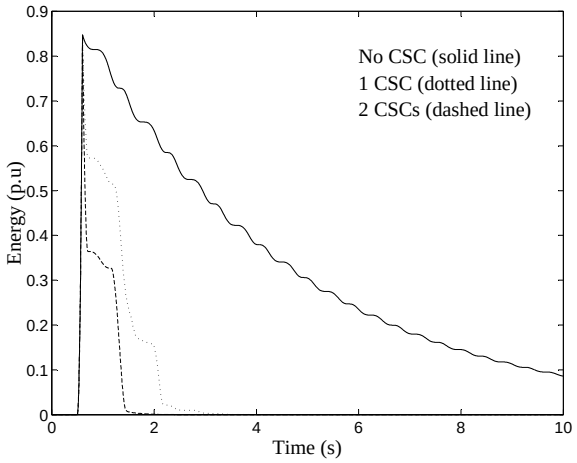

Figure 6.6. Variation of the energy function.

To summarize this section, just as the existence of a Lyapunov function is necessary and sufficient for the stability of a system without input, the existence of a CLF is necessary and sufficient for the stabilizability of a system with a control input.

6.2 Application of CLF to the Structure Preserving Model

Consider the differential–algebraic system given by (3.12) and (3.14). Let it be called the uncontrolled system. For this uncontrolled system, the energy function (5.23) is proposed. The time derivative of this energy function along the trajectories of the uncontrolled system is given by (5.28) which is not positive. Let it be denoted by $\dot{\mathcal{V}}_{NOCSD}$, that is,

$$\dot{\mathcal{V}}_{NOCSD} = -\sum_{k=1}^{n} D_k(\tilde{\omega}_k)^2 - \sum_{k=1}^{n} \frac{T'_{dok}}{x_{dk} - x'_{dk}}(\dot{E}'_{qk})^2 \leq 0$$

Assume that a CSD is located between buses **i** and **j** in the transmission system, see Figure 4.9. Let the energy function (5.23) be a Lyapunov function candidate for the system with CSD, i.e. the control system.

The introduction of the CSD does not alter the energy function (5.23), since it is an energy function for the uncontrolled system. However, the introduction of the CSD does alter $\dot{\mathcal{V}}(x)$; in particular the terms (5.25) and (5.26) no longer sum to zero. To see this, consider the i-th term of the (5.25), that is,

$$(P_i + P_{Li})\,\dot{\tilde{\theta}}_i$$

Without a CSD connected to bus **i**, we have $P_i + P_{Li} = 0$, resulting in the zero summation of (5.25). However, when the CSD is connected, power balance gives $P_i + P_{Li} + P_{si} = 0$. Therefore, with the CSD connected, the i-th term of (5.25) becomes

$$(P_i + P_{Li})\,\dot{\tilde{\theta}}_i = -P_{si}\,\dot{\tilde{\theta}}_i$$

A similar argument follows for the j-th term of (5.25) and the corresponding terms of (5.26), resulting in

$$\begin{aligned}[\frac{d\mathcal{V}_{22}}{dt} + \frac{d\mathcal{V}_{24}}{dt} + \frac{d\mathcal{V}_{25}}{dt} + \frac{d\mathcal{V}_{26}}{dt}]_{\tilde{\theta}} \\ = -P_{si}\dot{\tilde{\theta}}_i - P_{sj}\dot{\tilde{\theta}}_j\end{aligned} \tag{6.32}$$

$$\begin{aligned}[\frac{d\mathcal{V}_{22}}{dt} + \frac{d\mathcal{V}_{24}}{dt} + \frac{d\mathcal{V}_{25}}{dt} + \frac{d\mathcal{V}_{26}}{dt}]_{V} \\ = -Q_{si}\frac{\dot{V}_i}{V_i} - Q_{sj}\frac{\dot{V}_j}{V_j}\end{aligned} \tag{6.33}$$

Note that (5.24) and (5.27) are unaffected by the introduction of a CSD.

Therefore, the time derivative of the energy function becomes

$$\frac{d\mathcal{V}}{dt} = \dot{\mathcal{V}}_{NOCSD} + \dot{\mathcal{V}}_{CSD} \leq \dot{\mathcal{V}}_{CSD} \tag{6.34}$$

Note that all CSD models have $P_{si} = -P_{sj}$, see (4.5)–(4.7). This allows (6.34) to be written

$$\frac{d\mathcal{V}}{dt} \;\leq\; \dot{\mathcal{V}}_{CSD} = -P_{si}\dot{\theta}_{ij} - Q_{si}\frac{\dot{V}_i}{V_i} - Q_{sj}\frac{\dot{V}_j}{V_j} \tag{6.35}$$

By virtue of (4.5)–(4.7), we have for

UPFC:

$$\begin{aligned}\dot{\mathcal{V}}_{CSD} =& - b_s V_i[\ u_{up1}(\ \dot{V}_i + V_j \sin(\theta_{ij})\dot{\theta}_{ij} - \dot{V}_j \cos(\theta_{ij})\ ) \\ &+\ u_{up2}(\ V_j \cos(\theta_{ij})\dot{\theta}_{ij} + \dot{V}_j \sin(\theta_{ij})\ )\ ] \\ =& - b_s V_i[\ u_{up1}\frac{d}{dt}(V_i - V_j \cos(\theta_{ij})) + u_{up2}\frac{d}{dt}(V_j \sin(\theta_{ij}))\ ]\end{aligned} \tag{6.36}$$

QBT:

$$\begin{aligned}\dot{\mathcal{V}}_{CSD} =& - b_s[u_q\frac{d}{dt}(V_i V_j \sin(\theta_{ij})) + \frac{1}{2}u_q^2\frac{d}{dt}(V_i^2)] \\ \approx& - b_s u_q\frac{d}{dt}(V_i V_j \sin(\theta_{ij}))\end{aligned} \tag{6.37}$$

CSC:

$$\begin{aligned}\dot{\mathcal{V}}_{CSD} =& - \frac{1}{2}b_s u_c\frac{d}{dt}[V_i^2 + V_j^2 - 2V_i V_j \cos(\theta_{ij})] \\ =& - \frac{1}{2}b_s u_c\frac{d}{dt}|\overline{V}_{ij}|^2 = -\frac{1}{2}b_s u_c\frac{d}{dt}[x_L I_{csc} - V_{csc}]^2\end{aligned} \tag{6.38}$$

where in (6.38), I_{csc} is the absolute value of current through CSC and V_{csc} is the absolute value of voltage over CSC. Simulation results have shown that the influence of the second term of (6.37) is very small compared to the first term. Therefore, the second term is neglected.

The energy function (5.23) becomes a CLF for the control system if $\dot{\mathcal{V}}_{CSD}$ is negative. Therefore, the following control (feedback) laws are suggested (note that V_i and b_s are positive):

Control law for UPFC:

$$\begin{aligned}u_{up1} =& k_1\frac{d}{dt}(V_i - V_j \cos(\theta_{ij})) \\ u_{up2} =& k_2\frac{d}{dt}(V_j \sin(\theta_{ij}))\end{aligned} \tag{6.39}$$

Control law for QBT:

$$u_q = k_3\frac{d}{dt}(V_i V_j \sin(\theta_{ij})) \tag{6.40}$$

Control law for CSC:

$$u_c = k_4\frac{d}{dt}|\overline{V}_{ij}|^2 = k_4\frac{d}{dt}[x_L I_{csc} - V_{csc}]^2 \tag{6.41}$$

where k_1, k_2, k_3 and k_4 are positive gains which are chosen individually to obtain appropriate damping.

Once again, u_c can be replaced by x_c in (6.41), since u_c and x_c have the same sign, see (4.8). Thus,

$$x_c = k_5 \frac{d}{dt} |\overline{V}_{ij}|^2 = k_5 \frac{d}{dt} [x_L I_{csc} - V_{csc}]^2 \tag{6.42}$$

For a power system with CSDs, (6.35) is always valid, irrespective of the generator and load models used in the development of the various energy functions in [11]. Different models contribute with different terms to the left–hand sides of (6.32) and (6.33), but the right–hand sides remain unchanged. Thus, the control laws based on the CLF rely only on locally measurable information and are independent of system topology and modeling of power system components. Also, these control laws do not require information about the post–fault stable equilibrium point.

A similar analysis can also be found in [35]. The results in [35] are based on the statement "controllability implies stabilizability". By linearizing the control system, it has been shown in [35] that the linearized system is controllable, and therefore, the control law $u = u(x)$ is a stabilizer for the linearized system, and also for the nonlinear control system.

6.3 Summary

Lyapunov theory deals with dynamical systems without input. For this reason, it has traditionally been applied only to closed–loop control systems, that is, systems for which the input has been eliminated through the substitution of a predetermined feedback control. However, it may be difficult to find a Lyapunov function for the closed–loop control system.

The concept of the Control Lyapunov Function, however, allows us to use the Lyapunov function of the uncontrolled system (which is much easier to find) as a Lyapunov function candidate for the system with input (i.e. the control system). Then, the feedback control can be chosen by making the Lyapunov derivative negative.

Just as the existence of a Lyapunov function is necessary and sufficient for the stability of a system without input, the existence of a CLF is necessary and sufficient for the stabilizability of a system with a control input.

Chapter 7

Numerical Example

In this chapter, the control laws (6.39), (6.40) and (6.42) are applied to various test systems. The power system model used in development of these control laws had a very specific (and also restrictive) form. It was convenient for obtaining a Lyapunov function, but it only approximately described actual power system behavior. More precisely, for obtaining a Lyapunov function for the actual system

$$\dot{x} = F(x) = f_o(x) + p(x)$$

we assumed that $p(x) = 0$.

The following questions arise.

- How do these control laws, derived for $f_o(x)$, affect $p(x)$?
- In the context of CSD control, how good are these control laws when the system is lossy and more detailed models are used for generators and loads, i.e. when $p(x) \neq 0$?

Simulation results in this chapter provide a partial answer when the control laws (6.39), (6.40) and (6.42) are applied to real systems that are not subject to those modeling restrictions, i.e $p(x) \neq 0$. They indicate that these control laws are not sensitive to the model approximations. However, it is important to obtain an analytical justification of this observation. The analysis and theorems in Section 5.3 may also provide a partial answer.

All simulation are performed by using SIMPOW [36] and the results are plotted in MATLAB.

7.1 Two–Area Test System

Figure 7.1 shows a simple two–area system. The system data can be found in [37]. If not otherwise stated, the exact data from [37] is used. In [37], generators are modeled with one field winding, one damper winding in d–axis and two damper windings in q–axis. Saturation is considered. The active and reactive components of loads have constant current (i.e. $mp = 1$) and constant impedance (i.e. $mq = 2$) characteristics, respectively.

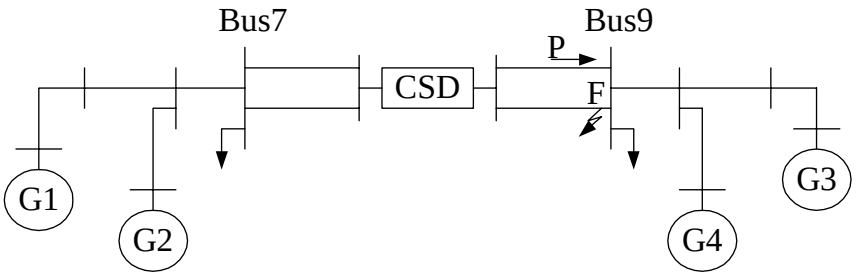

Figure 7.1. The two–area test system.

A three–phase fault occurs at point F. The fault is cleared after 100 ms by opening of the faulted line. The following system models are used in simulation.

- **System model 1:** The one–axis model is used for generators ($D = 2$ $(p.u)$) with excitation system (see Fig. E12.9 in [37]). $K_A = 300$, $T_B = 0.01$ and $T_R = T_A = 0$. No PSS.
- **System model 2:** The generators are modeled as in [37] with the same excitation system as in system model 1. Also, turbine and governor regulators are used. $D = 0$.
- **System model 3:** The same as in system model 2, but $P_{G1} = P_{G2} = 730$ (MW), i.e. $\Delta P_{G1} = \Delta P_{G2} = 30$ (MW).
- **System model 4:** The same as in system model 3, but active loads have also constant impedance characteristics.

The following figures show the variation of P $(p.u)$ vs time for those various system modeling. P is the real power through the unfaulted line between the CSD and Bus 9, see Figure 7.1. The CSDs have the following data, (r_{max} and x_{cmax} in $(p.u)$)

- **UPFC:** $r_{max} = 0.094, \quad 0 \leq r \leq r_{max}.$
- **QBT:** $r_{max} = 0.1, \quad 0 \leq r \leq r_{max}.$
- **CSC:** $x_{cmax} = 0.047, \; 0 \leq x_c \leq x_{cmax}.$

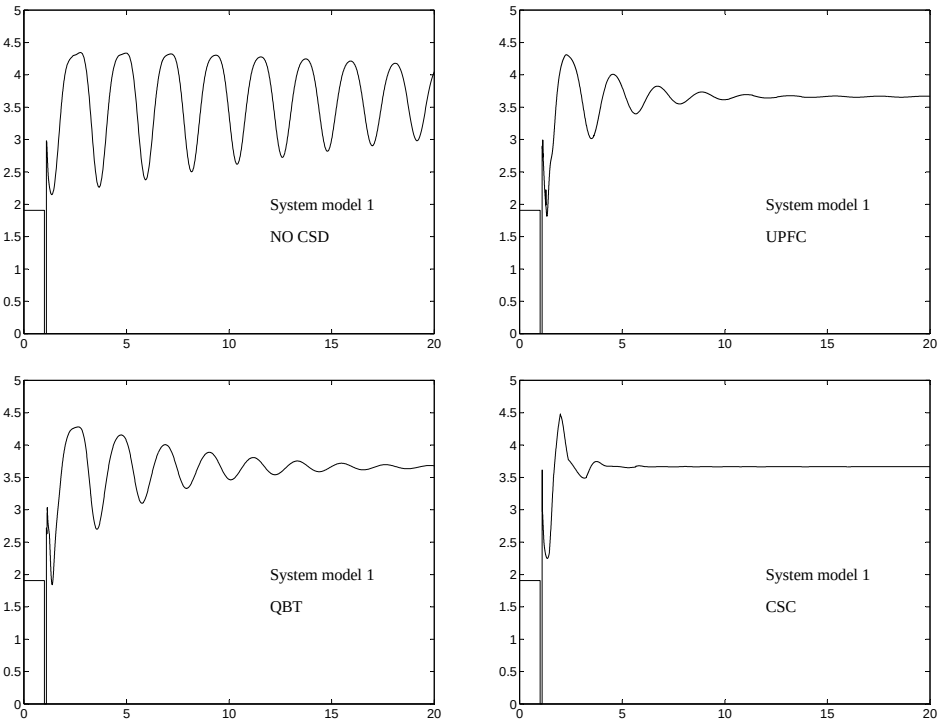

Figure 7.2. Variation of P vs time for the system model 1.

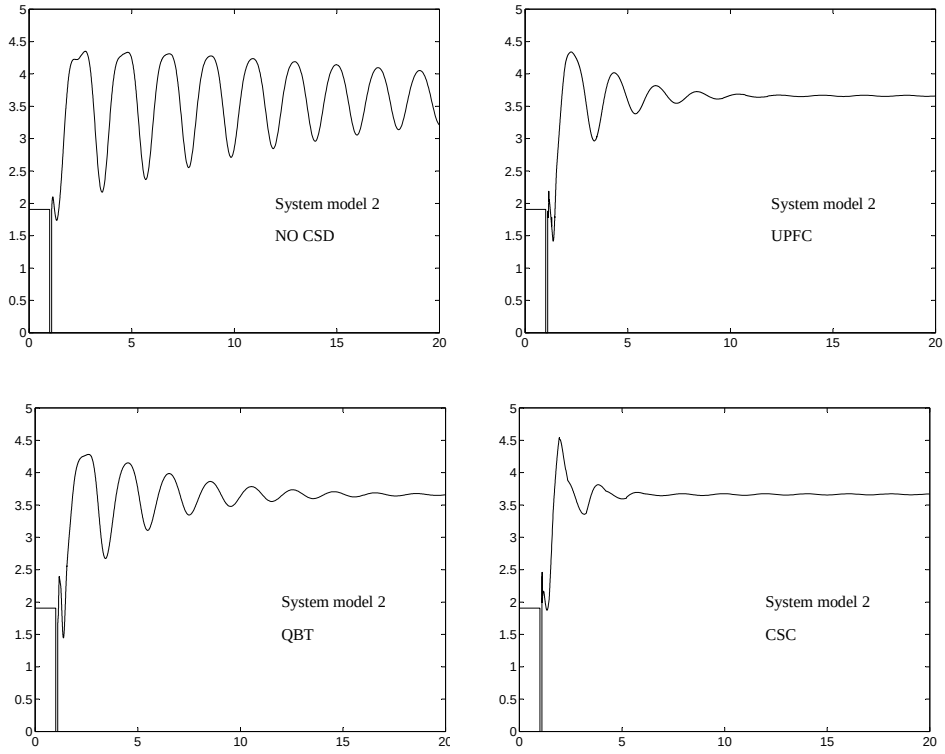

Figure 7.3. Variation of P vs time for the system model 2.

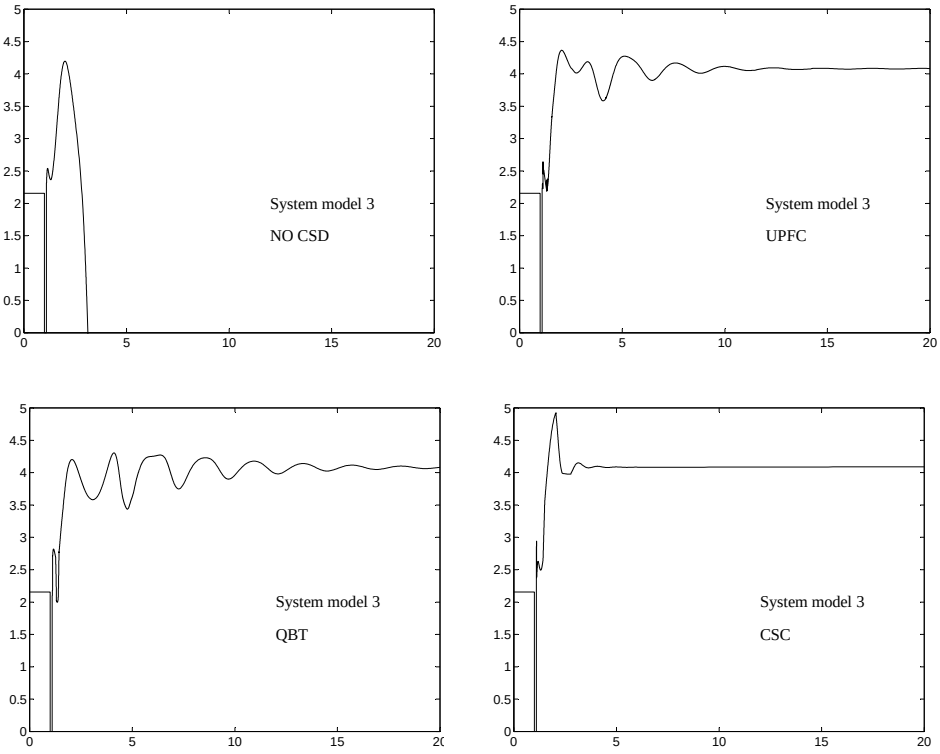

Figure 7.4. Variation of P vs time for the system model 3.

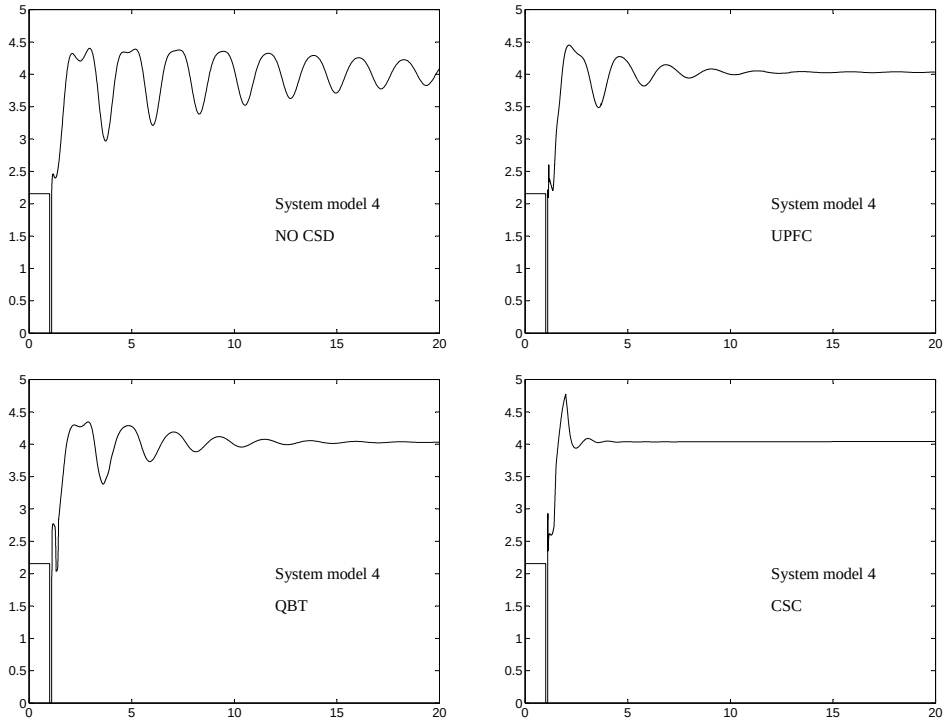

Figure 7.5. Variation of P vs time for the system model 4.

The simulation results show the ability of the control laws to stabilize and damp the proposed power system for different system models. System model 3 shows clearly that the CSDs which are controlled by the CLF, enlarge the stability region. Obviously, the size of the enlargement depends on the rating of the CSDs. For example in system model 3, having the same CSDs data, the QBT and the UPFC cannot achieve first–swing stability when $P_{G1} = P_{G2} > 740$ (MW) and for the CSC when $P_{G1} = P_{G2} > 770$ (MW). Also, system model 3 and system model 4 show that the load modeling does not significantly affect the performance of the CLF controlled CSDs.

7.2 IEEE 9-Bus Test System

Figure 7.6 shows the IEEE 9-bus test system. The system data can be found in [38]. The one–axis model is used for the generators ($D = 0$) including excitation system. PSS and turbine regulator are excluded. The active and reactive components of loads have constant current and constant impedance characteristics, respectively. In this example, it will

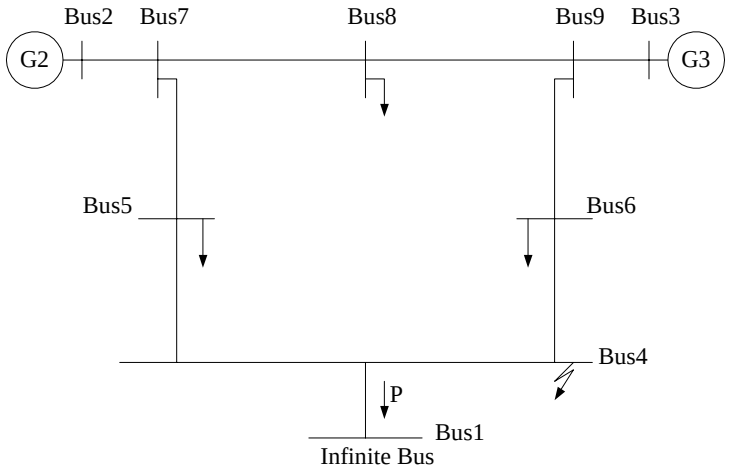

Figure 7.6. The IEEE 9–bus test system.

be shown that several CLF controlled CSDs do not adversely affect each other. Indeed, they improve damping of the electromechanical oscillations.

A three–phase fault occurs at Bus 4. The fault is cleared after 100 ms. No line is tripped. A UPFC, a QBT and a CSC are installed in the line between Bus 9 and Bus 6, respectively . Also, a CSC (say CSC1) is installed in the line between Bus 7 and Bus 5. The CSDs have the following data, (r_{max} and x_{cmax} in $(p.u)$)

- **UPFC:** $r_{max} = 0.013, \quad 0 \leq r \leq r_{max}.$
- **QBT:** $r_{max} = 0.012, \quad 0 \leq r \leq r_{max}.$
- **CSC:** $x_{cmax} = 0.04, \ 0 \leq x_c \leq x_{cmax}.$
- **CSC1:** $x_{cmax} = 0.05, \ 0 \leq x_c \leq x_{cmax}.$

Figure 7.7 shows the variation of P (MW) (identified in Figure 7.9) when there are no CSDs in the system.

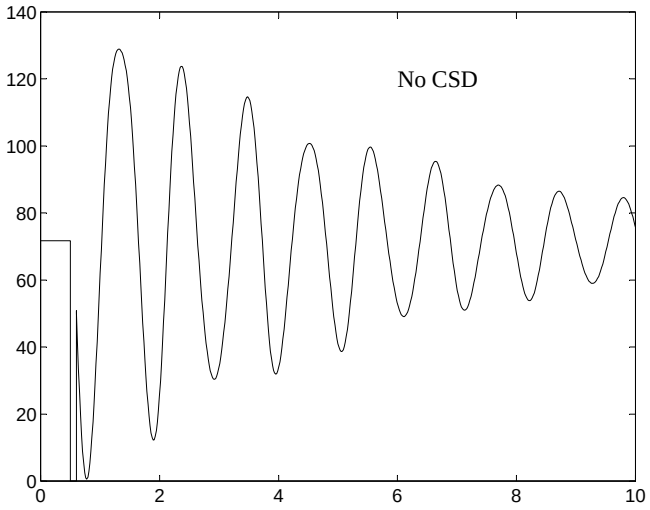

Figure 7.7. Variation of P vs time in the IEEE 9–bus test system.

The following figures show the variation of P for CLF control of a UPFC, a QBT and a CSC, respectively, with CLF controlled CSC1 and without it.

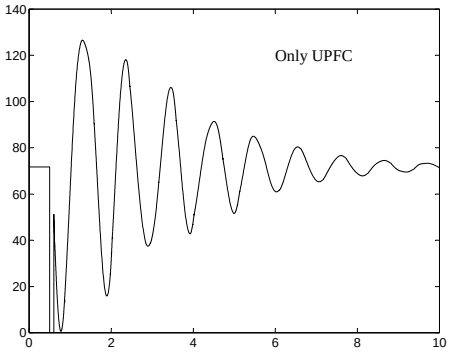

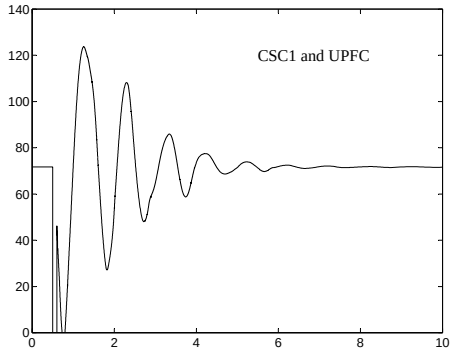

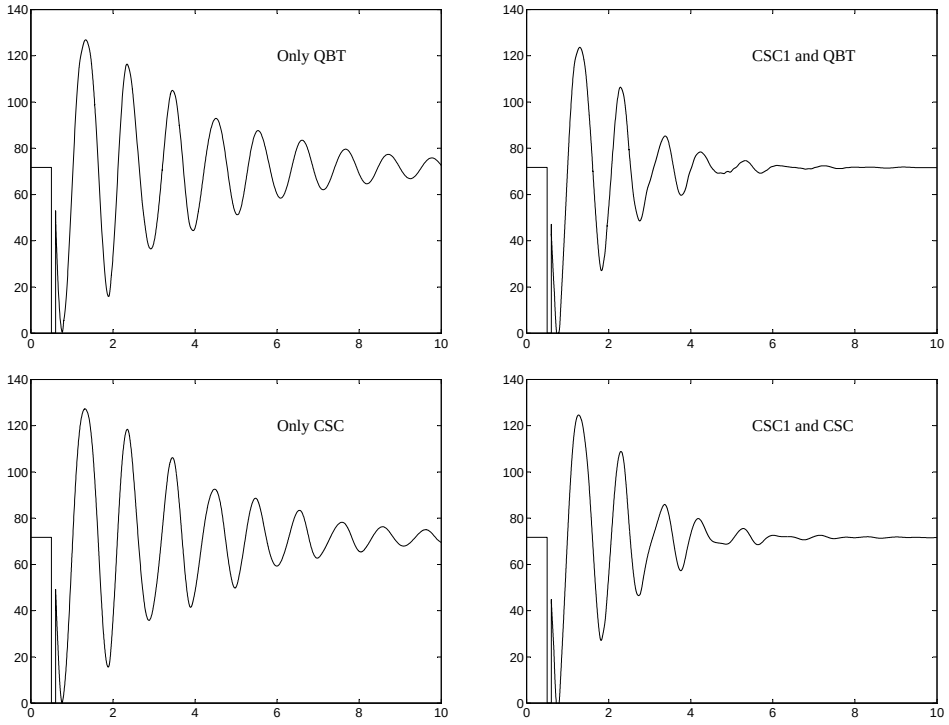

Figure 7.8. Variation of P vs time with CSDs in the IEEE 9–bus system.

7.3 Nordic32A Test System

Nordic32A (Figure 7.9) is a test system for simulation of transient stability and long term dynamics proposed by CIGRE Task Force 38.02.08 [39]. The exact data from [39] is used with the exception that no PSS is used in the system. The system contains 32 high voltage buses. The main transmission system is designed for 400 kV. There are also some regional systems at 220 kV and 130 kV. Both hydro power plants and thermal power plants with a total of 23 generators are modeled. The hydro power plants are located in the North and External regions of the system and are equipped with salient pole generators whose models include models of AVR, saturation, one field winding, one damper winding in d–axis and one damper winding in q–axis. The thermal power plants are located in the Central and South regions and each plant includes a round rotor generator whose model includes all features included in the salient pole model but

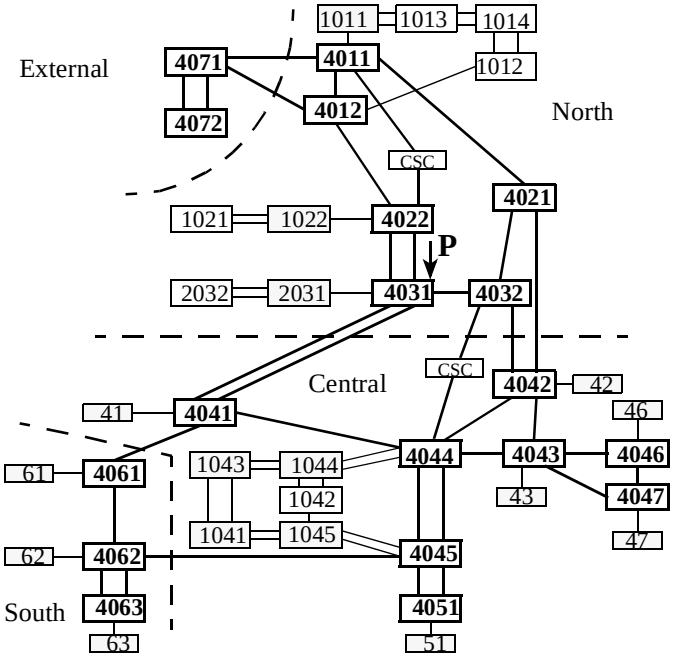

Figure 7.9. The Nordic32A test system proposed by CIGRE.

also a second damper winding in q–axis and saturation in the resulting air–gap flux. Only the hydro power units are using governors. No explicit damping is modeled in the generators, i.e. the damping constant D is zero. The active and reactive components of loads have constant current and constant impedance characteristics, respectively.

Two loading cases are considered, namely LF32–028 and LF32–029. In LF32–028, the transfers are high from North to Central. The load level is at peak load. The case is sensitive to many types of faults. In fact the transfer situation is above that recommended by normal reliability standards. LF32-029 is similar to LF32-028 but transfers from North to Central are decreased. It is made by an extra generation at bus 4051 and a decreasing of generating powers in some generators in North.

Two CSCs are used in the system. The first CSC is located in line 4011–4022 and the second one in line 4032–4044. The steady–state set points of both CSCs are 12.8 Ω, that is, each CSC is defined by $x_c = x_{co} + \Delta x_c$, where x_{co} is the steady–state set point and Δx_c is the control modulation

which is controlled by the CLF control law, i.e. (6.42). Since x_{co} is a constant, the reactance of the line in which the CSC is installed, can be given by $x_s = x_L^{new} = x_L - x_{co}$. Thus, x_c in (6.42) is replaced by Δx_c. For the first CSC, $8 \leq x_c \leq 30\ \Omega$ and for the second one $8 \leq x_c \leq 20\ \Omega$.

Various faults and contingencies (i.e. various large disturbances as well as small disturbances) have been studied for both LF32-028 and LF32-029. For all cases the CLF controlled CSCs damped power oscillations in an effective and robust manner. Also, various load characteristics were applied for this system and simulation results showed that the damping effect of the CLF controlled CSCs was not sensitive to the load modeling. In this section, we only show the simulation results of one case, that is, a three–phase fault imposed on transmission line 4011-4021 at a position very close to bus 4021. The fault is cleared by disconnecting both ends of line 4011-4021 after 100 ms.

In Figure 7.10 and Figure 7.11, the dotted and solid curves show the variation of P (identified in Figure 7.9) when the CSCs are uncontrolled, and controlled using CLF, respectively. Note that these two CLF controlled CSCs do not adversely affect each other. The reason is that each device contributes to make the time derivative of the energy function negative.

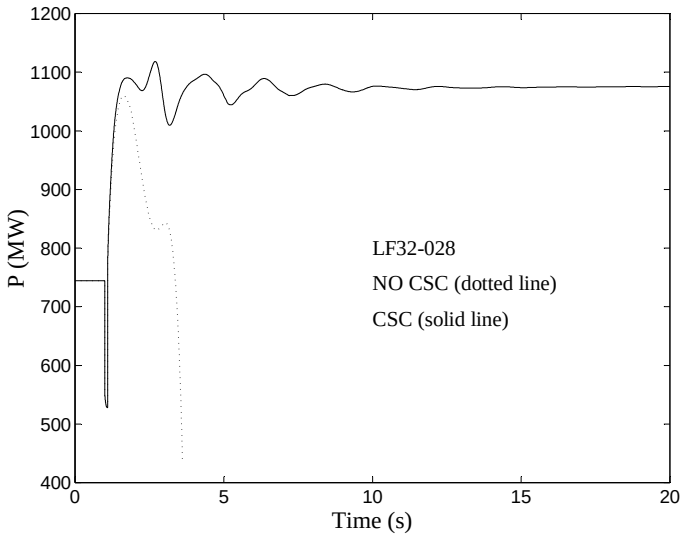

Figure 7.10. Variation of P vs time in the Nordic32A test system, LF32–028.

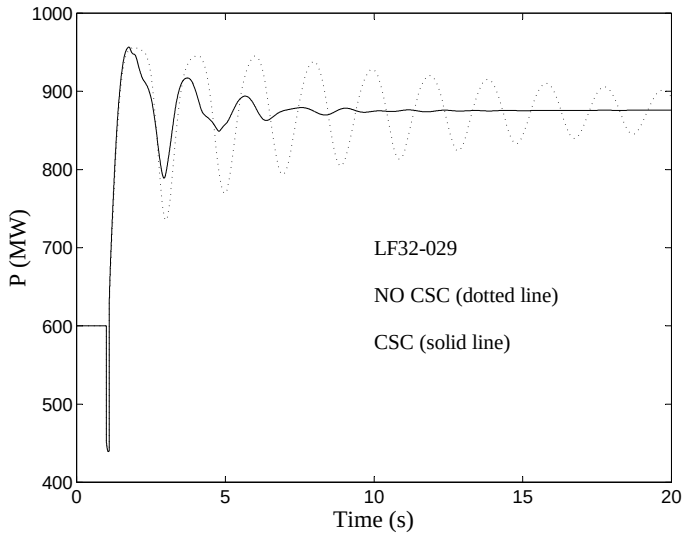

Figure 7.11. Variation of P vs time in the Nordic32A test system, LF32–029.

7.4 Summary

The CSDs provide an effective means of adding damping to power systems and significantly enlarge the stability region of the post–fault stable equilibrium point.

The control laws (6.39)–(6.41) have been derived based on a simplified Structure Preserving Model. However, these control laws have been applied for the actual systems. The simulation results indicate that the control laws are effective and robust for small and large disturbances as well as meshed and radial systems, and they are not sensitive to the model approximations.

These control laws rely only on locally measurable information and are independent of system topology and modeling of power system components. Thus, the input signals are inexpensive, fast and reliable. For these control laws, information about the post–fault stable equilibrium point is not required. Furthermore, the CSDs with CLF control (i.e. control laws (6.39)–(6.41)) do not adversely affect each other.

Chapter 8

Single Machine Equivalent

It has been shown that the control laws (6.39), (6.40) and (6.42) rely only on input signals that can easily be obtained from locally measurable variables. It has also been shown in Chapter 7 that the local signals can effectively damp the electromechanical oscillations initiated by both large and small disturbances. However, a remote input signal may be more effective for this purpose. A pertinent question is, for which power system conditions would this be the case?

In the case of using remote input signals, an important question is which (and/or which kind of) remote information should be chosen in a multi–machine power system, such that the concept of the CLF is fulfilled.

For selecting remote input signals, the SIngle Machine Equivalent (SIME) method, [40]–[42], may be a relevant choice. This method assesses the behavior of a power system in its post–fault configuration in terms of a Generalized One–Machine Infinite Bus (GOMIB) transformation to which the CLF can be applied.

8.1 Foundations

SIME is a hybrid direct-temporal transient stability method, which transforms the trajectories of a multi–machine power system into the trajectory of a GOMIB system of the form 5.8, whose parameters are time–varying [40]. The GOMIB parameters are its rotor angle (δ), rotor speed (ω), inertia coefficient (M), mechanical power (P_m), and electrical power (P_e).

Basically, SIME deals with the post-fault configuration of a power system subjected to a disturbance which presumably drives it to instability[1]. Under such condition, SIME uses a time–domain program in order to identify the mode of separation of its machines into two groups, namely critical (subscript C) and non-critical machines (subscript N) which are replaced by successively a two–machine equivalent. Then, this two–machine equivalent is replaced by a GOMIB system. By definition, the critical machines are the machines responsible of the loss of synchronism.

Let

$$M_C = \sum_{i \in C} M_i \quad , \quad M_N = \sum_{j \in N} M_j \quad , \quad M_T = \sum_{k=1}^{n} M_k = M_C + M_N$$

The angle and the speed of the GOMIB system are expressed by

$$\begin{aligned} \delta_{GOMIB} &= \delta_C - \delta_N \\ \omega_{GOMIB} &= \omega_C - \omega_N \end{aligned} \tag{8.1}$$

where

$$\begin{aligned} \delta_C = M_C^{-1} \sum_{i \in C} M_i \delta_i \quad , \quad \delta_N = M_N^{-1} \sum_{j \in N} M_j \delta_j \\ \omega_C = M_C^{-1} \sum_{i \in C} M_i \omega_i \quad , \quad \omega_N = M_N^{-1} \sum_{j \in N} M_j \omega_j \end{aligned} \tag{8.2}$$

By refreshing the GOMIB parameters at each integration time–step, SIME provides a faithful replica of the transient stability assessment of the multi–machine system, and also additional interesting pieces of information, such as stability margins, identification of the mode of instability and corresponding critical machines, sensitivity analysis and control techniques [42].

[1] By continuation, the GOMIB is also valid on a borderline stable case [41].

8.2 Control Law Based on SIME

Consider the two–area power system shown in Figure 8.1.

Figure 8.1. Two–area power system.

After a large disturbance, the post–fault dynamics of the corresponding GOMIB system of this two–area power system are given by

$$\begin{aligned} \dot{\delta}_{GOMIB} &= \omega_{GOMIB} \\ \dot{\omega}_{GOMIB} &= M_T^{-1} \left[P_{m_{GOMIB}} - P_{e_{GOMIB}} \right] \end{aligned} \tag{8.3}$$

where $P_{m_{GOMIB}}$ is the equivalent mechanical input power and $P_{e_{GOMIB}}$ is the equivalent electrical output power calculated by the time simulation program.

Let $P_{m_{GOMIB}}$ be approximated by a constant $P_{m_{app}}$, such that

$$\| P_{m_{GOMIB}} - P_{m_{app}} \| \tag{8.4}$$

is small.

Let also $P_{e_{GOMIB}}$ be approximated by $P_{e_{app}} = P_{max_{app}} \sin(\delta_{GOMIB})$ where $P_{max_{app}}$ is a constant, such that

$$\| P_{e_{GOMIB}} - P_{e_{app}} \| \tag{8.5}$$

is small.

Now, the right–hand side of the (8.3) is simplified by

$$\begin{aligned} \dot{\delta}_{GOMIB} &= \omega_{GOMIB} \\ \dot{\omega}_{GOMIB} &= M_T^{-1} \left[P_{m_{app}} - P_{max_{app}} \sin(\delta_{GOMIB})\right] \end{aligned} \tag{8.6}$$

Let $x = [\delta_{GOMIB} \quad \omega_{GOMIB}]^T$. Let also $F(x)$ and $f_o(x)$ denote the right–hand sides of (8.3) and (8.6), respectively. System (8.3) can now be rewritten as

$$\begin{aligned} \dot{x} &= F(x) \\ &= f_o(x) + [F(x) - f_o(x)] \\ &= f_o(x) + p(x) \end{aligned} \tag{8.7}$$

Assuming $p(x) = 0$, the GOMIB system has the same dynamics as the physical OMIB system, i.e. system (5.8) with $D = 0$. Consequently, a similar Lyapunov function to (5.11) (in which M, P_m, P_{max}, ω and δ are replaced by M_T, $P_{m_{app}}$, $P_{max_{app}}$, ω_{GOMIB} and δ_{GOMIB}, respectively) can be used for the GOMIB system.

Having a CSC between the two systems in Figure 8.1, the dynamics of the GOMIB system with the CSC is similar to the dynamics of the physical OMIB system with the CSC, i.e. system (6.19). Thus, the control strategy for the CSC in the GOMIB system is similar to (6.26), that is,

$$x_c = k \sin(\delta_{GOMIB})\, \omega_{GOMIB} \tag{8.8}$$

where k is a positive gain.

8.3 Numerical Examples

Example 8.1:

Consider again the power system shown in Figure 7.1. System model 2 is used in this example with $P_{G1} = P_{G2} = 750$ (MW). Two cases are studied. In case 1, a three–phase fault occurs at point **F**. The fault is cleared after 100 ms by opening of the faulted line. In case 2, 20% of the load at bus 9 is disconnected during 100 ms.

In an off–line simulation, the GOMIB system of the test system is determined by the SIME method for corresponding case. In case 1 (for which

the system is unstable), the critical machines are machine 1 and machine 2, and the non–critical machines are machine 3 and machine 4. Thus,

$$\begin{aligned} \delta_{GOMIB} &= \frac{M_1\delta_1 + M_2\delta_2}{M_1 + M_2} - \frac{M_3\delta_3 + M_4\delta_4}{M_3 + M_4} \\ \omega_{GOMIB} &= \frac{M_1\omega_1 + M_2\omega_2}{M_1 + M_2} - \frac{M_3\omega_3 + M_4\omega_4}{M_3 + M_4} \end{aligned} \tag{8.9}$$

Since the system is stable for case 2, the SIME method fails to determine a GOMIB system for this case. However, (8.9) is also used for case 2.

A CSC is located in the system (see Figure 7.1). The purpose of this example is to compare the dynamic behavior of the system for these two cases when the CSC is controlled by (6.42) (i.e. with local input signals) and (8.8) (i.e. with remote input signals), respectively.

Note, however, that the same system with the same CSC is simulated in the same time simulation program (SIMPOW). The only difference is the input data into the CSC, that is, the control laws. For control law (8.8), we need only an additional arithmetic operation to calculate (8.9) at each integration time–step.

The following figures show the variation of P (identified in Figure 7.1) vs. time for both cases. They also show the phase portrait of the corresponding GOMIB system.

Obviously, both control laws (which are based on the CLF) stabilize the system (case 1) and damp the electromechanical oscillations in the system (case 2). The dynamic behavior of this system is almost identical for both control laws.

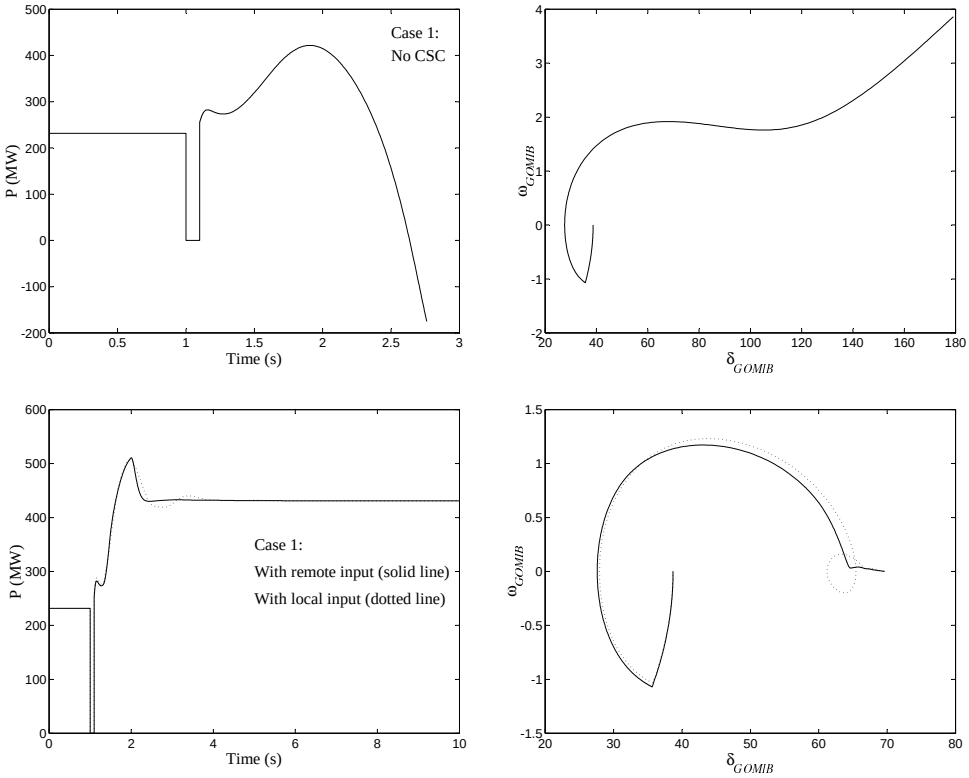

Figure 8.2. Case 1: Variation of P vs. time in the two–area test system and phase portrait of the corresponding GOMIB system.

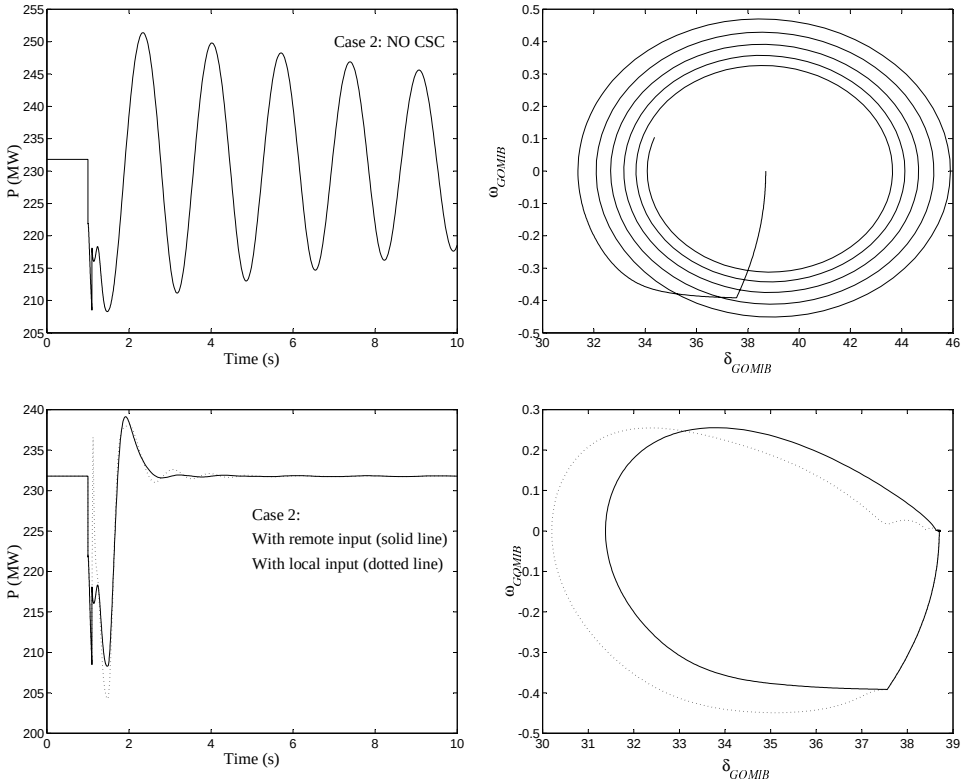

Figure 8.3. Case 2: Variation of P vs. time in the two–area test system and phase portrait of the corresponding GOMIB system.

In the next case (case 3), the generating powers of generator 1 and generator 2 increase with another 20 (MW), that is, $P_{G1} = P_{G2} = 770$ (MW). Figure 8.4 shows the variation of P vs. time. Obviously, both control laws are not able to stabilize the system for this case. This is not a question about the control laws, but the rating of the CSC ($x_{cmax} = 0.047$ $(p.u)$), that is, the size of the stability region. In case 1, both control laws enlarge the stability region of the post–fault stable equilibrium point. Thus, when the fault is cleared, the system trajectories lie within the enlarged stability region in which the Lyapunov function is positive definite. Therefore, both control laws act as a stabilizer. However, using the same rating in case 3, the post–fault system trajectories lie outside the enlarged stability region where we cannot prove the Lyapunov function is still positive definite. Having a larger rating, it can be shown that the system will be stabilized by both control laws.

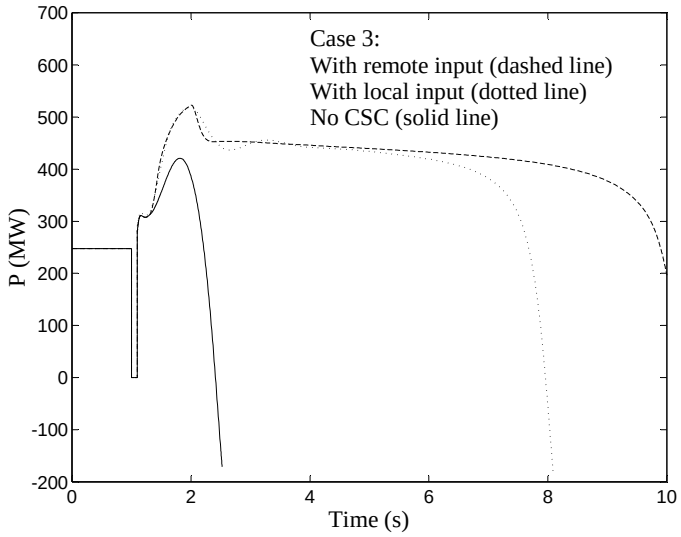

Figure 8.4. Case 3: Variation of P vs. time in the two–area test system.

Example 8.2:

In this example, the same case for the simple meshed system shown in Figure 7.6 is studied. Figure 8.5 shows the variation of P (identified in Figure 7.6) when CSC is controlled by control laws (6.42) and (8.8), respectively.

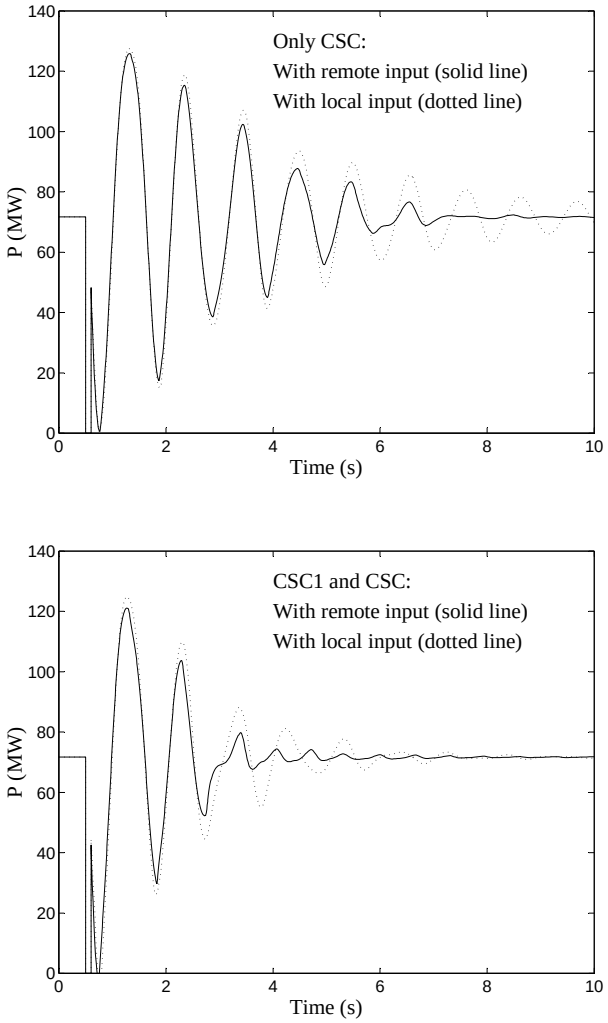

Figure 8.5. Variation of P vs time in the IEEE 9–bus system.

Clearly, the system is better damped with the remote input signals than the local input signals.

Example 8.3:

In this example, the same fault in the Nordic32A test system (shown in Figure 7.9) is considered. The loading case LF32–028 is used with the exception that:

- **Case 1:** the power generating of a generator in South is decreased with 100 (MW), so that the transmission system North–Central becomes more loaded.
- **Case 2:** the power generating of the same generator is decreased with another 30 (MW).

Figure 8.6 shows the variation of P (identified in Figure 7.9) when CSCs are controlled by control laws (6.42) and (8.8), respectively.

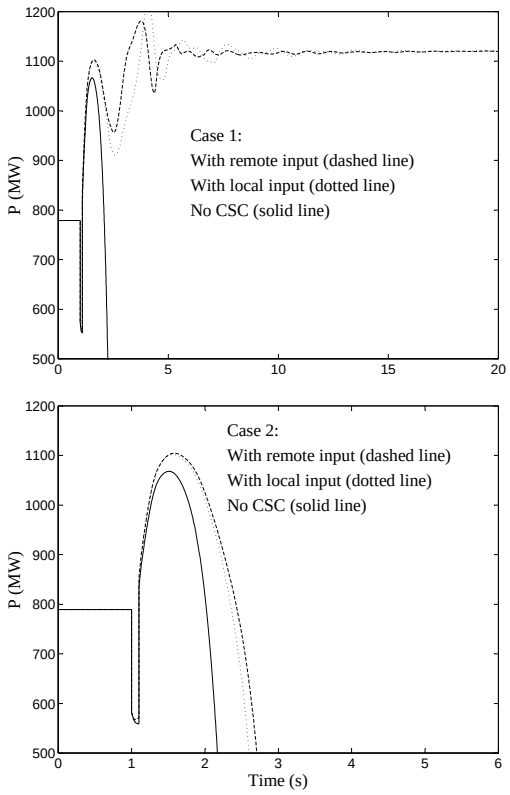

Figure 8.6. Variation of P vs time in the Nordic32A test system.

Example 8.4:

Figure 8.7 shows a sketch of the Brazilian North–South interconnection system described in [43]. The North/Northeast interconnected system consists of large hydro-generating complexes that are linked to 230 and 500 kV transmission networks. The South/Southeast/Midwest interconnected system consists of a large number of hydro–generating plants linked to the main load centers by transmission networks operating in the 138 and 750 kV. The North–South interconnect transmission line is 1028 km with a circuit rating of 1300 (MW). Full details are given in [43].

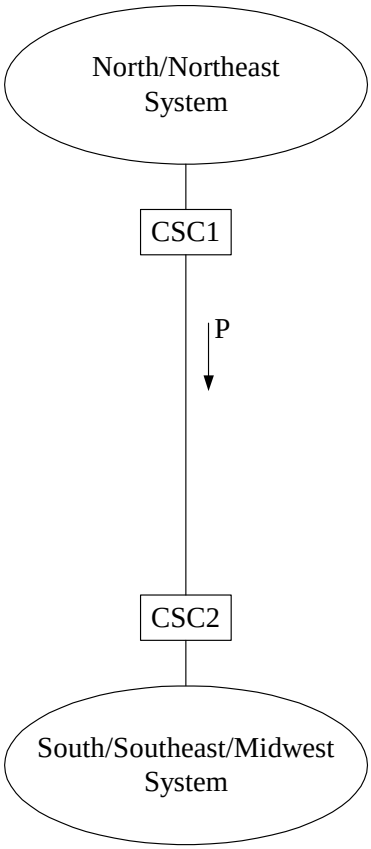

Figure 8.7. The Brazilian North–South interconnection system.

Four cases are studied.

- **case 1:** a line and a shunt in the North/Northeast system is tripped after a fault. The fault is cleared after 100 ms.
- **case 2:** a line and a shunt in the South/Southeast/Midwest system is tripped after a fault. The fault is cleared after 100 ms.
- **case 3:** a generator with a production of 606 (MW) is disconnected in the North/Northeast system.
- **case 4:** a generator with a production of 395 (MW) is disconnected in the South/Southeast/Midwest.

For both CSCs, the steady–state set points (i.e. x_{co}) are 15.84 Ω, and $13.2 \leq x_c \leq 40\,\Omega$.

In an off–line simulation, the SIME method has been used to determine the corresponding GOMIB system for each case when CSCs were not controlled. In case 1 and case 2, a longer clearing–time was applied to make the system unstable, so that the SIME method would be able to determine the corresponding GOMIB system. For the same reason, a three–phase fault at the terminal bus of the corresponding generator was also applied for case 3 and case 4. Having determined the corresponding GOMIB system, its variables $\delta_{_{GOMIB}}$ and $\omega_{_{GOMIB}}$ are calculated at each integration time–step in the time simulation program (SIMPOW).

The purpose of this example is also to compare the dynamic behavior of this system for these four cases when the CSCs are controlled by (6.42) and (8.8), respectively.

The following figures show the variation of P (identified in Figure 8.7) vs. time for each case. They also show the phase portrait of the corresponding GOMIB system.

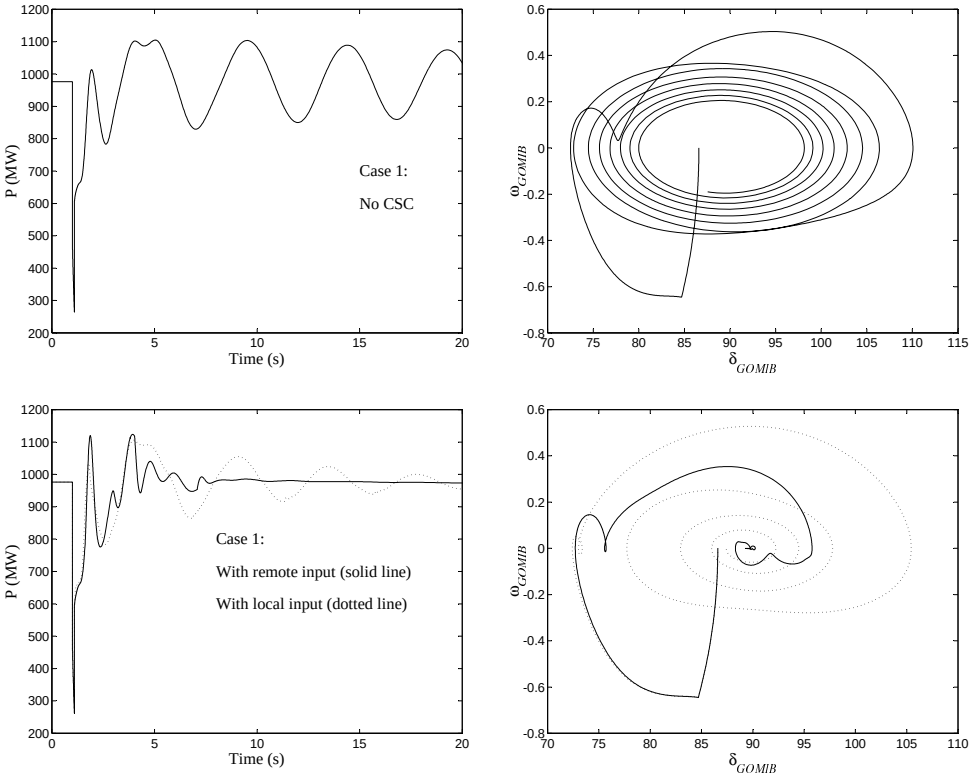

Figure 8.8. Case 1: Variation of P vs. time in the Brazilian North–South interconnection system and phase portrait of the corresponding GOMIB system.

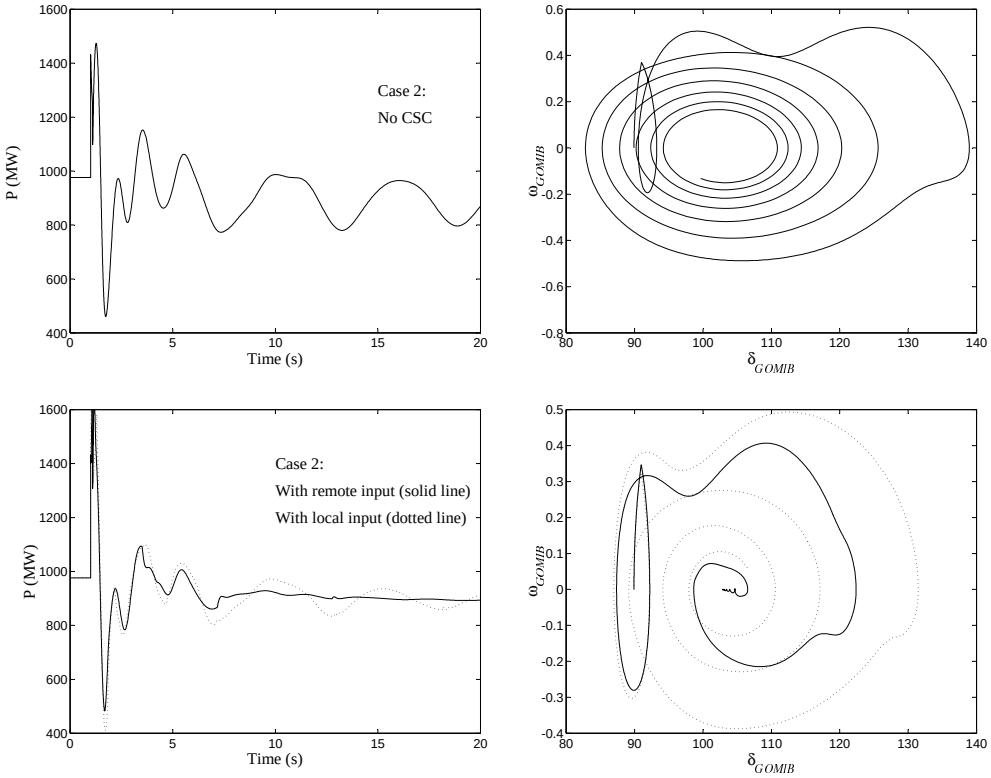

Figure 8.9. Case 2: Variation of P vs. time in the Brazilian North–South interconnection system and phase portrait of the corresponding GOMIB system.

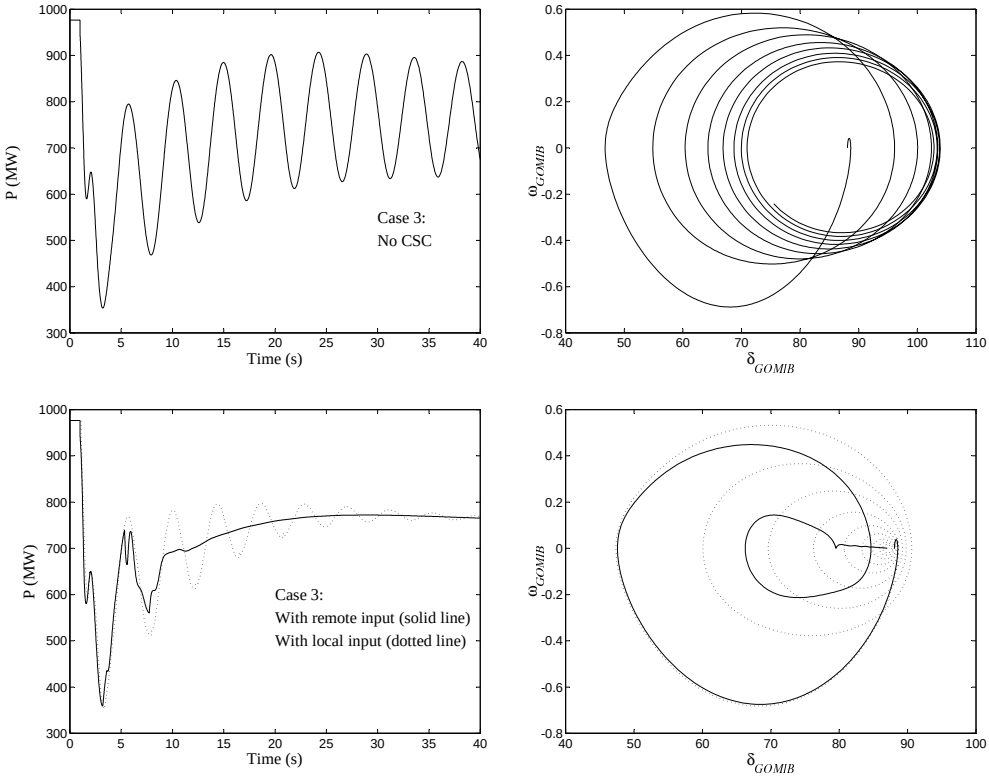

Figure 8.10. Case 3: Variation of P vs. time in the Brazilian North–South interconnection system and phase portrait of the corresponding GOMIB system.

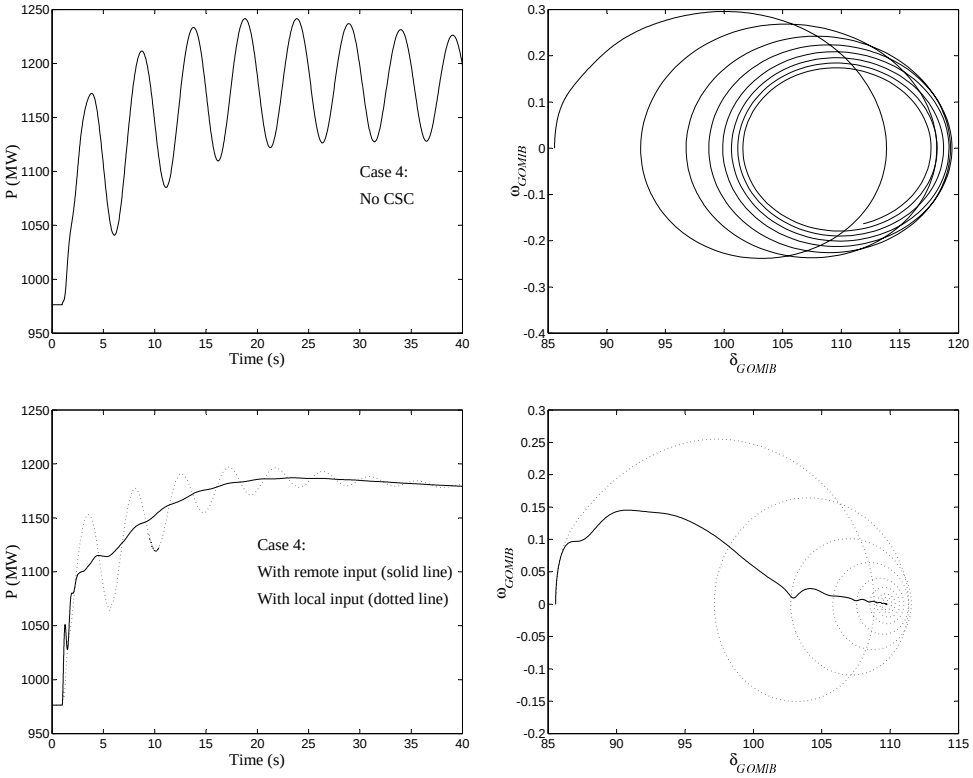

Figure 8.11. Case 4: Variation of P vs. time in the Brazilian North–South interconnection system and phase portrait of the corresponding GOMIB system.

The simulation results show the ability of both control laws to damp the power system oscillations initiated by these four cases. They also show that the proposed test system has better damping with control law (8.8) than control law (6.42). The reason may be that control law (8.8) uses data from all machines in the system. This comprehensive data is indeed compacted into two variables (i.e. δ_{GOMIB} and ω_{GOMIB}) which give a better information of the post–fault dynamics of the system. However, the system is still well damped by (6.42) which is inexpensive, faster and more reliable since it relies only on locally measurable information.

Next, an extreme case (case 5) is studied. In this case, a generator with a production of 800 (MW) is disconnected in the South/Southeast/Midwest. This case implies that the power through the North–South interconnect transmission line (at the post–fault steady–state) is almost 1300 (MW)

which is the circuit rating of the North–South interconnect transmission line.

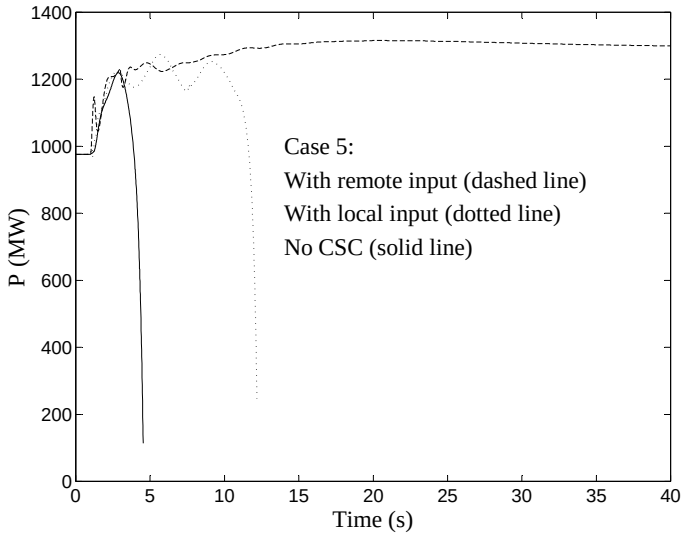

Figure 8.12. Case 5: Variation of P vs. time in the Brazilian North–South interconnection system.

Figure 8.12 shows that the control law based on the local input signals cannot stabilize the system for this case. However, the system is stabilized when the remote input signals are used.

In a further analysis (by using the SIME method), we found that the stability margin was -0.02 when control law (6.42) had been used, and it was almost zero (but positive) when control law (8.8) had been used. This analysis implies that the system trajectories lie close by the corresponding stability boundary of the post–fault equilibrium point at fault clearing. Obviously, the (enlarged) stability region by control law (8.8) is a little larger than the (enlarged) stability region by control law (6.42). Therefore, the system trajectories lie just inside the corresponding (enlarged) stability region at fault clearing when control law (8.8) is used. However, when control law (6.42) is used, the system trajectories lie outside the corresponding (enlarged) stability region at fault clearing.

Note, however, that both control laws are based on the CLF. They have also been derived based on a simplified system, i.e. $f_o(x)$.

8.4 Selection of the Gains of Control Laws

A question of importance is the selection of the gains k_1–k_5 and k in the control laws (6.39)–(6.42) and (8.8), respectively. Mathematically, any positive gain should stabilize the system. In practice, there are however limitations for these gains. To see that , we use the SIME method.

Consider again the power system in Example 8.1. Case 1 is considered. The control law for CSC is given by (6.42). Figure 8.13 shows the phase portrait of the GOMIB system of the test system for various values of k_5.

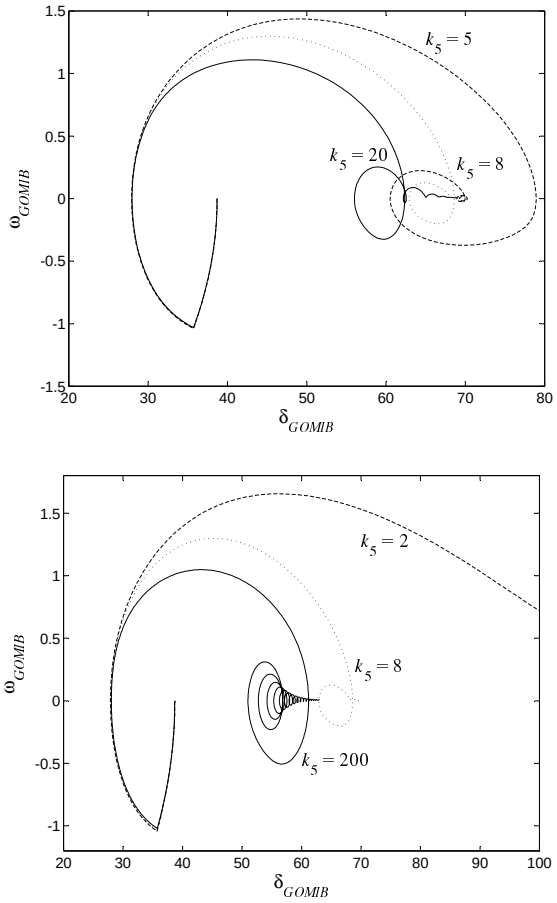

Figure 8.13. Phase portrait of the GOMIB system of the test system.

For $k_5 < 5$, the stability margin (calculated by the SIME method) is negative for this case, that is, the post–fault trajectories (when the fault is cleared) lie outside the stability region of the post–fault stable equilibrium point. For $5 \leq k_5 \leq 8$, the stability margin is positive and it significantly becomes larger by increasing the value of k_5. For around $k_5 = 8$, the system is well damped and the system trajectories rapidly tend towards the post–fault stable equilibrium point. For $k_5 > 8$, the stability margin is positive, but its value is almost the same as for $k_5 = 8$. However, for large k_5, the system trajectories slowly tend towards the post–fault stable equilibrium point.

8.5 Summary

The control law (6.42) relies only on locally measurable information. Thus, the input signals are inexpensive, fast and reliable, but the control law (8.8) (based on the SIME methos) uses data from all machines in the system. Thus, the input signals can be expensive and less reliable in a real power system. However, due to the latest development in signal and communication technology, these issues may be solved in the near future.

The simulation results indicate that using CSCs in a power system, the control law with remote input signals (i.e. control law (8.8)) is more effective than the control law with local input signals (i.e. control law (6.42)) for damping and stability of the power system.

Note that the control laws (6.42) and (8.8) do not require information about the post–fault stable equilibrium point.

Chapter 9

Variable Structure Control with Sliding Modes

This chapter briefly presents the concept of Variable Structure Control (VSC) with sliding modes, and its application to power systems with CSDs. For a comprehensive and detailed analysis of VSC with sliding modes , see [44]–[50] and references therein.

With VSC, dynamical systems are controlled with discontinuous feedback controllers. VSC has been developed during the last four decades, and is characterized by a control structure which is designed to drive the system trajectories onto a specified line (or surface) in the state space. The sliding mode describes the particular case when the system trajectories are constrained to lie upon a line (or surface).

9.1 Background

Consider the following system

$$\begin{bmatrix} \dot{x}_1 \\ \dot{x}_2 \end{bmatrix} = \begin{bmatrix} 0 & 1 \\ 1 & 0.2 \end{bmatrix} \begin{bmatrix} x_1 \\ x_2 \end{bmatrix} + \begin{bmatrix} 0 \\ 1 \end{bmatrix} u$$

where x is the state of the system and $u = kx_1$ is a control variable. Thus, the system can be rewritten as

$$\begin{bmatrix} \dot{x}_1 \\ \dot{x}_2 \end{bmatrix} = \begin{bmatrix} 0 & 1 \\ 1+k & 0.2 \end{bmatrix} \begin{bmatrix} x_1 \\ x_2 \end{bmatrix}$$

The eigenvalues of this system are given by

$$\lambda_{1,2} = 0.1 \pm \sqrt{1.01 + k}$$

Obviously, the system is unstable for any value of k. Let $k = -3$ and $k = 2$. The system eigenvalues for these structures (i.e. $k = -3$ and $k = 2$) are

- for $k = -3$, $\lambda_{1,2} = 0.1 \pm j1.4107$
- for $k = 2$, $\lambda_1 = -1.6349$ and $\lambda_2 = 1.8349$

As was mentioned above, the system is unstable for both structures as shown in Figure 9.1. Note, however, that the only trajectories converging to the origin are the trajectories along the the eigenvector corresponding to the stable eigenvalue for the structure $k = 2$.

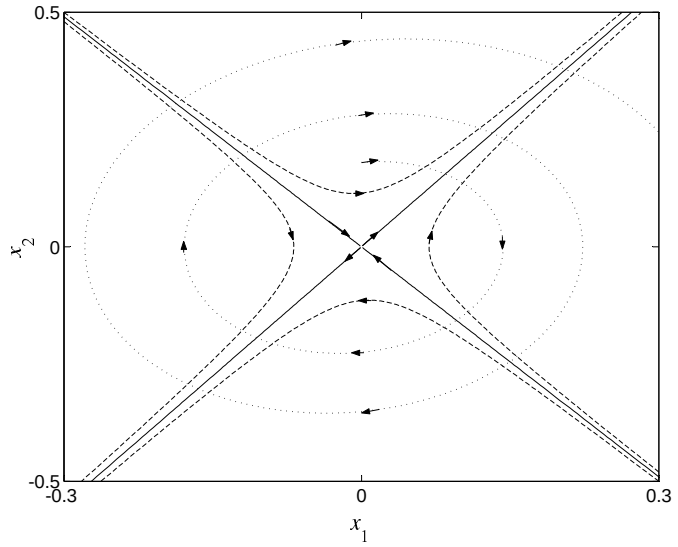

Figure 9.1. Phase portrait of the system for $k = -3$ (dotted line) and $k = 2$ (dashed line, and also solid lines which are indeed the eigenvectors).

The objective of the VSC is to drive the system trajectories to this eigenvector which is a positively invariant manifold (see (5.2)). To do this, we first define a switching line, that is,

$$S(x) = g_1 x_1 + x_2 = 0 \tag{9.1}$$

Choosing $g_1 = -\lambda_1 = 1.6349$, the switching line is indeed along the eigenvector corresponding to the stable eigenvalue. Next, we define the following switching (control) law,

$$k = \begin{cases} -3 & \text{if } S(x)\, x_1 > 0 \\ 2 & \text{if } S(x)\, x_1 \leq 0 \end{cases}$$

Applying the above switching laws, the system trajectories tend to the origin as shown in Figure 9.2.

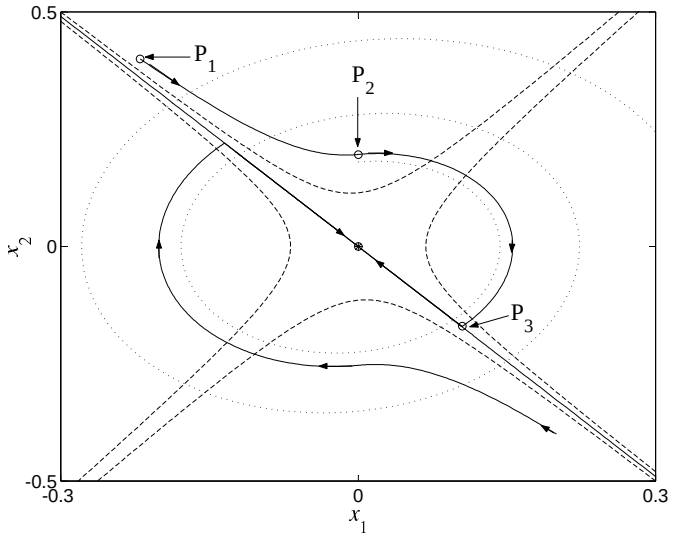

Figure 9.2. Phase portrait of the system controlled by VSC, $c_1 = \lambda_1$.

In Figure 9.2, point P_1 is the initial point. From this point, structure $k = 2$ is switched by the switching law. Thus, the system trajectory moves along the trajectory of this structure. At point P_2, the structure is switched to $k = -3$. Therefore, the system trajectory moves along the trajectory of this structure. Once the system trajectory encounters the switching line $S(x) = 0$ at point P_3, structure $k = 2$ is switched. Since the switching line $S(x)$ is a positively invariant manifold, the system trajectory remains in this line which is indeed the eigenvector corresponding to the stable eigenvalue for structure $k = 2$. Therefore, the system trajectory tends to the origin along the switching line.

In the above example, a new system property has been obtained by composing a desired trajectory from the parts of trajectories of different structures. An even more fundamental aspects of VSC is the possibility to obtain trajectories not inherent in any of the structures. Theses trajectories describe a new type of motion.

To show how such motion occurs, rename $S(x)$ to $S_1(x)$ in which $g_1 < \lambda_1$, and $S(x)$ to $S_2(x)$ in which $g_1 > \lambda_1$. The same switching law is used with exception that $S_1(x)$ and $S_2(x)$ replace $S(x)$, respectively.

Figure 9.3 show the phase portrait of the system when $g_1 < \lambda_1$ and $g_1 > \lambda_1$, respectively.

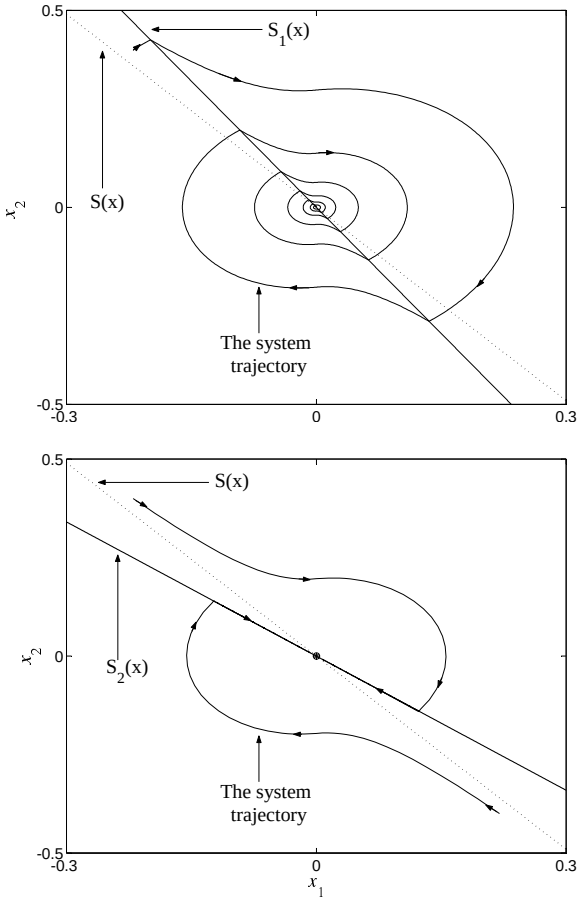

Figure 9.3. Phase portrait of the system when $g_1 < \lambda_1$ and $g_1 > \lambda_1$, respectively.

In Figure 9.3, the system trajectory does not remain on switching line $S_1(x)$, once the system trajectory intercepts $S_1(x)$. However, the system trajectory remains on switching line $S_2(x)$, once it intercepts $S_2(x)$. This property of remaining on the switching line once intercepted is called a sliding mode, and the switching line $S_2(x)$ is a sliding line.

A sliding mode will exist for a system $\dot{x} = f(x)$, if in the vicinity of the switching line, the state velocity vector $f(x)$ is directed towards the switching line.

Note, however, that the above example deals with an ideal VSC, that is, switching in the control law can occur infinitely fast. An ideal sliding mode exists only, once the system trajectory $x(t)$ intercepts the switching line at t_o, it satisfies $S_2(x) = 0$ at every $t \geq t_o$. In actual systems, various small nonidealities of time–delay, hysteresis etc. should be taken into consideration. Theses nonidealities force switching to occur at a finite frequency. The trajectory then oscillates within a neighborhood of the switching line. If the frequency of the switching is very high compared with the dynamic response of the system, the nonidealities and the finite switching frequencies are often negligible [48].

Consider the following control system with control input $u \in R^m$,

$$\dot{x} = f(x, u) \tag{9.2}$$

and the following general control law ($i = 1 \cdots m$),

$$u_i(x) = \begin{cases} u_i^+(x) & \text{if} \quad S_i(x) > 0 \\ u_i^-(x) & \text{if} \quad S_i(x) < 0 \end{cases} \tag{9.3}$$

where $S(x) = [S_1(x) \cdots S_m(x)]^T = 0$ is switching manifold (or surface).

The mathematical description of sliding modes is quite a challenge. It requires the design of special techniques. The solution of system $\dot{x} = f(x)$ is known to exist and be unique if a Lipshitz constant L may be found, such that for any x_1 and x_2

$$\|f(x_1) - f(x_2)\| \leq L \|x_1 - x_2\| \tag{9.4}$$

It is evident that in the dynamic system (9.2) with discontinuous control (9.3), condition (9.4) is violated in the vicinity of $S(x)$. Indeed, if x_1 and x_2 are on different sides of $S(x)$, and $\|x_1 - x_2\| \to 0$, condition (9.4) is

not true for any fixed value of L. Therefore, (at least formally) some additional effort is needed to find a solution to (9.2) and (9.3) at an occurrence of a sliding mode.

Various types of existence and uniqueness theorems have been presented in the literature. Filippov's method, [51], is one possible technique for determining the system motion in a sliding mode. A more promising technique (easily applicable to multi–input systems) is the method of equivalent control, as proposed by Utkin in [44]–[47].

9.2 Method of Equivalent Control

In this section, a formal procedure is suggested below to obtain sliding equations along the intersections of a set of discontinuity surfaces for systems (9.2) and (9.3).

Assume that a sliding mode exists on manifold $S(x) = 0$. The aim is to find a continuous control, such that under the initial position of the system trajectory on this manifold, it yields

$$\dot{S}(x) = \frac{\partial S}{\partial x} \cdot \dot{x} = \mathcal{G} \cdot f(x, u) = 0 \tag{9.5}$$

along the trajectory of system (9.2). In (9.5), $\mathcal{G} = \frac{\partial S}{\partial x}$ is a matrix of dimension $(m \times n)$. We assume that $\mathcal{G}$ is a constant matrix. Note that the rows of $\mathcal{G}$ are the gradients of the functions $S_i(x)$.

Assume that a solution exists for (9.2) with respect to m–dimensional control. Using this solution (hereinafter referred to as equivalent control $u_{eq}(x)$) in system (9.2), we obtain

$$\dot{x} = f(x, u_{eq}(x)) \tag{9.6}$$

which describes the motion on the switching manifold. It is also called the equation of sliding mode.

It is quite obvious that (by virtue of condition (9.5)) a motion starting in $S[x(t_o)] = 0$ will proceed along the trajectories which lie on the manifold $S(x) = 0$.

Consider now the following affine system

$$\dot{x} = f(x,u) = f_o(x) + \sum_{i=1}^{m} u_i f_i(x) = f_o(x) + \mathcal{B}(x) \cdot u \tag{9.7}$$

where $u = [u_1 \cdots u_m]^T$ and $\mathcal{B}(x)$ is an $n \times m$ matrix whose i–th column is $f_i(x)$.

The switching manifold is given by

$$S(x) = \mathcal{G} \cdot x = 0 \tag{9.8}$$

The conditions for the existence of a sliding mode are closely linked with the convergence of the system trajectory to the manifold $S(x) = 0$. Generally, there exists a sliding mode on $S(x) = 0$, if the system trajectory satisfies a generalized Lyapunov stability requirement to $S(x) = 0$.

A suitable function is

$$\mathcal{V}(x) = 0.5\, S^T \cdot S$$

which is positive definite. Note that this function is zero on $S(x) = 0$. Therefore, (9.9) is a sufficient condition for existence of a sliding mode.

$$\dot{\mathcal{V}} = 0.5\, \frac{d}{dt}(S^T \cdot S) < 0 \tag{9.9}$$

For the sake of the simplicity, assume that $m = 1$, i.e. single control input. Suppose that the system trajectory intercepts $S(x) = 0$ at t_o, and a sliding mode exists for $t \geq t_o$. The existence of a sliding mode implies that for all $t \geq t_o$, $S(x) = \mathcal{G} \cdot x = 0$, and

$$\dot{S}(x) = \mathcal{G} \cdot \dot{x} = \mathcal{G} \cdot [f_o(x) + u_{eq}\mathcal{B}(x)] = 0 \tag{9.10}$$

To compute u_{eq}, assume that $[\mathcal{G} \cdot \mathcal{B}(x)]^{-1}$ is nonsingular for all t and x. Thus,

$$u_{eq} = -[\mathcal{G} \cdot \mathcal{B}(x)]^{-1} \mathcal{G} \cdot f_o(x) \tag{9.11}$$

The equivalent control u_{eq} is found by recognizing that (9.10) is a necessary condition for the system trajectory to stay on the switching line

$S(x) = 0$. To satisfy condition (9.9), the control action must be chosen in the following way,

$$u(x) = \begin{cases} u^+(x) & \text{if} \quad S(x) > 0 \\ u^-(x) & \text{if} \quad S(x) < 0 \end{cases} \tag{9.12}$$

where $u^+ < u_{eq}$ and $u^- > u_{eq}$.

Using the control law

$$u = u_{eq} - \tilde{u} \tag{9.13}$$

where $\tilde{u} = k[\mathcal{G} \cdot \mathcal{B}(x)]^{-1} S(x)$ and $k > 0$. Then, $\tilde{u}$ assures that a sliding mode exists, that is, the condition (9.9) is satisfied.

Substitution of (9.13) into (9.7) yields

$$\dot{x} = f_o(x) - \mathcal{B}(x)[\mathcal{G} \cdot \mathcal{B}(x)]^{-1}[\mathcal{G} \cdot f_o(x) + kS(x)] = f(x, \mathcal{G}) \tag{9.14}$$

which is the equation of sliding mode.

Control strategy based on VSC with sliding mode can be summarized as follows:

- Design a switching manifold $S(x) = 0$ to represent a desired system dynamics.
- Design a control law u, such that the system trajectory outside the switching manifold is driven to reach $S(x) = 0$ in finite time. On the switching manifold, the sliding mode takes place, following the desired system dynamics.

Example 9.1 :

Consider again the OMIB system with CSC as shown in Figure 6.1.

Let $x_1 = \delta - \delta^s$, $x_2 = \omega$ and $x = [x_1 \quad x_2]^T$. Thus, the origin is the stable equilibrium point and the system dynamics are given by

$$\dot{x} = f_o(x) + u\mathcal{B}(x) \tag{9.15}$$

where

$$f_o(x) = \begin{bmatrix} x_2 \\ \\ (P_m - P_{max}\sin(x_1 + \delta^s))/M \end{bmatrix}$$

and

$$\mathcal{B}(x) = f_{csc} = \begin{bmatrix} 0 \\ \\ -P_{max}\sin(x_1 + \delta^s)/M \end{bmatrix}$$

Let also $S(x) = \mathcal{G}\cdot x = 0$ be the sliding line, where $\mathcal{G} = [g_1 \quad g_2]$. Applying the control law (9.13) and substituting it into (9.15), we obtain

$$\dot{x} = \begin{bmatrix} x_2 \\ \\ -\left(\frac{g_1}{g_2}x_2 + k\frac{g_1}{g_2}x_1 + kx_2\right) \end{bmatrix} \tag{9.16}$$

On the sliding line,

$$S(x) = g_1x_1 + g_2x_2 = 0 \;\Rightarrow\; x_1 = -\frac{g_2}{g_1}x_2 \quad \text{or} \quad x_2 = -\frac{g_1}{g_2}x_1$$

Therefore, (9.16) can be rewritten as

$$\dot{x} = -\frac{g_1}{g_2}\begin{bmatrix} x_1 \\ x_2 \end{bmatrix}$$

which is the equation of sliding mode, and it represents the original system dynamics (9.15) constrained to $S(x) = 0$. Obviously, the equation of sliding mode is asymptotically stable if $\frac{g_1}{g_2} > 0$ and $g_2 \neq 0$. Note , however, that $g_2 \neq 0$ is a necessary condition for $[\mathcal{G}\cdot\mathcal{B}(x)]^{-1}$ to be nonsingular. A similar analysis can be found in [52]. Application of VSC with sliding mode to the QBT and UPFC can be found in [4] and [5].

Figure 9.4 shows the stability boundary of the post–fault stable equilibrium point, and also, the post–fault system trajectory. x^s and x_{e1} are the

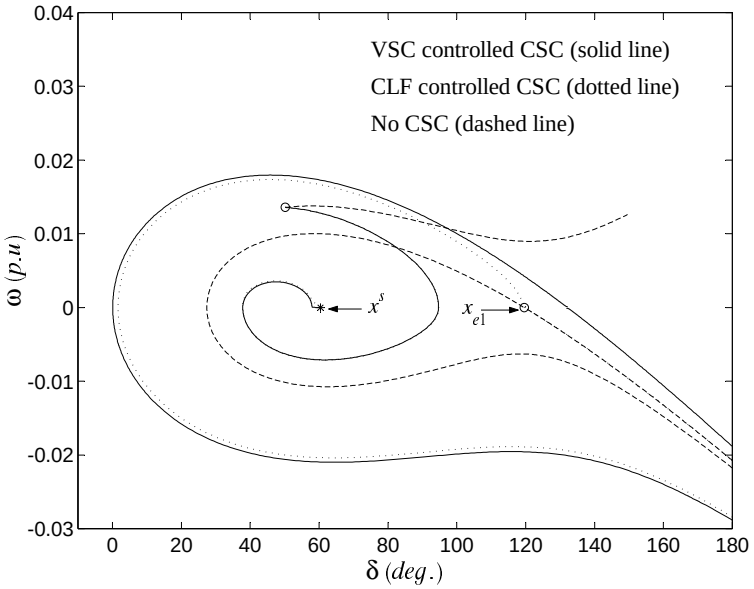

Figure 9.4. Phase portrait of the OMIB system after the fault, when CSC is controlled by CLF and VSC with sliding mode, respectively.

post–fault stable and unstable equilibrium points of $f_o(x)$, respectively. The values of these points are given by (5.10).

As shown in the figure, the behavior of the post–fault system dynamics is almost identical for both control laws. However, the stability region is larger, when CSC is controlled by control law (9.13) than control law (6.26). Specially, the difference is significant around x_{e1}. A reason for this significantly difference may be that the control law based on VSC with sliding mode (i.e. (9.13)) is zero only at the origin. However, the control law based on CLF (i.e. $x_c = k_5 \sin(\delta)\,\omega$) tends to zero whenever $\omega \to 0$ irrespective of the value of δ (i.e. for $0 < \delta < \pi$). The reason being that we use an energy function (which is not a true Lyapunov function) as a Lyapunov function candidate by virtue of the La Salle's theorem. Furthermore, in the neighborhood of x_{e1} with $\omega = -\epsilon$ (where $\epsilon > 0$), the control law (6.26) becomes negative, and the minimum value of x_c must be switched, that is, $x_c = x_{cmin} = 0$. Thus, the second term of the right–hand side of (6.19) becomes zero. Therefore, (from the initial point $x = [\delta_{e1} \quad -\epsilon]^T$) the system trajectory of (6.19) coincides with the stable manifold of the system without CSC (i.e. $\dot{x} = f_o(x)$).

A disadvantage with control law based on VSC with sliding mode is that it requires information about the post–fault stable equilibrium point for designing the switching manifold $S(x) = \mathcal{G} \cdot \dot{x} = 0$. Furthermore, for large multi–machine power systems, it is difficult and time–consuming to choose an appropriate $\mathcal{G}$, such that the equation of sliding mode becomes asymptotically stable.

As was mentioned, the control law (6.26) was derived by virtue of (6.12), when an energy function had been used as a Lyapunov function candidate, i.e.

$$\mathcal{V}(x) = 0.5Mx_2^2 - P_m\, x_1 - P_{max}[\cos(x_1 + \delta^s) - \cos(\delta^s)] \tag{9.17}$$

where $x_1 = \delta - \delta^s$, $x_2 = \omega$, that is, the post–fault stable equilibrium point is transformed to the origin.

Let us look for a Lyapunov function $\mathcal{V}(x)$ that would have a negative definite $\dot{\mathcal{V}}(x)$. Starting from the energy function, let $0.5Mx_2^2$ be replaced by the more general quadratic form $(0.5Mx^TPx)$ for some 2×2 positive definite matrix P, i.e.

$$\begin{aligned}\mathcal{V}(x) =& \frac{M}{2}x^TPx - P_m\, x_1 - P_{max}[\cos(x_1 + \delta^s) - \cos(\delta^s)] \\ =& \frac{M}{2}\begin{bmatrix} x_1 & x_2 \end{bmatrix}\begin{bmatrix} p_{11} & p_{12} \\ p_{12} & p_{22} \end{bmatrix}\begin{bmatrix} x_1 \\ x_2 \end{bmatrix} - P_m\, x_1 \\ & - P_{max}[\cos(x_1 + \delta^s) - \cos(\delta^s)]\end{aligned} \tag{9.18}$$

Note that P is positive definite if its pivots p_{11} and $p_{22} - p_{12}^2/p_{11}$ are positive [54].

The gradient of (9.18) is given by

$$grad(\mathcal{V}(x)) = \begin{bmatrix} Mp_{11}x_1 + Mp_{12}x_2 - P_m + P_{max}\sin(x_1 + \delta^s) \\ \\ Mp_{12}x_1 + Mp_{22}x_2 \end{bmatrix}^T$$

The time derivative of (9.18) is given by

$$\begin{aligned}\dot{\mathcal{V}}(x) &= grad(\mathcal{V}(x)) \cdot f_o(x) \\ &= x_2^2(Mp_{12} - Dp_{22}) + p_{12}x_1(P_m - P_{max}\sin(x_1 + \delta^s)) \\ &\quad + P_m x_2(p_{22} - 1) + P_{max}x_2\sin(x_1 + \delta^s)(1 - p_{22}) \\ &\quad + x_1x_2(Mp_{11} - Dp_{12})\end{aligned}$$

Now, we choose p_{11}, p_{12} and p_{22}, such that $\dot{\mathcal{V}}(x)$ becomes negative definite. Since the signs of the cross product terms $x_2 \sin(x_1 + \delta^s)$ and $x_1 x_2$ are indefinite, we remove them by taking $p_{22} = 1$ and $p_{11} = \frac{D}{M} p_{12}$. Thus,

$$\dot{\mathcal{V}}(x) = x_2^2(Mp_{12} - D) + p_{12}x_1(P_m - P_{max}\sin(x_1 + \delta^s)) \tag{9.19}$$

Taking $p_{12} < \frac{D}{M}$, the first term of (9.19) becomes negative, and the conditions for the pivots are also satisfied. It can also be proved that the second term of (9.19) is negative in a region surrounding the origin. Thus, (9.19) is negative definite.

Using the control law (6.12), we obtain

$$\begin{aligned} x_c &= -\, k_5 grad(\mathcal{V}(x)) \cdot f_{csc} \\ &= k_6(p_{12}x_1 + x_2)\sin(x_1 + \delta^s) \\ &= k_6(p_{12}(\delta - \delta^s) + \omega)\sin(\delta) \end{aligned} \tag{9.20}$$

since $x_1 = \delta - \delta^s$. In (9.20), $k_6 = -k_5(-P_{max}) = k_5 P_{max}$.

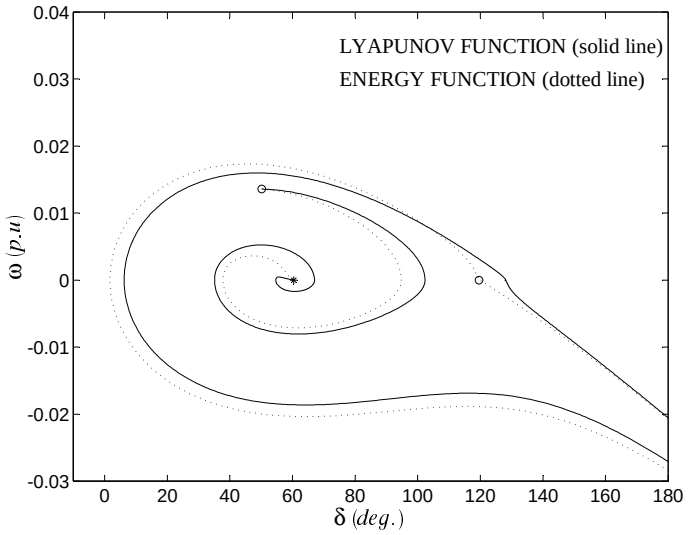

Figure 9.5. Phase portrait of the OMIB system after the fault, when an energy function (dotted line) and a Lyapunov function (solid line) are used for deriving the control law, respectively.

Figure 9.5 shows the stability boundary of the post–fault stable equilibrium point, and the post–fault system trajectory when energy function

(9.17) (dotted line) and Lyapunov function (9.18) (solid line) are used for deriving the control law, respectively. As shown in this figure, the stability region is larger, and the system is better damped when the control law is derived based on the energy function, i.e. control law (6.26). However, control law (9.20) (which is derived based on a true Lyapunov function) is not zero at x_{e1}, but it requires information about the post–fault stable equilibrium point.

9.3 Summary

Both control theories (i.e. CLF and VSC) can be applied to nonlinear systems. VSC receives much attention due to its robust response characteristics. Under certain conditions, the sliding mode of a VSC system is not affected by the system perturbations and external disturbances [53]. However, application of this control theory to CSDs in multi–machine power systems faces some difficulties, namely:

- In contrast to CLF, there exists mathematical (and also practical) unexplored issues for application of VSC to Differential–Algebraic Equations (DAE).
- In contrast to CLF, for the Reduced Network Model of the form (3.11), VSC does not require elimination of $p(x)$. However, two important problems arise regarding application of VSC to this model. First, one must find a good method to describe the sliding motion, that is, to define the equation of the sliding mode. The second challenge is the design of the matrix $\mathcal{G}$ to yield an asymptotically stable sliding motion.
- In contrast to the control law based on CLF, control law based on VSC requires information about the post–fault stable equilibrium point and also all information from the system (see (9.13)).

Chapter 10

Closure

10.1 Contributions of the Thesis

The main contributions of this thesis have been

1. to develop a general model for Controllable Series Devices (CSDs).
2. to observe the impact of CSDs on damping of electromechanical oscillations.
3. to clarify the difference between energy functions and Lyapunov functions.
4. to justify application of an energy function as a Lyapunov function candidate.
5. to clarify the difference between a Lyapunov Function and a Control Lyapunov Function (CLF).
6. to justify mathematically the control laws based on the CLF.
7. to show how the SIngle Machine Equivalent (SIME) method can be used to select remote input signals for CSDs.
8. to observe the impact of the CLF controlled CSDs on damping of electromechanical oscillations, when local and remote input signals are used, respectively.

9. to justify (both analytically and numerically) the effectiveness of control laws derived from simplified systems into actual systems.

10. to compare control laws based on Control Lyapunov Function and Variable Structure Control with sliding modes.

10.2 Conclusions

A general injection model for Controllable Series Devices (CSDs) has been developed. The injection model was derived in a single–phase–positive–sequence phasor frame. This model is helpful for understanding the impact of the CSDs on power systems dynamics.

It has been shown that the CSDs provide an effective means of adding damping to power systems and significantly enlarge the stability region (also called the region of attraction) of the post–fault stable equilibrium point with a suitable control strategy, see Figure 6.2 and Figure 6.3.

The damping effect of a Controllable Series Capacitor (CSC) increases as line loading increases, see (6.25), but the damping effect of a Quadrature Boosting Transformer (QBT) for a heavily loaded line is less than for a lightly loaded line, see (6.24). However, the damping effect of a Unified Power Flow Controller (UPFC) is robust with respect to the line loading, see (6.23). A similar result, based on small signal analysis, can be found in [7].

Based on Control Lyapunov Function (CLF) concepts, a general control strategy, see (6.35), for these three devices has been derived. The control laws (6.39)–(6.41) have been derived based on a simplified Structure Preserving Model (SPM). However, these control laws have been applied for the actual systems, and the simulation results in Chapter 7 indicate that the control laws are effective and robust for small and large disturbances as well as meshed and radial systems, and they are not sensitive to the model approximations. An analytical justification of this observation can be found in Section 5.3, i.e. the concept of total stability.

The control laws (6.39)–(6.41) rely only on locally measurable information and are independent of system topology and modeling of power system components. Thus, the input signals are inexpensive, fast and reliable.

Selecting remote input signals for the CSDs, the SIngle Machine Equivalent (SIME) method has been applied. The control law for a CSC based

on the SIME, see (8.8), relies on remote input signals, i.e. data from all machines in the system. Thus, the input signals can be expensive and less reliable in a real power system. However, due to the latest development in signal and communication technology, these issues may be solved in the near future. The simulation results in Section 8.3 indicate that using CSCs in a power system, the control law with remote input signals (i.e. control law (8.8)) is more effective than the control law with local input signals (i.e. control law (6.42)) for damping and stability of the power system.

It should be noted that both control laws (6.42) and (8.8) are derived based on CLF, and they do not require information about the post–fault stable equilibrium point. Furthermore, the CSDs with CLF control do not adversely affect each other.

Simulation results have shown that the electromechanical oscillation is damped, and the power system is stabilized under the proposed control (i.e. control laws based on CLF), if the initial states are in the region of attraction, or equivalently, the fault (or other contingency) is cleared before some maximum critical clearing time. The CLF controlled CSDs can certainly lengthen the maximum clearing time (i.e. enlarge the region of attraction), but there is obviously a limit on the increase, due to the physical limitation of the devices.

The concept of Variable Structure Control (VSC) with sliding modes has been presented in Chapter 9. A disadvantage with control law based on VSC with sliding mode is that it requires information about the post–fault stable equilibrium point for designing the switching manifold $S(x) = \mathcal{G} \cdot \dot{x} = 0$. Furthermore, for large multi–machine power systems, it is difficult and time–consuming to choose an appropriate $\mathcal{G}$, such that the equation of sliding mode becomes asymptotically stable.

10.3 Discussions and Future Work

In this thesis, the design of the controller has been done on phasor based model, which may be not appropriate at higher frequencies. Therefore, if the designed controller has a high gain at frequencies not adequately modeled in the phasor domain it might turn out to be unstable when tested in a full time-domain simulation. In order to investigate these issues, it is proposed to verify the design method in a full time-domain

simulation. This could either be done in a digital simulator, e.g. MASTA or EMTDC, or in a real time analogue simulator. This study should also result in guidelines regarding appropriate modifications to limit the possible adverse influence of high frequency dynamics.

For deriving control law (8.8), the right–hand side of the actual system (8.3) was simplified, and the simplified system was given by (8.6). In the the actual system (8.3), $P_{m_{GOMIB}}$ and $P_{e_{GOMIB}}$ (which are time–varying, and are calculated at each integration time–step) can be defined by

$$P_{m_{GOMIB}} = M_T^{-1} \left[M_N \sum_{i \in C} P_{mi} - M_C \sum_{j \in N} P_{mj} \right] \tag{10.1}$$

and

$$P_{e_{GOMIB}} = a \, \sin(b \, \delta_{GOMIB} + c) \tag{10.2}$$

where parameters a, b and c are time–varying, and are calculated at each integration time–step.

In a real power system (10.1) and (10.2) are indeed bounded. Therefore, it is reasonable to assume that there exists a $P_{m_{app}}$ and a $P_{max_{app}}$ such that (8.4) and (8.5) are small.

The simulation results in Section 8.3 indicate that using CSCs in a power system, the control law with remote input signals (i.e. control law (8.8)) is more effective than the control law with local input signals (i.e. control law (6.42)) for damping and stability of the power system. However, these results cannot be basis for a general conclusion regarding the SIME method. But, they may be good reasons for further research regarding this control law. The following questions may be the basis for this research.

- How does this control law work in a meshed system in which several CSCs are located in different locations?
- How fast can SIME predict on-line a GOMIB system for large as well small disturbances?
- How effective is this control law, (especially in extreme cases), if we only use information from the most sensitive generators (not all generators in the system)? How should these most sensitive generators be identified? (Application of Trajectory Sensitivity Analysis [55]–[57] may be useful to identify the most sensitive generators.)

Bibliography

[1] I. A. Hiskens, "Analysis Tools for Power Systems–Contending with Nonlinearities", *Proceedings of the IEEE*, Vol. 83, No. 11, pp. 1573–1587, November 1995.

[2] N. G. Higorani, "Flexible AC Transmisson", *IEEE, Spectrum*, pp. 40–45, April 1993.

[3] CIGRE Task Force 38.01.06, *"Load Flow Control in High Voltage Systems Using FACTS Controllers"*, CIGRE Technical brochure 51, 1996.

[4] M. Ghandhari, *Control of Power Oscillations in Transmission Systems Using Controllable Series Devices*, *Licentiate Thesis, Royal Institute of Technology*, TRITA–EES–9705, ISSN 1100–1607, 1997.

[5] M. Ghandhari et al., "Non–linear Control of Controllable Series Devices (CSD)", *Proceedings of the* 29^{th} *North American Power Symposium (NAPS)*, pp. 398–403, October 1997.

[6] M. Ghandhari and G. Andersson, "Two Various Control Laws for Controllable Series Capacitor (CSC)", *Power Tech. Budapest 99*, September 1999.

[7] M. Noroozian, *Exploring benefits of controllable series compensators on power systems*, *Ph. D. Thesis, Royal Institute of Technology*, TRITA–EES–9402,ISSN 1100–1607, 1994.

[8] A. Herbig, *On Load Flow Control in Electric Power Systems* , *Ph. D. Thesis, Royal Institute of Technology*, TRITA–EES–0001,ISSN 1100–1607, 2000.

[9] L. E. Jones, *On Zero Dynamics and Robust Control of Large AC and DC Power Systems* , *Ph. D. Thesis, Royal Institute of Technology*, TRITA–EES–9904,ISSN 1100–1607, 1999.

[10] CIGRE Task Force 38.01.07, *"Analysis and Control of Power System Oscillations"*, CIGRE Technical brochure, 1996.

[11] M. A. Pai, *Energy Function Analysis for Power System Stability*, Kluwer Academic Publishers, 1989.

[12] M. Pavella and P.G. Murthy, *Transient Stability of Power Systems, Theory and Practice*, John Wiley & Sons, 1994.

[13] H. K. Khalil, *Nonlinear Systems (second edition)*, Prentice-Hall, Inc., 1996.

[14] W. Hahn, *Stability of Motion*, Springer–Verlag Berlin. Heidelberg, 1967.

[15] N. N. Krasovskii and J. L. Brenner, *Stability of Motion*, Stanford University Press. Stanford, California, 1963.

[16] T. L. Vincent and W. J. Grantham, *Nonlinear and Optimal Control Systems*, John Wiley & Sons, INC., 1997.

[17] A. Bacciotti, *Local Stabilizability of Nonlinear Control Systems*, World Scientific Publishing Co. Pte. Ltd., 1996.

[18] A. Bacciotti, *The Local Stabilizability Problem for Nonlinear Systems*, IMA Journal on Mathematical Control and Information 5, pp. 27–39, 1988.

[19] E. W. Kimbark, *Power System Stability*, John Wiley and Sons, Inc., New York, 1948.

[20] A. R. Bergen and D. J. Hill, "A structure preserving model for power system stability analysis", *IEEE Trans. on Power Apparatus and Systems* Vol. PAS-100, No. 1, pp. 25–35, January 1981

[21] L. Gyugyi et al., "The Unified Power Flow Controller: A new approach to power transmission control", *IEEE Trans. on Power Delivery* Vol. 10, No. 2, pp. 1085–1097, April 1995

[22] H. D. Chiang et al., "Stability Regions of Nonlinear Autonomous Dynamical Systems ", *IEEE Trans. on Automatic Control*, Vol. AC–33, No. 1, pp. 16–27, January 1988.

[23] R. E. Kalman and J. E. Bertram, "Control System Analysis and Design Via the Second Method of Lyapunov", *Journal of Basic Engineering*, pp. 371–393, June 1960.

[24] P. C. Magnusson, "Transient energy method of calculating stability", *AIEE Transaction*, Vol. 66, pp. 747–755, 1947.

[25] V. Venkatasubramanian et al., "Dynamics of Large Constrained Nonlinear Systems–A Taxonomy Theory", *Proceedings of the IEEE*, Vol. 83, No. 11, pp. 1530–1561, November 1995.

[26] C. L. DeMarco and A. R. Bergen, "Application of Singular Perturbation Techniques to Power System Transient Stability Analysis", *Proceedings of I.S.C.A.S, Monteral, Canada*, pp. 597–601, May 1984.

[27] A. R. Bergen et al., "Lyapunov function for multimachine power systems with generator flux decay and voltage dependent loads", *International Journal of Electric Energy and Power Systems*, Vol. 8, No. 1, pp. 2–10, January 1986.

[28] H. D. Chiang et al., "Direct Stability Analysis of Electric Power Systems Using Energy Functions: Theory, Applications, and Perspective", *Proceedings of the IEEE*, Vol. 83, No. 11, pp. 1497–1529, November 1995.

[29] D. J. Hill and I. M. Y. Mareels, "Stability for Differential/Algebraic Systems with Application to Power Systems", *IEEE Trans. on Circuits and Systems* , Vol. 37, No. 11, pp. 1416–1423, November 1990.

[30] N. A. Tsolas et al., "A Structure Preserving Energy Function for Power System Transient Stability Analysis", *IEEE Trans. on Circuits and Systems*, Vol. CAS–32, No. 10, pp. 1041–1049, October 1985.

[31] Z. Artstein, "Stabilization with relaxed controls", *Nonlinear Analaysis, Theory, Methods and Applications*, Vol. 7, No. 11, pp. 1163–1173, 1983.

[32] E. Sontag, "A universal construction of Artstein's theorem on nonlinear stabilization", *Systems and Controll Letters 13*, pp. 117–123, 1989.

[33] V. Jurdjevic and J. P. Quinn, "Controllability and Stability", *Journal of Differential Equations 28*, pp. 381–389, 1978.

[34] R. A. Freeman and P. V. Kokotovic, *Robust Nonlinear Control Design*, Birkhäuser, 1996.

[35] J. F. Gronquist et al., "Power Oscillation Damping Control Strategies for FACTS Devices Using Locally Measurable Quantities", *IEEE, Trans. on Power Systems*, Vol. 10, No. 3, pp. 1598–1605, 1995.

[36] H. R. Fankhauser et al., "SIMPOW- a digital power system simulator", *Reprint of ABB Review*, No. 7, 1990.

[37] P. Kundur, *Power System Stability and Control*, McGraw–Hill, 1994.

[38] P. M. Andersson and A. A. Fouad, *Power System Control and Stability*, The Iowa State University Press, 1977.

[39] CIGRE Task Force 38.02.08, *"Longer term dynamics phase II"*, Final report, January 1995.

[40] M. Pavella et al., *Power System Transient Stability Analysis and Control*, Kluwer Academic Publishers, 2000.

[41] A. L. Bettiol et al., "Transient Stability–Constrained Maximum Allowable Transfer", *IEEE Trans. on Power Systems*, Vol. 14, No. 2, pp. 654–659, May 1999.

[42] Y. Zhang et al., "SIME : A hybrid approach to fast transient stability assessment and contingency selection", *International Journal of Electrical Power and Energy Systems*, Vol. 19, No. 3, pp. 195–208, 1997.

[43] B. Carraro and J. Salomao, "Power Corridor Unites Brazil's Network", *Transmission and Distribution World*, pp.70–74, June 1999.

[44] V. I. Utkin, *Sliding Modes in Control Optimization*, Springer–Verlag Berlin, Heidelberg 1992.

[45] V. I. Utkin, "Variable structure systems with sliding modes", *IEEE Trans. on Automatic Control*, Vol. AC–22, No. 2, pp. 212–222, April 1977.

[46] V. I. Utkin, "Variable structure systems: present and future", *Automat. Remote Control*, No. 9, pp. 1105–1120, 1983.

[47] V. I. Utkin, "Equations of the slipping regime in discontinuous systems, II", *Automat. Remote Control*, No. 2, pp.211–219, 1972.

[48] R. A. DeCarlo et al., "Variable structure control of nonlinear multivariable systems: A tutorial", *Proceedings IEEE*, Vol. 76, No. 3, pp. 212–232, 1988.

[49] S. Jayasuriya and S. Choi, "On the sufficiency condition for existence of a sliding mode", *American Control Conf.*, pp. 84–89.

[50] B. A. White and P. M. Silson, "Reachability in variable structure control systems", *Proceedings IEEE*, Vol. 131, No. 3, pp. 85–91, May 1984.

[51] A. F. Filippov, "Differential equations with discontinuous right hand sides", *Am. Math. Soc. Transl.*, Vol. 42, pp. 199–231, 1964.

[52] Y. Wang et al., "Variable–structure FACTS Controllers for Power Transient Stability", *IEEE Trans. on Power Systems*, Vol. 7, No. 1, pp. 307–313, February 1992.

[53] W. Gao and J. C. Hung, "Variable Structure Control of Nonlinear Systems: A New Approach", *IEEE Trans. on Industrial Electronics*, Vol. 40, No. 1, pp. 45–55, February 1993.

[54] G. Strang, *Introduction to Applied Mathematics*, Wellesley–Cambridge Press, 1986.

[55] I. A. Hiskens and M. A. Pai , "Trajectory Sensitivity Analysis of Hybrid Systems", *IEEE Trans. on Circuits and Systems I: Fundamental Theory and Applications*, Vol. 47, No. 2, pp. 204–220, February 2000.

[56] I. A. Hiskens and M. Akke, "Analysis of the Nordel Power Grid Disturbance of January 1, 1997 Using Trajectory Sensitivities", *IEEE Trans. on Power Systems*, Vol. 14, No. 3, pp. 987–994, August 1999.

[57] M. J. Laufenberg and M. A. Pai, "A New Approach to Dynamic Security Assessment Using Trajectory Sensitivities", *IEEE Trans. on Power Systems*, Vol. 13, No. 3, pp. 953–958, August 1998.